NATIONAL ADVISORY COMMITTEE FOR AERONAUTICS

TECHNICAL NOTE 2130

CALCULATION OF TRANSONIC FLOWS PAST THIN AIRFOILS BY AN INTEGRAL METHOD

By William Perl

Lewis Flight Propulsion Laboratory
Cleveland, Ohio

Washington
July 1950

TABLE OF CONTENTS

NATIONAL ADVISORY COMMITTEE FOR AERONAUTICS

TECHNICAL NOTE 2130

CALCULATION OF TRANSONIC FLOWS PAST THIN AIRFOILS BY AN INTEGRAL METHOD

By William Perl

SUMMARY

A method of calculating two-dimensional compressible flows past thin airfoils is presented with particular reference to the transonic speed range. The method is based on the integral form of the equation of continuity and on the intrinsic form, in terms of the streamline curvature, of the irrotationality condition. The application to the transonic range conforms with, and is carried out within the framework of, the transonic similarity theory. The results include velocity distributions for various symmetric sections in the continuous-potential-flow speed range and for the symmetric biconvex airfoil at zero angle of attack through the transonic speed range and the associated variation of terminal- and head-shock location and pressure drag with Mach number. Comparisons with other theories and with available experimental data indicate at least qualitatively good agreement. The location and the movement of the terminal shock in the lower transonic speed range are discussed, as well as the limiting-line phenomenon.

INTRODUCTION

Considerable effort has been expended in recent years on the investigation of the flow phenomena that occur when aerodynamic bodies travel at transonic speeds. Experimentally, the main features of steady transonic flow patterns about airfoil sections have been established. (See, for example, references 1 to 5.)

Thus, the succession of flow patterns, of which an approximate theoretical description is attempted herein, may be briefly outlined as follows: Consider the zero-lift flow relative to an airfoil that is symmetric with respect to its chord line (fig. 1). At low subsonic free-stream velocities, the flow pattern is likewise symmetric with respect to the chord line and is everywhere subsonic. Above a certain subsonic free-stream velocity, a symmetric-type local supersonic region, bounded by the locus of sonic speed indicated by 1 (fig. 1), starts to develop in the

neighborhood of the maximum-thickness location of the airfoil. If the airfoil had fore-and-aft symmetry with respect to its midchord location, these local supersonic regions would likewise have fore-and-aft symmetry with respect to midchord. As the free-stream velocity is further increased, the fore-and-aft type of symmetry of the flow pattern disappears and an asymmetric pattern develops. The local supersonic region, indicated by the sonic boundary 2 in figure 1, is now of an asymmetric type (that is, would be asymmetric fore and aft even if the airfoil were symmetric fore and aft) and is terminated on the downstream side by an approximately normal shock. Near the airfoil especially, this terminal shock is actually a more or less complex shock structure depending on the Reynolds number and interacts with the boundary layer in a complex manner. As the free-stream velocity increases toward sonic, the asymmetric-type local supersonic region increases in extent and the terminal shock increases in intensity and moves downstream toward the trailing edge. At slightly supersonic free-stream velocities, an additional shock, the bow wave, appears ahead of the airfoil and approaches it as the free-stream speed is increased. The subsonic part of the flow field has now become finite in extent, as indicated by the sonic boundary 3 (fig. 1). The terminal shock has reached, and remains in, the neighborhood of the trailing edge and begins to slope in a downstream direction. At a certain supersonic free-stream speed the forward shock attaches at the nose of the airfoil, if the nose is sharp-edged, and shortly thereafter the flow field becomes, usually, everywhere supersonic, except, of course, in the boundary layer.

On the theoretical side, much of the effort expended on the transonic problem has gone into the solution of the mathematically well-defined problem of the continuous compressible potential flow past an airfoil, corresponding to the symmetric-type flow pattern described. (See, for example, references 6 to 20.) Emmons and Maccoll and Codd (references 18 to 20), however, have included shocks in some of their relaxation calculations. Progress with the methods cited has so far not been rapid, primarily because of mathematical and computational difficulties. Perhaps the most significant theoretical result that has emerged is the probability that a subsonic free-stream speed exists for a given aerodynamic shape, such that continuous symmetric-type flow patterns containing local supersonic regions can, at least in principle, be derived for this shape below this speed but not above. In regard to the other main ingredient of real transonic flows, namely, the boundary layer and its interaction with the terminal shock, interpretation and analysis is only in a preliminary stage. (See, for example, references 3, 4, and 21 to 24.) It must be noted, however, that progress with a

complete theory is hampered by the practical difficulties involved in carrying out good experiments in the transonic speed range.

In the present report an integral method is applied to the calculation of transonic flow patterns. Starting from the equation of continuity in integral form and conservation of energy in the integrated form of Bernoulli's equation, which suffice for the analysis of quasi one-dimensional flows, two-dimensional effects are then taken into account by inclusion of the equation of motion normal to the streamlines, expressed in terms of the streamline curvature. By an appropriate choice of the streamline curvature, the flow pattern can then be calculated in a comparatively simple manner.

This method has long been known and applied to the calculation of flows through curved channels, for example, between turbine blades, or in wind tunnels (references 25 and 26). Application has recently been made to isolated airfoils in continuous compressible potential flow (references 27 to 29).

The small-perturbation form of the method of reference 29 is developed herein. The resulting simplifications make feasible the approximate calculation of some of the more complicated, shock-containing, flow patterns previously described. The small-perturbation form also shows explicitly the agreement of the method of reference 29 with the more general transonic similarity theory of von Kármán (reference 30) and Oswatitsch, to which any nonviscous-type explicit solution for thin airfoils in the transonic speed range must conform.

The mathematical simplicity of the present method preserves the possibility of interpreting results and difficulties at all stages in terms of the basic conservation laws. The insight thus permitted into the nature of transonic flows makes it easy to understand, for example, the previously mentioned phenomenon of an upper-limiting subsonic flight speed for the existence of continuous potential flows.

In order not to unduly disturb the continuity of presentation of the main ideas, certain mathematical details are relegated to appendices A to D and a list of the main symbols used is contained in appendix E.

The main developments of this report were worked out at Columbia University in the winter of 1947-1948 under the stimulus of a lecture given by Professor Theordore von Kármán on the subject of transonic similarity. The report was completed at the NACA Lewis laboratory.

The author wishes to express his thanks to Professor Theodore von Kármán for having inspired the present treatment of the transonic problem. This inspiration was not only direct; for, Professor von Kármán has probably done most to demonstrate the power and utility in fluid mechanics of the two foundational ideas on which the present theory is built, namely, the integral-method approach and the similarity concept. It is to be hoped that the present structure does not rest too lightly on the foundations.

COMPRESSIBLE POTENTIAL FLOW

Governing equations. - The flow is considered steady, two-dimensional, isentropic, irrotational, and symmetric with respect to the airfoil chord (x-axis). The equations of motion can be expressed in terms of the local fluid density ρ, speed v, pressure p, Mach number M, the corresponding free-stream values (denoted by the subscript o), the specific-heat ratio γ, and the streamline curvature C, as follows (fig. 2): (The main symbols are defined in appendix E.)

Equation of continuity:

$$\int_0^{y_o} \rho_o v_o dy = \int_0^n \rho v dn \tag{1}$$

Irrotationality condition (reference 31):

$$\frac{\partial v}{\partial n} + Cv = 0 \tag{2}$$

Bernoulli-state equation:

$$\frac{\rho}{\rho_o} = \left(\frac{p}{p_o}\right)^{\frac{1}{\gamma}} = \left[1 - \frac{\gamma-1}{2} M_o^2 \left(\frac{v^2}{v_o^2} - 1\right)\right]^{\frac{1}{\gamma-1}} \tag{3}$$

The differentials dy and dn in equation (1) are elements of length along a potential line in the free stream far ahead of the airfoil and along a potential line in the region of the airfoil, respectively. The lower limits of integration lie on the zero

streamline, that is, on the x-axis and on the airfoil contour. The upper limits lie on a streamline DBF, which, as y_o approaches infinity, becomes parallel to the x-axis. It is assumed for the present that as y_o approaches infinity the displacement component δ in the y-direction between any two points on the same streamline, such as D and B, approaches zero. This assumption is valid for circulation-free (zero-lift) flows that are subsonic at infinity and that have no wakes or unclosed portions of airfoil contour extending to infinity in the x-direction, inasmuch as such flows can be represented at infinity by a collection of incompressible-type source-sink doublets in the finite part of the plane, and for such doublets the assumption is valid. This assumption can also be regarded, perhaps more generally, as restricting the flow pattern to that produced in a closed, straight-walled, two-dimensional wind tunnel in the limiting case in which the walls are infinitely for apart.

The element of length dn in equation (1) is now approximated by the element of length dy in the y-direction, that is, the potential lines are replaced by the lines x = constant. This replacement is exactly valid for the potential line starting from the midchord location of a symmetric airfoil that has also fore-and-aft symmetry. In appendix A, this replacement is shown to be justified, in general, for the case of small perturbation of the free-stream flow by an airfoil.

Next let the lower limit on the right side of equation (1) start from a point on the airfoil at which the airfoil ordinate is Y. Set ρ_o, v_o, and p_o equal to unity, so that the corresponding local quantities ρ, v, and p henceforth represent nondimensional fractions of free-stream density, velocity, and pressure, respectively. Furthermore, let the unit of length be the airfoil chord c so that the lengths x, y, and 1/C henceforth represent nondimensional fractions of the airfoil chord length. Subtracting y_o-Y from both sides of equation (1), letting y_o approach infinity, and using the preceding assumption for δ and approximation for dn yields

$$Y = \int_Y^\infty (\rho v - 1)\,dy \tag{4}$$

Equations (2) and (3) become, respectively,

$$dy = -\frac{dv}{Cv} \tag{5}$$

$$\rho = p^{\frac{1}{\gamma}} = \left[1 - \frac{\gamma-1}{2} M_o^2(v^2-1)\right]^{\frac{1}{\gamma-1}} \qquad (6)$$

The form of the continuity equation (4) is analogous to that defining the displacement thickness in the boundary-layer theory. The airfoil ordinate Y here takes the place of the boundary-layer displacement thickness. Whereas the subtraction and limiting process leading to equation (4) is performed in the boundary-layer theory mainly for definiteness in defining a boundary-layer thickness, the process is here essential in order to subtract out the infinite mass flow crossing a potential line and initially introduced perhaps somewhat artificially by considering the fluid as moving relative to the stationary airfoil.

The streamline curvature C, considered positive when the streamline curves in the same sense as the corresponding contour of the airfoil at the maximum thickness location, is a function of the position coordinates x and y of the flow field. At a given chordwise location x, the streamline curvature is a function of y that varies continuously from the curvature C_a of the airfoil contour at $y = Y$ to the value zero at $y = \infty$. It proves convenient to consider the curvature C at a given x as a function of the local velocity v rather than of y. In the applications made herein, v will be a monotonic function of y. Hence, at least for such applications, C can be expressed as

$$C = C_a f(x,v) \qquad (7)$$

The assumption that the streamline curvature can be as well expressed by a function of x and v as by a function of x and y may be more generally justified as follows: Of the four basic variables of the problem, namely, the vector velocity given by the two variables v and θ, where θ is the angle of inclination of the local stream direction to the x-axis, and the vector distance given by the two variables x and y, two variables are to be regarded as independent and two as dependent. The solution of the so-called direct problem of airfoil theory is required in the form where $v(x,y)$, $\theta(x,y)$, and in particular the velocity $V(x,Y)$ on the given airfoil contour $\theta_a(x,Y)$ are finally known. The analysis of the problem, however, can be made, at least in principle, with any two of the variables considered as independent and the remaining two as dependent. The hodograph method, for example, is based on v and θ as the independent and x and y as the dependent variables.

The present method is based on v and x as the independent and θ and y as the dependent variables. Conceivably, other possible combinations might be advantageous in particular problems. Similar remarks apply with the potential, or the stream function, or both, replacing one or two of the present variables.

The present method is thus a sort of semihodograph method. Whereas it retains the principal advantage of the hodograph method, namely, that the velocity v and hence, by equation (6), the density ρ becomes essentially an independent variable, it avoids the well-known disadvantage of the hodograph method; namely, difficulty in satisfying the boundary conditions in obtaining flows past given fixed airfoils as a function of Mach number.

Equation (4) becomes, upon substitution of equations (5) and (7),

$$YC_a = \int_1^V \frac{\rho - \frac{1}{v}}{f(x,v)}\, dv \tag{8}$$

in which V is the sought-for velocity at the airfoil at chordwise location x, the quantity x being held constant in the integration. Equations (6) and (8) constitute an expression for the velocity V at a point on an airfoil in terms of the shape parameter YC_a of the airfoil at that point, the free-stream Mach number M_o, and the curvature function $f(x,v)$. (From the point of view of the inverse problem, that is, designing an airfoil to satisfy a prescribed velocity distribution, the shape parameter YC_a would be regarded as dependent upon V, M_o, and f.) The basic reason for expressing the airfoil velocity V in terms of a streamline-curvature function f is that, in the form of equation (8), V is relatively insensitive to choice of f. As will be seen, a reasonable choice of f can therefore be made that leads with comparatively little computation to fairly accurate values of V.

The relation between the local velocity v and the lateral distance y at a given x is obtained by integration of equation (5) from an airfoil point (x,Y) or (x,V) to a field point (x,y) or (x,v) as

$$y = Y + \frac{1}{C_a} \int_v^V \frac{dv}{vf(x,v)} \tag{9}$$

Solution of equation (8) for V enables the local velocity $v(x,y)$ at any point in the flow field to be determined from equation (9). The streamline inclination $\theta(x,y)$ can then also be obtained, as will be subsequently shown.

The only approximation thus far made is to replace the element of length dn along a potential line by the element of length dy perpendicular to the chord line. The resulting equations (6), (8), and (9), together with an assumed form for the curvature function $f(x,v)$, have been applied in reference 29 to calculate (finite perturbation) compressible potential flows past airfoils. An approximation for the density $\rho(v)$ is next made, which leads to the general small-perturbation form of the preceding theory.

Small-perturbation case. - By small perturbation is herein meant that the local velocity increment $v-1$ produced by the airfoil is small relative to unity. The density ρ is, by equation (6), thereby expressible as a power series in $v-1$. Thus, the numerator of the integrand in equation (8) can be developed as

$$\rho - \frac{1}{v} = \mu v - \Gamma_c v^2 + \cdots \tag{10}$$

where

$$v \equiv v - 1 \tag{11a}$$

$$\mu \equiv 1 - M_o^2 \tag{11b}$$

$$\Gamma_c \equiv 1 + \frac{M_o^2}{2} - \frac{2-\gamma}{2} M_o^4 \tag{11c}$$

$$\lim_{M_o \to 1} \Gamma_c \equiv \Gamma = \frac{\gamma+1}{2} \tag{11d}$$

The velocity increment Λ at the airfoil, a normalized local-velocity variable z, and a Mach number parameter K are next defined as

$$\Lambda \equiv V - 1 \tag{12a}$$

$$z \equiv \frac{v}{\Lambda} = \frac{v - 1}{V - 1} \tag{12b}$$

$$K \equiv \frac{\mu}{(\tau\Gamma)^{2/3}} = \frac{1-M_o^2}{(\tau\Gamma)^{2/3}} \tag{12c}$$

In terms of the reduced local velocity z, the curvature function (equation (7)) can be expressed as

$$C = C_a\, f(x,z,K) \tag{13}$$

Equation (13) can easily be shown, from the general transonic similarity theory of reference 30, to be the most general possible form for the streamline-curvature function in the small-perturbation transonic range. (This possibility was pointed out by Professor Theodore von Kármán.) Conversely, it will be presently verified that the use of equation (13) with the present formulation of the equations of motion leads to the transonic similarity laws of reference 30. The curvature function $f(x\ z,K)$ in equation (13) must satisfy the boundary conditions $f(x,1,K) = 1$ at the airfoil and $f(x,0,K) = 0$ at infinity.

Substitution of equation (10) into equation (8) and changing the variable of integration from v to z by equations (11a), (12), and (13) yields

$$\frac{YC_a}{\mu\Lambda^2} = \int_0^1 \left(z - \frac{\Gamma_c \Lambda}{\mu} z^2\right) \frac{dz}{f(x,z,K)} \tag{14}$$

Similarly, the relation (9) between local velocity v and lateral distance y becomes, for small perturbations,

$$y = Y + \frac{\Lambda}{C_a} \int_z^1 \frac{dz}{f(x,z,K)} \tag{15}$$

Prandtl-Glauert range. - In the subsonic or Prandtl-Glauert range, defined by $0 < M_o << 1$ or $K \to \infty$, the dependence of the

curvature function (equation (13)) on K must disappear. Hence, in the small-perturbation case, $\Lambda << 1$, and for sufficiently subsonic free-stream Mach numbers M_o, the second term in the integrand of equation (14) can be neglected relative to the first, and equation (14) can be written as

$$\frac{YC_a}{\mu\Lambda^2} = F(x) \tag{16}$$

where $F(x)$ is a function of x of the order of magnitude of unity. For smoothly curved, thin airfoils, the shape parameter YC_a can be expressed as the product of the square of the thickness ratio τ (τ = maximum thickness/chord length) and a function of x of the order of magnitude of unity over most of the airfoil. Equation (16) can therefore be written as

$$\Lambda = \frac{\tau}{\sqrt{\mu}} G(x) \tag{17}$$

where $\tau << 1$ and $G(x) \sim 1$. Equation (17) expresses the basic result of thin-airfoil theory that the velocity increment at chordwise location x of one of a series of thin airfoils, all having the same geometric shape but differing in thickness ratio τ, is proportional to the thickness ratio τ of that airfoil. Equation (17) also expresses the Prandtl-Glauert rule that the effect of compressibility in the lower subsonic range is to increase the airfoil velocity increment by the factor $1/\sqrt{1-M_o^2}$.

Lower transonic range; similarity rules. - As the free-stream Mach number M_o is increased toward unity, or $\mu \to 0$, the airfoil contour being such as to maintain a small velocity perturbation $\Lambda << 1$, a value of $\mu << 1$ must eventually be reached where $\Gamma\Lambda/\mu$ becomes comparable to unity. The second term in the integrand of equation (14) is then comparable with the first. Additional terms in the expansion of the integrand, however, evidently would remain negligible relative to the first two terms. Hence, at transonic speeds defined by $\mu \sim 0$, instead of the relation of equation (16) between the two parameters x and $YC_a/\mu\Lambda^2$, equation (14) constitutes a relation among four parameters; thus

$$H\left(x, \frac{\tau^2}{\mu\Lambda^2}, \frac{\Gamma\Lambda}{\mu}, \frac{\mu}{(\tau\Gamma)^{2/3}}\right) = 0 \tag{18}$$

The last three parameters indicated in equation (18) are not independent, however, but can be expressed in terms of two independent parameters. Thus, using the third parameter of equation (18) to eliminate Λ from the second yields the equivalent expression of equation (14)

$$I\left(x, \frac{\mu}{(\tau\Gamma)^{2/3}}, \frac{\Gamma\Lambda}{\mu}\right) = 0 \tag{19}$$

or also, using the second parameter of equation (19) to alter the third,

$$J\left(x, \frac{\mu}{(\tau\Gamma)^{2/3}}, \frac{\Gamma^{1/3}\Lambda}{\tau^{2/3}}\right) = 0 \tag{20}$$

Inasmuch as the pressure coefficient P at a point on the airfoil is obtained in terms of the velocity from equation (3) in the small-perturbation case as

$$P \equiv \frac{p-p_o}{\frac{1}{2}\rho_o v_o^2} = -2\Lambda \tag{21}$$

relation (20) can be written as

$$P = \frac{\tau^{2/3}}{\Gamma^{1/3}}\mathscr{P}(x,K) \tag{22}$$

The function $\mathscr{P}$ in equation (22) is determined by the shape of the airfoil and is of the order of magnitude of unity. Equations (22) and (12c) agree with the transonic-similarity theory as regards velocity distributions on airfoils.

By multiplying equation (15) by $\sqrt{\mu}$ and using the preceding relations, there results for the velocity increment in the flow field

$$v = \frac{\tau^{2/3}}{\Gamma^{1/3}}\mathscr{N}_1\left[x, \sqrt{\mu}(y-Y), K\right] = \frac{\tau^{2/3}}{\Gamma^{1/3}}\mathscr{N}_2\left[x, (\tau\Gamma)^{1/3}(y-Y), K\right] \tag{23}$$

where $\mathcal{N}_1$ and $\mathcal{N}_2$ are functions of the order of magnitude of unity and $\sqrt{\mu}(y-Y)$, the affinely transformed lateral distance of the Kármán theory (reference 30) is of the order of magnitude of unity by equation (15). Equation (23) agrees with the transonic-similarity theory as regards conditions in the flow field. Equation (23) reduces to equation (22) on the airfoil.

Equation (22) states that if the pressure coefficient has a certain value P_1 at a chordwise location x on an airfoil of thickness ratio τ_1 in a flow at speed $M_{o,1} \sim 1$ and in a fluid of specific-heat ratio γ_1, then the pressure coefficient P_2 at the same chordwise location of a geometrically similar airfoil of thickness ratio τ_2 in a fluid of specific-heat ratio γ_2 and at a speed $M_{o,2}$ given by

$$\frac{1-M_{o,1}^2}{(\tau_1\Gamma_1)^{2/3}} = \frac{1-M_{o,2}^2}{(\tau_2\Gamma_2)^{2/3}} \tag{24}$$

will be related to P_1 by

$$\frac{P_2}{P_1} = \left(\frac{\tau_2}{\tau_1}\right)^{2/3}\left(\frac{\Gamma_1}{\Gamma_2}\right)^{1/3} \tag{25}$$

The Prandtl-Glauert rule is included in equation (22) if an inverse square root is chosen for the K-dependent part of the function $\mathcal{P}$. This result necessarily follows because the Prandtl-Glauert case is obtainable from the general formulation, equations (14) and (19), by letting $\Gamma\Lambda/\mu \to 0$.

A further similarity rule that concerns the local Mach number may be noted. In isentropic flow, the local Mach number M is related to the local velocity v and the free-stream Mach number M_o as follows:

$$M^2 = \frac{M_o^2 v^2}{1 - \frac{\gamma-1}{2} M_o^2 (v^2-1)} \tag{26}$$

In the small-perturbation case $v - 1 = \nu << 1$, equation (26) becomes

$$M^2-1 = -\mu + 2\Gamma_M \nu \tag{27}$$

where

$$\Gamma_M = M_o^2 \left(1 + \frac{\gamma-1}{2} M_o^2\right) \tag{28a}$$

and

$$\lim_{M_o \to 1} \Gamma_M = \Gamma = \frac{\gamma+1}{2} \tag{28b}$$

Equations (23), (27), and (28b) yield the transonic similarity rule for local Mach number

$$\frac{M^2-1}{(\tau\Gamma)^{2/3}} = \mathcal{M}\left[x,\ (\tau\Gamma)^{1/3}(y-Y),\ K\right] \tag{29}$$

Equation (29) may be applied in a manner similar to equations (24) and (25) to relate local Mach numbers M_1 and M_2 at the corresponding points

$$x_1 = x_2 \tag{30a}$$

$$(\tau_1\Gamma_1)^{1/3}(y_1-Y_1) = (\tau_2\Gamma_2)^{1/3}(y_2-Y_2) \tag{30b}$$

in the flow fields of similar airfoils τ_1 and τ_2 in fluids characterized by Γ_1 and Γ_2 at corresponding free-stream Mach numbers $M_{o,1}$ and $M_{o,2}$ given by equation (24). Instead of equation (25), the following relation, obtained from equation (29), applies:

$$\frac{M_2^2-1}{(\tau_2\Gamma_2)^{2/3}} = \frac{M_1^2-1}{(\tau_1\Gamma_1)^{2/3}} \tag{31}$$

Various special cases of this similarity rule have been previously given in references 4, 32, and 33.

It may be noted that although the use of $\Gamma = (\gamma+1)/2$ in such expressions as equations (23) and (29) is valid in the transonic limit $M_o = 1$, in applications for which M_o is finitely different from unity equations (28a) and (11c) for Γ_M and Γ_c, respectively, should more properly be used. The reason is that in the approximating equations (10) and (27), only the small-perturbation approximation $\nu << 1$ was made and not the transonic approximation $\mu << 1$. This transonic approximation was made in equation (18), and so forth, only to show the agreement between the common transonic limiting value of Γ_M and Γ_c with the Γ of reference 30.

Explicit solution by choice of curvature function. - Before choosing a form for the curvature function $f = C/C_a$ and thence calculating the flow pattern explicitly, a few general remarks, which may be helpful in judging the degree of approximation of the resulting solution, will be made. The present formulation of the airfoil flow problem is in terms of longitudinal distance x and local velocity v as independent variables and local streamline curvature C and lateral distance y as dependent variables, that is, the solution for given stream Mach number M_o is required in the form $C(x, v)$, $y(x, v)$. Various possible procedures for obtaining this solution suggest themselves. For example, an iterative procedure would be to assume in first approximation a curvature function $C(x, v)$, and thence calculate $y(x, v)$ and, in particular, the streamlines, using equations (1) to (9). The curvature of these streamlines would then yield a second approximation $C(x, v)$ and the procedure would be repeated until satisfactory convergence was achieved. Again, a network-type procedure would be to set up the continuity integral (1) between n pairs of streamlines rather than between the one pair (airfoil and infinity) in equation (4). The number n would increase in successive steps of the calculation. In each step a curvature function based on the curvature values obtained in the preceding step would be used to yield by simultaneous solution of the continuity and distance equations (1) and (9) an increased number of curvature and corresponding distance values for use in the next step.

The rapidity of convergence of the preceding types of procedure could be expected to depend strongly on the initial choice of curvature function in the first approximation. It is therefore sensible for computational reasons to choose an initial curvature function in the light of the information supplied by experiment and other theory as to the behavior of the streamline curvature in the type of flow field under consideration.

Only the first approximation is considered herein and free use is made of experiment and other theory in setting up an initial curvature function. In view of the preceding remarks, this use of experiment and other theory should not be construed as inherently limiting the degree of rigor in principle attainable in solutions by the present approach. This ultimate degree of rigor can be expected to be about the same as with existing perturbation or network formulations of the airfoil flow problem.

An explicit form for the curvature function $C/C_a = f(x, z, K)$, equation (13), in the small-perturbation case is now set up. This function must satisfy the boundary conditions of the problem; namely,

at airfoil,

$$\left.\begin{aligned} y &= Y \\ v &= \Lambda \\ z &= 1 \\ C &= C_a \\ f(x,1,K) &= 1 \end{aligned}\right\} \qquad (32a)$$

at infinity,

$$\left.\begin{aligned} y &\to \infty \\ v &\to 0 \\ z &\to 0 \\ C &\to 0 \\ f(x,0,K) &\to 0 \end{aligned}\right\} \qquad (32b)$$

Furthermore, it may be expected, at least in subsonic flow and at the chordwise locations near the maximum velocity or thickness regions of the airfoil (which are of most interest), that the streamline curvature will decrease monotonically from the positive value C_a at the airfoil to zero at infinity. A simple curvature function that satisfies these requirements is (reference 29)

$$f = z^r \qquad (33)$$

in which the parameter r is a function of x and K to be determined.

Substitution of equation (33) into equation (14) and integration yields

$$YC_a = \frac{\mu\Lambda^2}{2-r} - \frac{\Gamma_c\Lambda^3}{3-r} \tag{34}$$

Equation (34) gives the local velocity increment Λ on a symmetric airfoil in compressible potential flow in terms of the local shape parameter YC_a, the Mach number parameter μ, the specific-heat-ratio parameter Γ_c, and the parameter r.

In order to determine r, it is first noted that to satisfy the boundary condition at infinity (equations (32b)), r must be positive and the integral for the lateral distance y in equation (15) must diverge at $z = 0$, and therefore $r \geq 1$. In addition, the continuity integral (equation (14)) must converge at $z = 0$, which it does for $r < 2$. Hence r is restricted to the range

$$1 \leq r < 2 \tag{35}$$

In the speed range for continuous potential flow, the flow pattern is largely subsonic, as mentioned in the INTRODUCTION. Hence, in this speed range the determination of r will be completed (1) by assuming r to be independent of K, and (2) by requiring equation (34) to yield the (presumed) known velocity distribution $\Lambda_i(x)$ in the incompressible case $M_o = 0$. Conditions (1) and (2) are appropriate to the Prandtl-Glauert speed range. In the higher speed ranges discussed in subsequent sections in which the flow pattern differs very substantially from Prandtl-Glauert type, these conditions on r will be discarded for new ones. By condition (2) and equations (11b) and (11c), equation (34) yields for the determination of r

$$YC_a = \frac{\Lambda_i^2}{2-r} - \frac{\Lambda_i^3}{3-r} \tag{36}$$

The values of r determined by equation (36) turn out to be in the range of equation (35) over the maximum-velocity region of the airfoil, for which the curvature function (equation (33)) was set up. This type of inner consistency will recur often in this report.

The second term on the right side of equation (36) can, in principle, be neglected in the small-perturbation case considered.

Better results are obtained, however, in applications to airfoils of finite thickness ratio (of the order of 0.1) if it is retained. Some theoretical explanation for this improvement and hence retention of the term in question can be made as follows: The right side of equation (34) actually consists of the first two terms of an infinite series in the velocity increment Λ, which is evident for any curvature function f, from equations (8), (10), and (14). If the coefficients multiplying the powers of Λ are of comparable magnitude, as in equation (36), it may therefore be expected that for small but finite Λ the first two terms of the series would be a better approximation to the complete series than the first term alone.

Thus, finally, in order to calculate a velocity increment Λ at a chordwise location x on a symmetric airfoil at zero lift at Mach number M_o by the present method, the shape parameter YC_a and the low-speed velocity increment Λ_i at that point are determined first. The quadratic equation (36) for r is then solved for the value of r in the range of equation (35). (If such a root of equation (36) does not exist, the present explicit solution based on the curvature function (equation (33)) fails.) While keeping this value of r constant as M_o varies and using the values of μ and Γ_c corresponding to the desired M_o, equation (34) is solved for the desired velocity increment $\Lambda(x)$ at free-stream Mach number M_o. For convenience in solving the cubic equation (34) for Λ for various values of the other parameters, these other parameters can be combined as follows: Let

$$\lambda \equiv \left(\frac{2-r}{3-r}\right) \frac{\Gamma_c \Lambda}{\mu} \tag{37a}$$

$$\chi \equiv \frac{(2-r)^3}{(3-r)^2} \frac{\Gamma_c{}^2 YC_a}{\mu^3} \tag{37b}$$

Equation (34) then becomes

$$\chi = \lambda^2 - \lambda^3 \tag{38}$$

Equation (38) is plotted in figure 3. The most significant feature, the double-valuedness of (positive) λ for given χ, will be subsequently discussed in connection with the potential-limit phenomenon.

Conditions in flow field. - Once the velocity increment Λ at the airfoil has been obtained, the variation of local velocity v in the field with distance y from the airfoil can be determined from equation (15). With the curvature function (equation (33)), equation (15) yields

$$z = \frac{v}{\Lambda} = \left[1 + \frac{(r-1)(y-Y)C_a}{\Lambda}\right]^{\frac{-1}{r-1}} \tag{39}$$

The streamline curvature is expressed in terms of y by equations (33) and (39) as

$$f = \frac{C}{C_a} = \left[1 + \frac{(r-1)(y-Y)C_a}{\Lambda}\right]^{\frac{-r}{r-1}} \tag{40}$$

The preceding equations show that both the local velocity and the streamline curvature decrease monotonically with y from their values at the airfoil to zero at infinity. The actual manner of this decrease depends, at a given chordwise location x, on the airfoil curvature C_a and on the equations of motion through the parameters r and Λ. Actually there is therefore not a great deal of arbitrariness in the values of streamline curvature obtained here. Once a basic form such as equation (33) is chosen, the actual values of streamline curvature in the flow field are determined by the equations of motion and in such a way as to satisfy these equations on the average or in the large (inasmuch as the integral, rather than the differential, form of the continuity equation was used). The insensitivity of airfoil velocity and hence also of the flow pattern generally to the choice of a particular form of curvature function such as equation (33) is thus plausible.

A streamline in the flow field can be traced out as follows: A streamline is defined by a constant value of y_o in the continuity equation (1), which can be written as

$$y_o = \int_Y^y \rho v dy \tag{41}$$

Eliminating v in equation (41) by the irrotationality relation (5) gives the equation of the streamline

$$y = S(x,y_o) \tag{42}$$

Thus y_o is in effect the stream function. In the small-perturbation case, equation (41) can be transformed as follows:

$$y_o - (y-Y) = \int_Y^y (\rho v - 1)dy = \int_v^V \left(\rho - \frac{1}{v}\right)\frac{dv}{C}$$

$$= \frac{1}{C_a}\int_\nu^\Lambda \frac{(\mu\nu - \Gamma_c\nu^2)}{f(x,\nu)}\,d\nu = \frac{\mu\Lambda^2}{C_a}\int_z^1 \left(z - \frac{\Gamma_c\Lambda}{\mu}z^2\right)\frac{dz}{z^r}$$

$$= \frac{\mu\Lambda^2}{C_a}\left[\frac{\left(1-z^{2-r}\right)}{2-r} - \frac{\Gamma_c\Lambda}{\mu}\frac{\left(1-z^{3-r}\right)}{3-r}\right]$$

Hence, using equation (34),

$$y - y_o = \frac{\mu\Lambda^2}{C_a}\left(\frac{z^{2-r}}{2-r} - \frac{\Gamma_c\Lambda}{\mu}\frac{z^{3-r}}{3-r}\right) \tag{43}$$

Elimination of z in equation (43) by use of equation (39) gives the equation of the streamline (equation 42). The inclination θ of the local stream direction to the x-axis can then be obtained as the slope of the streamline.

It is of interest to note that for $r = 3/2$, which is in the middle of its permissible range (equation (35)), the local velocity increment far from the airfoil is given in the Prandtl-Glauert range by equations (39) and (16) as

$$\lim_{y\to\infty} v \sim \frac{\tau}{y^2\mu^{3/2}} \tag{44}$$

This expression agrees with that obtained for a source-sink doublet by conventional methods.

Illustrative examples. - In order to illustrate the preceding explicit solution, consider first the Kaplan section (reference 6) of thickness ratio $\tau = 0.1$. This contour, indicated in figure 4, can be expressed in parametric form as (reference 34)

$$2Y \equiv \eta = \frac{3}{4}\tau\left(\sin\varphi - \frac{1}{3}\sin 3\varphi\right) \tag{45a}$$

$$2x-1 \equiv \xi = \left(1 - \frac{\tau}{4}\right)\cos\varphi + \frac{\tau}{4}\cos 3\varphi \tag{45b}$$

where $0 < \varphi < 2\pi$. When the shape parameter $YC_a(x)$, as determined by equation (45), and the incompressible velocity distribution $\Lambda_i(x)$, as determined by conformal transformation, are substituted into equation (36), the parameter $r(x)$ is found to vary from $r = 1.301$ at the midpoint $\xi = 0$ to $r = 2$ at $\xi = 0.645$ (because $\Lambda_i = 0$ but $YC_a \neq 0$ at $\xi = 0.645$). Thus, by equation (35), the preceding explicit solution fails outside the range $0 < |\xi| < 0.645$. The velocity distributions $\Lambda(x)$ at various Mach numbers M_o, as obtained from equation (34) within this chordwise range, are shown in figure 4. For comparison, the results obtained (reference 29) without making the small-perturbation approximation of equation (10) for the density and the results of Kaplan (reference 6) are shown. The results of Kaplan were obtained by substituting a series for the potential in powers of τ into the partial differential equation for the potential and successively solving the Poisson equations obtained by equating orders of magnitude in τ. The calculation was carried out to the third order, τ^3.

The three sets of distributions in figure 4 are seen not to differ greatly except for Mach numbers near the potential limit, that is, the maximum Mach number for which the method yields a solution. This limiting case will be discussed in the next section.

As a further illustration, $\Lambda(M_o)$ at the maximum thickness locations of the three $\tau = 0.1$ sections - Kaplan, symmetric biconvex, and ellipse - as calculated by the small-perturbation integral method, the finite-perturbation integral method (reference 29), and by various other authors is shown in figure 5.

The results of Hantzsche (reference 7) for the ellipse were obtained by a method similar to that used by Kaplan. The calculations

were carried to the third order in a thickness-ratio parameter, which in successive orders equalled τ, τ^2, and $\tau^3 + O(\tau^4 \log \tau)$, respectively.

In the method of Göthert and Kawalki (reference 17), the influence of compressibility was represented by a finite number (12 per quadrant) of sources and sinks (Rayleigh-Janzen idea) located in the incompressible-flow field, as corrected by the Prandtl-Glauert rule, outside a given airfoil. The source-sink strength used for calculating velocity increments caused by compressibility was computed by iteration from the flow-field velocities themselves so as to satisfy continuity. As many successive steps in the calculations (~ 10 near the potential limit) were made as required for obtaining a self-consistent compressible-flow field that could be regarded as an incompressible-flow field, with the given spatial arrangement of sources and sinks superimposed.

Finally, the velocity increments given by the Prandtl-Glauert and Kármán-Tsien rules, (reference 35) are included in figure 5. It can be seen from figure 5 that the results of the present method differ from those of the other methods by about the same amounts as the results of the other methods differ amongst themselves.

The Prandtl-Glauert rule has an interesting connection with the present method. This rule results when the second term in equation (34) is negligible relative to the first term, as is the case in the subsonic speed range for small perturbations. The transonic term is also negligible, however, for higher speeds or larger perturbations if $r \sim 2$. As previously noted, $r \to 2$ at those points on the airfoil where $\Lambda_i \sim 0$ but $YC_a \neq 0$. Near these (locally subsonic) locations the Prandtl-Glauert rule may therefore be expected to apply. On the other hand, the maximum velocity increments on airfoils of the type illustrated in figure 5 turn out to vary with Mach number in the subsonic range in a manner approximating the Kármán-Tsien rule. (See also reference 29). Inasmuch as the Kármán-Tsien rule itself approaches the Prandtl-Glauert rule for small velocity increments, the present method therefore gives results in the subsonic speed range not greatly different from those obtained by the Kármán-Tsien rule.

Potential-limit phenomenon. - In computing a velocity distribution on an airfoil at a fixed free-stream Mach number M_o by equation (34) as plotted in figure 3, a portion of the airfoil contour is put into correspondence with a portion of the lower branch of figure 3. For example, on the Kaplan section at $M_o = 0$, the

region of airfoil $0.178 < x < 0.823$ corresponds to the portion AD in figure 3, such that traversing the stretch $0.178 < x < 0.5$ on the airfoil corresponds to traversing the stretch AD and traversing the stretch $0.5 < x < 0.823$ on the airfoil corresponds to traversing the stretch DA.

As the Mach number increases, the same region of the airfoil corresponds to a greater portion of the lower branch of figure 3, the point A corresponding to $x = 0.178$ and 0.823 remaining at the origin but the point D corresponding to $x = 0.5$ moving away from the origin. For example, the fixed airfoil location $x = 0.5$ corresponds at $M_o = 0.5$ to point D_1, at $M_o = 0.75$ to point D_2, and at $M_o = M_{o,l} = 0.807$ to the turning point B between lower and upper branches in figure 3. Thus, at a certain lowest free-stream Mach number $M_{o,l}$ a point x_l on an airfoil comes into correspondence with the turning point B in figure 3. For higher but still subsonic free-stream Mach numbers, the stretch AB remains fixed at its maximum extent but now corresponds to a diminishing region of airfoil, such that the gap on the airfoil for which no solutions for the velocity are yielded by equation (34) or figure 3 spreads out from x_l as M_c increases in the range $M_{o,l} < M_o < 1$. For example, on the Kaplan section the forbidden region at $M_o = 0.85$ is $0.35 < x < 0.65$. Thus, $M_{o,l}$ is the maximum free-stream Mach number for which continuous potential-flow solutions are obtainable by the present method. Herein $M_{o,l}$ is termed "the potential-limit Mach number," and the corresponding flow pattern, "the potential-limit solution."

Quantitatively, the turning point B corresponds to the condition $d\chi/d\lambda = 0$ in equation (38) or, equivalently, the condition $(d\mu/d\Lambda)_{r,YC_a = \text{const}} = 0$ in equation (34). Hence, at the potential limit (denoted by the subscript l),

$$\lambda_l = \frac{2}{3} \tag{46a}$$

$$\chi_l = \frac{4}{27} \tag{46b}$$

or, by equation (37)

$$\left(\frac{\Gamma_c \Lambda}{\mu}\right)_l = \frac{2}{3}\left(\frac{3-r}{2-r}\right) \tag{47a}$$

$$\left(\frac{\mu^3}{\Gamma_c^2}\right)_l = \frac{27}{4}\frac{(2-r)^3}{(3-r)^2} YC_a \qquad (47b)$$

The procedure for obtaining the potential-limit Mach number for a symmetric airfoil at zero lift is then to plot the right side of equation (47b) as a function of chordwise location x. The potential-limit chordwise location x_l is that where the right side attains a maximum value. This maximum value yields, by equation (47b), a value of μ^3/Γ_c^2 that, by equations (11b) and (11c), determines the potential-limit Mach number $M_{o,l}$. The corresponding velocity increment Λ_l is obtained from equation (47a). The velocity distribution over the rest of the airfoil at Mach number $M_{o,l}$ is determined as usual from equation (34) or (38) using figure 3.

The potential-limit velocity distributions for the Kaplan section by the small- and finite-perturbation integral methods are shown in figure 4. The potential-limit Mach numbers by these two methods are 0.807 and 0.843, respectively. Kaplan (reference 6) estimates from the first three terms of his expansion for the potential that the entire series would diverge beyond $M_o = 0.83$. Göthert and Kawalki (reference 17) also locate a limiting Mach number above which their method does not converge to a self-consistent solution regardless of the number of iterations performed. Although the various determinations of limiting Mach number $M_{o,l}$ and the corresponding velocity increment Λ_l, indicated by the circled points in figure 5, do not agree extremely closely, nevertheless, considering the diversity of the methods used, the inference appears warranted that a unique, upper-limiting, subsonic free-stream Mach number exists beyond which a continuous potential flow past a given airfoil cannot be derived.

Various properties of the potential-limit flow pattern can be derived by the present method, which not only make it easy to understand why this limiting flow pattern should exist but also connect it with the so-called limiting-line phenomenon encountered in the hodograph method. (See, for example, reference 36.) In the first place, at the potential limit the local Mach number M_l at the

chordwise location x_l on the airfoil must be greater than 1, and hence a local supersonic region must exist in the flow field. By equations (27) and (47a),

$$M_l^2 - 1 = \mu_l \left[\frac{4}{3} \frac{\Gamma_M}{\Gamma_c} \left(\frac{3-r}{2-r} \right) - 1 \right] \tag{48}$$

In the permissible range (35) for r, the right side of equation (48) is positive down to at least $M_{o,l} = 0.63$. For the thin airfoils contemplated here, $M_{o,l} > 0.63$ and hence $M_l > 1$, as indicated by the constant local Mach number contours in figure 5.

Secondly, the velocity gradient Λ_x is finite and suffers a finite discontinuity at $x = x_l$ when $M_o = M_{o,l}$. Differentiation (denoted by a subscript) of equation (34) with respect to x yields

$$\Lambda_x \left(\frac{2\mu\Lambda}{2-r} - \frac{3\Gamma_c\Lambda^2}{3-r} \right) = (YC_a)_x - r_x \left[\frac{\mu\Lambda^2}{(2-r)^2} - \frac{\Gamma_c\Lambda^3}{(3-r)^2} \right] \tag{49}$$

The quantity in parentheses on the left side of equation (49) is zero for $M_o = M_{o,l}$, by equation (47a). The right side of equation (49) is zero at $x = x_l$ for $M_o = M_{o,l}$, as can be seen from equation (47a) and from the potential-limit condition that μ^3/Γ_c^2 in equation (47b) be a maximum at $x = x_l$; that is, that its derivative by x is zero at x_l. Thus, $_x$ in equation (49) is given by an indeterminate form at $M_o = M_{o,l}$, $x = x_l$. Application of l'Hospital's rule to this indeterminate form and use of equation (47) yields a quadratic equation for Λ_x. For the usual airfoil shapes, the two roots of this quadratic are real and of opposite sign. (For two-way symmetric airfoils such as in fig. 5, the two roots are numerically equal.) Hence Λ_x undergoes, in general, a finite discontinuity at $x = x_l$ for $M_o = M_{o,l}$ of an amount equal to the difference between these two roots. This discontinuity in velocity gradient is indicated for the Kaplan section in figure 4 at $x = 0.5$ and $M_{o,l} = 0.807$, $M_{o,l} = 0.843$ by the small- and finite-perturbation methods, respectively. If $(YC_a)_{xx} = r_x = r_{xx} = 0$ at $x = x_l$, $M_o = M_{o,l}$, then also $\Lambda_x = 0$ and no discontinuity occurs in Λ_x at the potential-limit point

in this case. The preceding statements for Λ_x also hold for the fluid acceleration on the airfoil inasmuch as the acceleration is given by $(1+\Lambda)\Lambda_x$.

Third, by eliminating y between equations (39) and (43) and differentiating the result by x, an expression for the velocity gradient $(\nu_x)_s$ along a streamline in the flow field is obtained that is a linear function of Λ_x, $(YC_a)_x$, r_x, and $C_{a,x}$, with coefficients dependent on Λ, YC_a, r, and C_a. Furthermore, the slope of a constant velocity, or constant local Mach number, line $(y_x)_M$, multiplied by the local streamline curvature C, equals $(\nu_x)_s$. Hence $(\nu_x)_s$, the local fluid acceleration along a streamline, and $(y_x)_M$ are associated with Λ_x at a given x in being finite or infinite together.

Fourth, the present method yields a second flow pattern at and above the potential limit, which overlaps the first. This pattern is given by the upper branch of the cubic curve, figure 3; for, at the potential limit, the turning point B is just reached from along the lower branch AB upon traversing the airfoil to its potential-limit chordwise location x_l. In retracing the airfoil in the opposite direction, the upper branch BC could be used. For $M_o > M_{o,l}$, instead of a single chordwise location x_l, two chordwise locations $x_{l,1}$ and $x_{l,2}$ correspond to the turning point B, as previously mentioned. Between the two lines $x = x_{l,1}$ and $x = x_{l,2}$ is thus a region of space for which no solution can be found by the present method. Outside this region two overlapping flow patterns are derivable, corresponding to the two branches in figure 3. At the lines $x = x_{l,1}$, $x = x_{l,2}$, the velocity gradient Λ_x is, in general, infinite. (The left factor in equation (49) is zero by equation (47a), but the right side is not zero, because μ^3/Γ_c^2 of equation (47b) is here not a maximum.) These results and those of the preceding paragraph show that the lines $x = x_{l,1}$ and $x = x_{l,2}$, which are potential lines in the present approximation, are envelopes of constant-velocity, or constant Mach number, lines. Furthermore, it is plausible that the lines $x = x_{l,1}$ and $x = x_{l,2}$ are also envelopes of Mach lines or characteristics; a point of infinite velocity gradient in a supersonic region requires a spacing of Mach lines closer by an order of magnitude than does a point of finite velocity gradient, and an envelope of Mach lines satisfies this condition.

The preceding properties indicate that $x = x_{l,1}$ and $x = x_{l,2}$ may be limiting lines in the sense of the hodograph method and that the potential-limit solution is the boundary solution between continuous potential-flow patterns, for $M_o < M_{o,l}$, and flow patterns with limiting lines bounding forbidden regions, for $M_o > M_{o,l}$. This inference is supported by a closer examination of the limiting-line phenomenon as follows:

A limiting line in a flow field is defined as the locus of points at which the Jacobian $J = \partial(\Phi,\Psi)/\partial(v,\theta)$ from the hodograph (v,θ)-plane to the physical (Φ,Ψ)-plane vanishes. (Constant Φ and Ψ define the potential and streamlines, respectively, in the physical plane.) Consider the reciprocal of this Jacobian

$$J^{-1} = \frac{\partial(v,\theta)}{\partial(\Phi,\Psi)} = \frac{\partial v}{\partial \Phi}\frac{\partial \theta}{\partial \Psi} - \frac{\partial v}{\partial \Psi}\frac{\partial \theta}{\partial \Phi} \tag{50}$$

The differential equations of motion in intrinsic form are (reference 35)

$$\frac{\partial \theta}{\partial \Psi} = \frac{(M^2-1)}{\rho v}\frac{\partial v}{\partial \Phi} \tag{51a}$$

$$\frac{\partial \theta}{\partial \Phi} = \frac{\rho}{v}\frac{\partial v}{\partial \Psi} \tag{51b}$$

Substituting equations (51) into equation (50) and noting that $d\Phi \equiv v\,ds$ and $d\Psi \equiv \rho v\,dn$ yields

$$j^{-1} \equiv \rho v^3 J^{-1} = \left(M^2-1\right)\left(\frac{\partial v}{\partial s}\right)^2 - v^2\left(\frac{\partial \theta}{\partial s}\right)^2 \tag{52}$$

where $\partial v/\partial s$ is the velocity gradient along a streamline and $-\partial\theta/\partial s$ is the streamline curvature.

The variation of j^{-1} along the $\tau = 0.1$ biconvex airfoil, determined by equation (52) and the velocity distributions previously calculated, is shown in figure 6 for various values of M_o. Figure 6 shows that the present method yields finite values of j^{-1} in the range $M_o \leq M_{o,l}$. The only discontinuity in behavior occurs at $x = x_l = 0.5$ at which point $j^{-1}(M_o)$ undergoes a finite

discontinuity for $M_o = M_{o,l}$ (because, as previously discussed, $\partial v/\partial s$ undergoes here a finite discontinuity as a function of M_o).

It may be inferred, in general, that $j^{-1} < 0$ everywhere for $M_o \leq M_{o,l}$. For, equation (52) can be solved for $(\partial v/\partial\theta)_s$ as (subscript s denotes values along a streamline)

$$\left(\frac{\partial v}{\partial \theta}\right)_s = \pm\sqrt{\frac{v^2}{M^2-1} + \frac{j^{-1}}{(\partial\theta/\partial s)^2}} \tag{53}$$

For $j^{-1} = 0$, equation (53) yields the Prandtl-Meyer rate of change for $(\partial v/\partial\theta)_s$ in supersonic regions. For $j^{-1} > 0$, equation (53) yields a numerically greater rate. Now, in a local supersonic region embedded in a subsonic flow field, it is known that $(\partial v/\partial\theta)_s$ must be numerically less than the Prandtl-Meyer value (references 37 and 38) because the sonic boundary reflects Mach waves of opposite sign to those incident upon it. Flows having finite fluid accelerations and streamline curvatures and containing local supersonic regions must therefore have a finite $j^{-1} < 0$ everywhere (in subsonic regions $j^{-1} < 0$ by equation (52)). Hence, also $j < 0$ within such flow fields. The preceding discussion may be regarded as an indication of a simple proof of a theorem of Friedrichs (reference 39) to the effect that if a continuous potential-flow solution $v(x,y,M_o)$, $\theta(x,y,M_o)$ varies continuously with M_o and approaches a limit as M_o approaches some limiting value, then this limiting solution itself cannot contain any points at which $j = 0$; that is, a limiting line.

The relatively small region of positive values of j^{-1} indicated in figure 6 for $M_o \lesssim M_{o,l}$ must therefore be regarded as due to, and indicating the extent of, the approximations in the present method. A plot of j^{-1} would appear to be a useful indication for assessing and possibly improving the accuracy of transonic velocity distributions. The finite discontinuity in $j^{-1}(M_o)$ at $x = x_l$ for $M_o = M_{o,l}$ may well exist (in theory). The present method thus illuminates the theorem of Friedrichs.

For $M_o > M_{o,l}$, figure 6 shows that $j^{-1} \to \infty$, hence $j \to 0$ at a point $x_{l,1}(M_o)$ and at the symmetrically disposed point $x_{l,2} = 1 - x_{l,1}$ (because here $\partial v/\partial s \to \infty$, as previously noted).

Thus, formal continuation of the present method to $M_o > M_{o,l}$ yields discontinuous solutions containing forbidden regions $x_{l,1} < x < x_{l,2}$ bounded by limiting lines, as previously inferred.

The reason for the existence of two values of λ for a given χ in figure 3, and hence two overlapping flow patterns, of which one corresponds to either subsonic or slightly supersonic conditions and the other to highly supersonic conditions, is essentially similar to the reason for the existence of two possible velocities for a given flow area in one-dimensional flow, as in a converging-diverging nozzle. Indeed, the present method, which makes use of the equation of continuity in quasi-one-dimensional or hydraulic fashion, shows rather directly that the potential-limit solution occurs for essentially the same reason that a converging-diverging nozzle chokes when a sufficiently high but subsonic Mach number occurs ahead of the throat (reference 29). (The mass-flow density ρv passes through a maximum at a local Mach number of 1.) The manner by which steady-flow patterns can nevertheless exist for the subsonic free-stream Mach numbers between $M_{o,l}$ and unity, in spite of the analog of this choking phenomenon (which prevents higher subsonic Mach numbers from being obtained ahead of the throat in nozzles) is considered in the next section. In particular, it will be seen that the purely mathematical extrapolation made herein leading to the limiting lines $x = x_{l,1}$ and $x = x_{l,2}$, has no physical significance in connection with the shock that actually appears at these Mach numbers.

LOWER TRANSONIC ASYMMETRIC FLOW WITH TERMINAL SHOCK

Velocity distributions. - In this section, asymmetric flow patterns with a single terminal shock will be derived for free-stream Mach numbers from the potential-limit Mach number to unity. The analysis, particularly that connected with the terminal shock, is more uncertain in this range than in the neighboring speed ranges because the terminal shock is no longer at most a boundary of the region of interest, but exists within it.

The procedure for obtaining a symmetric solution at the potential-limit Mach number, derived in the preceding section, indicates how asymmetric solutions may be obtained at higher Mach numbers.

Thus, in determining the airfoil velocity increments at the potential-limit free-stream Mach number as a function of chordwise location, the lower branch of the curve in figure 3 was traversed from A to B, the potential-limit point B being reached, say, at the midchord location for the symmetric biconvex airfoil. In going from midchord toward the trailing edge on the airfoil, the curve was traced back from B to A, giving the symmetric solution. Because the turning point B at midchord has just been attained, however, it is possible to continue around and have part of the upper branch BC correspond to the rear part of the airfoil. The chordwise location $x = x_l$ in the present speed range therefore has the property of a branch point, as previously explained. This property maintains the analogy with conditions at the throat of a converging-diverging nozzle.

The preceding procedure yields an asymmetric solution at the potential-limit Mach number. In order to obtain a solution, and in particular an asymmetric solution, without forbidden regions at higher subsonic Mach numbers, the basic cubic equation (34) must be modified. The modification made herein is to introduce a nonvanishing, lateral streamline displacement δ at infinity (fig. 2). Such a displacement, of the order of the airfoil thickness, is clearly necessary for steady-flow patterns to exist near sonic speed if the free-stream flow is to "get by" the airfoil in accordance with steady-state continuity relations. (That a steady-flow solution is yielded by the equations of motion at precisely sonic speed has been demonstrated by Guderley, references 38, 40 and 41.) The streamline at infinity can still be considered straight and parallel to the x-axis, relative to the airfoil slope, if its lateral displacement δ is assumed to occur gradually over an infinite distance along the streamline. Thus, δ will not be a function of airfoil chordwise location but will be constant for the entire airfoil. It will, however, be a function of free-stream Mach number. The introduction of a nonvanishing, lateral streamline displacement δ in the present speed range $M_o < M_{o,l} < 1$ does not conflict with the proof previously indicated that δ vanishes for subsonic-flow conditions and no wakes at infinity; the simultaneous introduction of a shock terminating an asymmetric local supersonic region implies a shock wake of slightly decreased total head extending to infinity. Such a wake provides a mechanism for producing a nonvanishing displacement δ similar to that provided by an ordinary subsonic wake produced by boundary-layer action.

By subtracting a suitable displacement function $\delta(M_o)$ from Y in the basic cubic equation (34), both branches in figure 3 can now be correlated continuously with the airfoil contour in the speed range $M_{o,l} < M_o < 1$ to yield an asymmetric solution. In order actually to calculate this solution, the variation of the curvature parameter r with x and K, or its equivalent, must first be determined. To this end, the assumption is first made that the potential-limit condition of equation (47), with Y replaced by $Y-\delta$, will apply throughout the speed range $M_{o,l} < M_o < 1$ to the same chordwise location $x = x_l$ first found to require the potential-limit condition. In more geometric terms, if the basic cubic equation (34) is viewed as a surface in the Λ, x, and M_o space, then the potential-limit condition, which has been regarded as determining an absolute maximum of M_o on the projections of this surface in the Λ, M_o plane, can therefore be regarded as determining the saddle point of this surface. Hence, in the Λ, x plane, the potential-limit point is a branch point. Secondly, it is noted that the velocities obtained along the rear portion of the airfoil, corresponding to the upper branch in figure 3, and using the subsonic values of r previously determined, become much greater than those corresponding to a Prandtl-Meyer distribution. As pointed out by Tsien and Fejer in reference 37, however, the velocity in a local supersonic region should be less than that in a Prandtl-Meyer expansion through the same angle of turn, the difference being due to compression waves reflected from the sonic boundary and striking the airfoil. Inasmuch as these compression waves will probably be of small influence compared to the expansion waves emanating from the airfoil for the size and the shape of local supersonic regions to be expected in the present speed range, it will be assumed that the supersonic portion of the velocity distributions to be derived will be Prandtl-Meyer distributions. (It would not be difficult to obtain more accurate velocity distributions in local supersonic regions on the basis of the shape and extent of the supersonic region determined by the first approximation considered herein.) The Prandtl-Meyer velocity-distribution formula can be written in the transonic small-perturbation limiting case as (reference 30)

$$M^2-1 = \bar{\mu} + 2\Gamma\Lambda = 3\Gamma(\theta-\theta_e)^{2/3} \tag{54}$$

where

$$\bar{\mu} \equiv -\mu = M_o^2-1 \tag{55}$$

and $\theta-\theta_e$ is the (positive) angular change, in radians, of slope of airfoil contour from the value θ_e at which the local Mach number is 1 to the value θ at which it is M. Throughout this section and the next, for simplicity in the calculations, all Γ's that arise, such as the Γ_M of equation (28), which should appear in equation (54), are replaced by $\Gamma = 1.2$ unless otherwise mentioned. Hence, the calculations are limiting calculations for $M_o = 1$; that is, the transonic approximation is made more strictly than in the preceding section, where the functions $\Gamma_c(M_o)$ and $\Gamma_M(M_o)$ were used.

By assuming a Prandtl-Meyer distribution, the problem of calculating the supersonic portion of velocity distributions in a given speed range is reduced to determining one point of this distribution (that is, velocity and airfoil location) at each free-stream Mach number M_o in the range, which is necessary to evaluate the constant θ_e in equation (54). This one point will be chosen as the velocity at the potential-limit, or branch-point, location $x = x_l$ in the present speed range. It is convenient to carry out the determination with the basic cubic equation (34), as modified by inclusion of δ, and the potential-limit condition of equation (47) in explicity similarity form, thus:

$$\frac{(Y-\delta)C_a}{\tau^2} = \frac{KL^2}{2-r} - \frac{L^3}{3-r} \tag{56}$$

$$L_l = \frac{2}{3}\left(\frac{K_l}{2-r}\right)(3-r) \tag{57a}$$

$$\frac{(Y-\delta)C_a}{\tau^2} = \frac{4}{27}\left(\frac{K_l}{2-r}\right)^3 (3-r)^2 \tag{57b}$$

where

$$K = \mu/(\tau\Gamma)^{2/3} \tag{58a}$$

$$L = \Gamma\Lambda/(\tau\Gamma)^{2/3} \tag{58b}$$

Explicit calculations will be made for the thin symmetric biconvex airfoil. This airfoil contour is given, for small thickness ratio τ, by

$$\xi \equiv 2x-1 = -\frac{\theta}{2\tau} \tag{59a}$$

$$Y = \frac{\tau}{2}(1-\xi^2) \tag{59b}$$

The left side of equation (56) becomes, by equations (59)

$$\frac{(Y-\delta)C_a}{\tau^2} = 2\left(1 - \frac{2\delta}{\tau} - \xi^2\right) \tag{60}$$

The potential-limit location for the symmetric biconvex airfoil is $x_l = 0.5$ or $\xi_l = 0$. Inasmuch as a unique steady-flow pattern at $M_o = 1$ is assumed, which is continuous with the flow patterns existing on either side of $M_o = 1$, the velocity at $\xi = \xi_l = 0$ in particular must have this property. In the next section, the value $L_l = 2^{1/3}$ is derived for the velocity parameter at $\xi = \xi_l = 0$ at $K = 0$ or $M_o = 1$, by an analysis for $M_o > 1$. In order for equation (57a) to yield this value also, it is necessary that $r \to 2$ as $K \to 0$ and in such a way that

$$\lim_{K \to 0} \frac{K_l}{2-r} = \frac{3}{2^{2/3}} = 1.890 \tag{61}$$

At sonic speed, a nonvanishing streamline displacement at infinity δ is thereby obtained, given by equations (57b), (61), and (60) with $\xi = 0$ as

$$2\delta/\tau = 0.5 \tag{62}$$

This value of δ, half the maximum airfoil ordinate, is of the right order of magnitude inasmuch as at precisely sonic speed a streamline displacement at infinity somewhat greater than the maximum airfoil ordinate is clearly required by steady-state continuity considerations.

The velocity at the potential-limit chordwise location $\xi_l = 0$ can now be obtained as a function of M_o by an interpolation procedure. The value of $K/(2-r)$ at $M_o = M_{o,l} = 0.831$ and $\xi = \xi_l = 0$ is 1.60 from the results of the preceding section. This

value does not differ greatly from that at $M_o = 1$ given by equation (61). Accordingly, a linear variation of $K/(2-r)$ at $\xi = 0$ as a function of K can be assumed in this range that yields $r(K)$ and thence $L_l(K)$ and $\delta(K)$ at $\xi = 0$, by equations (57) and (60). The values $L_l(K)$ at $\xi = 0$ enable Prandtl-Meyer velocity distributions to be determined over the airfoil at each Mach number M_o corresponding to K by equation (54).

As a possible refinement, the velocity distribution over the front portion of the airfoil can be interpolated between the Prandtl-Meyer distribution at $M_o = 1$ and the potential-limit distribution at $M_o = M_{o,l}$ found in the preceding section. The interpolation is made at each chordwise location x between the values of $K/(2-r)$ given by equation (56) using equation (62) and the values of L given by the Prandtl-Meyer distribution at $M_o = 1$, and the values of $K/(2-r)$ at $M_{o,l} = 0.831$ determined in the preceding section. The resulting values of $r(x,K)$ and $\delta(K)$ determined from equation (57b) then yield intermediate velocity distributions by equa-equation (56).

The asymmetric-type velocity distributions determined as just outlined are so far incomplete in two basic respects. First, the subsonic portion from the leading edge to the point where free-stream velocity is first reached locally is lacking. This lack, as explained in the preceding section, is mainly due to the inadequacy of the simple curvature function (equation (33)) in this region. For the purpose of calculating pressure drag in the transonic range, this portion is not needed. (See section PRESSURE DRAG; USE OF MOMENTUM INTEGRAL.) The second and more important omission, the terminal shock, is discussed next.

Terminal shock. - The terminal shock is observed to form the downstream boundary of the local supersonic region and to move toward the trailing edge as the free-stream Mach number increases toward unity. Assume for the present that this shock is normal rather than oblique. This assumption appears valid, at least under the experimental conditions reported in reference 2, in which the measured pressure rises across the shock and outside the region of shock-boundary-layer interaction corresponded fairly closely to those of ideal (that is, Rankine-Hugoniot) normal shocks.

The velocities across an ideal normal shock are related by Prandtl's equation, derivable from the Rankine-Hugoniot relations,

$$v_1 v_2 = a^{*2} \tag{63}$$

where a^* is the speed of sound at sonic speed $M = 1$ in an isentropic flow. In the small-perturbation transonic case, equation (63) becomes, for the shock element near the airfoil (appendix C),

$$\Gamma\Lambda_1 + \Gamma\Lambda_2 = \mu \tag{64}$$

In terms of the local Mach numbers $M_1 \equiv \sqrt{1 + \bar{\mu}_1}$ and $M_2 \equiv \sqrt{1 + \bar{\mu}_2}$ upstream and downstream of the shock, respectively, equation (64) becomes by equations (27) and (28b)

$$\bar{\mu}_1 + \bar{\mu}_2 = 0 \tag{65}$$

Equations (64) and (65) are unsatisfactory for determining terminal-shock locations; because first if no boundary layer is assumed and subsonic values of Λ_2 are determined either by a subsonic rule as in reference 34, or equivalently by the subsonic results of the preceding section, then the chordwise locations at which such subsonic values of Λ_2 will "match" the supersonic values of Λ_1 previously determined to satisfy equation (64) or (65) are within about 20 percent of the chord length of the trailing edge for the symmetric biconvex airfoil. This result would probably not be substantially altered by a more exact calculation of viscosity-free flow patterns with single terminal shock, such as by the relaxation method of, reference 18. Experiment shows, however, (references 3 and 4) that a well-developed shock exists forward of the aforementioned location. On the other hand, if a boundary layer is assumed that, in traversing the shock, separates so completely as to make the pressure downstream of the shock approximately equal to free-stream pressure, then $\Gamma\Lambda_2$ (the velocity outside the boundary layer) drops out of equation (64). The shock locations determined by $\Gamma\Lambda_1 = \mu$, however, move forward instead of rearward as sonic free-stream speed is approached from below. An intermediate situation, in which Λ_2 could be determined from velocity distributions calculated to allow for the presence of a boundary layer that has interacted with the shock, might yield satisfactory terminal-shock locations by equation (64). Such a calculation of Λ_2 has not yet been attempted because of the difficulties of calculating the shock-boundary-layer interaction and its effect on the downstream velocity distribution.

Some understanding of the rearward movement of the terminal shock can be had, however, from a modification of equation (64). Assume that the actual pressure rise across the normal shock differs from the Rankine-Hugoniot, or ideal value, by an amount Δp_s. This difference can be caused inside the region of shock-boundary-layer interaction by friction processes, in which case the actual pressure rise is less than the ideal value. A pressure drop Δp_s can also occur outside the boundary layer, according to references 2, 18, and 19. This drop occurs over a short distance just downstream of the (ideal) normal shock and exists because of the necessity for the flow to make a quick reversal of curvature from the negative value given it by the shock to the positive value required by the airfoil contour. Farther out along the shock, this pressure drop becomes a pressure rise for the same reason (reference 2). In any event, this type of pressure change must physically "join on" continuously with that in the boundary-layer region. In view of the preceding discussion, a shock pressure-drop coefficient c_s, representing the over-all departure of a normal-shock element from Rankine-Hugoniot behavior, can be defined in the small-perturbation transonic case as

$$c_s \equiv \frac{\Delta p_s}{\frac{1}{2}\rho_1 v_1^2} = \frac{(p_2-p_o)_{ideal}}{\frac{1}{2}\rho_o v_o^2} - \frac{(p_2-p_o)_{actual}}{\frac{1}{2}\rho_o v_o^2}$$

$$= -2\Lambda_2 - P_2 \qquad (66)$$

If the element of shock front under consideration is near the airfoil, as is the case here, then P_2 in equation (66) is the pressure coefficient at the airfoil just downstream of the shock and Λ_2 is the Rankine-Hugoniot velocity that would exist just downstream of the shock if c_s were zero. Substitution for Λ_2 from equation (64) yields

$$c_s = 2\left(\Lambda_1 - \frac{\mu}{\Gamma}\right) - P_2 \qquad (67)$$

The additional assumption is now made that the pressure on the downstream side of the shock equals free-stream pressure, or $P_2 = 0$. (In a conversation with the author, von Kármán mentioned having used this condition some years ago.) This condition, in general, requires separation of the boundary layer as it traverses

the shock. If c_s were known as a function of M_1 (and of a suitable Reynolds number at the shock if c_s represents a frictional effect), shock locations could be determined from equation (67) with $P_2 = 0$. In the absence of such knowledge, however, an assumed rearward shock movement can be used to calculate c_s. Thus assume the following boundary conditions on the terminal-shock location: (a) At the potential-limit Mach number $M_{o,l}$, the terminal shock occurs at the potential-limit chordwise location x_l ($x_l = 0.5$ for the biconvex airfoil); and (b) At a free-stream Mach number of unity, the terminal shock is at the trailing edge, $x = 1$.

These boundary conditions are, of course, approximate. The terminal shock appears to be formed by the ever-present random pressure disturbances that are continually propagating through the flow field at locally sonic speed. Some of these disturbances, traveling upstream (reference 1), encounter the locally supersonic region and tend to pile up; that is, the terminal shock appears to form as an envelope of characteristics in the x,y,t space (t is time) rather than as an envelope of characteristics in the x,y plane (limiting line). It may be necessary, however, for the symmetric-type locally supersonic region to reach a finite size before the unsteady disturbances can coalesce to form a steady terminal shock (reference 4). The boundary condition (a) idealizes this process by assuming no shock and a symmetric solution up to the potential-limit Mach number, thence a sudden change-over to an asymmetric solution with steady terminal shock. Presumably, the disturbances that form the terminal shock have a tendency to pile up as far upstream as possible. The terminal shock could hardly form upstream of the potential-limit location, however, because of the "choked" condition at this location. (See preceding section. In this connection compare the experimental data and the semiempirical analysis of reference 24.) As regards boundary condition (b), there are no experimental data on terminal-shock location and structure at Mach number unity. In the supersonic speed range, this shock becomes the oblique shock, which does start close to the trailing edge. The schlieren photographs of Liepmann (reference 3) suggest that the terminal shock will reach the vicinity of the trailing edge at sonic speed but will also be curved in the direction ultimately required in the completely supersonic regime.

Boundary condition (a) and equation (67), with $P_2 = 0$, now yield for the $\tau = 0.1$ biconvex airfoil, at $M_o = M_{o,l} = 0.831$ and $\Lambda_1 = \Lambda_l = 0.389$ (values shown in fig. 5), the shock pressure-drop coefficient $c_s = 0.26$. At $M_o = 1$ and $x = 1$, $\Lambda_1 = 0.47$

(from the following section and fig. 7) giving $c_s = 0.94$. The assumption of a linear variation of Λ_1 with μ between the preceding end values (the extreme values of Λ_1 do not differ greatly) determines, from the velocity distributions previously calculated, the variation of terminal-shock location x_s with Mach number M_o (fig. 8). Typical velocity distributions as thus completed by location of the terminal shock are shown in figure 7. (The velocity increment Λ is related to the pressure coefficient P by $P = -2\Lambda$. By the assumption $P_2 = 0$, Λ is therefore indicated as zero behind the shock. This Λ refers to conditions outside the boundary layer.)

Other shock conditions have been advanced. Tsien and Fejer (reference 37) regard the shock as an oblique shock producing maximum outward deflection of the streamline outside the boundary layer. Theodorsen (reference 42) regards the shock as the oblique shock that produces locally sonic speed on its downstream side. In the small-perturbation transonic case, these shock conditions lead to equations similar in form to equation (64): namely (appendix C),

Maximum deflection: $$\Gamma\Lambda_1/3 + \Gamma\Lambda_2 = 2/3\ \mu \qquad (68)$$

Crocco's point: $$\Gamma\Lambda_1/7 + \Gamma\Lambda_2 = 4/7\ \mu \qquad (69)$$

Sonic point: $$\Gamma\Lambda_2 = 1/2\ \mu \qquad (70)$$

An additional shock condition has been included in equation (69). This condition is the oblique shock for which the streamline curvature on the downstream side is zero (if the oblique shock has finite curvature, reference 43). It is defined by Crocco's point on the shock polar (appendix C).

From the similarity between the preceding equations and equation (64), essentially the same objections as regards ability to predict shock location that have been made to equation (64) can be made to the preceding equations. In addition, as has been mentioned, measurements indicate the terminal shock to be normal under the experimental conditions of reference 2. Making the same modifications, however, in equations (68) and (69) as were made in equation (64), that is, introducing a shock pressure-drop coefficient c_s and assuming $P_2 = 0$, yields, with the same shock boundary conditions as before, practically the same variation of shock location

with Mach number M_o but different ranges of variation of c_s. These conditions are listed in table I. (Equation (70) does not yield a solution for shock location inasmuch as, unlike the previous equations, it does not relate conditions across the shock but specifies only the velocity on its downstream side. Equation (70) therefore depends in an essential way on the knowledge of the velocity distribution downstream of the shock.)

TABLE I

Terminal-shock condition	Shock-pressure-drop coefficient, c_s	
	$M_{o,l} = 0.831$	$M_o = 1$
Normal	0.26	0.94
Maximum deflection	- .09	.31
Crocco's point	- .18	.14
Sonic point	- .26	0

The pressure measurements of reference 2 indicate values of c_s of about 0.1 just outside the boundary layer and of about 0.3 at the surface of the airfoil at an effective free-stream Mach number probably much closer to the potential-limit Mach number than to unity. The surface-pressure and wake survey measurements of reference 44 can be interpreted as indicating values of c_s up to about 0.5 in the boundary-layer region. These estimates of c_s would appear to favor the normal-shock condition (table I), particularly inasmuch as the negative values calculated in table I are probably unrealistic. The actual shock-boundary-layer structure near the airfoil is, of course, considerably more complicated than that of a single straight shock, whether normal or oblique. The introduction of a coefficient such as c_s to represent an over-all departure from ideal single-shock behavior, however, may possibly be useful practically.

The reason for the rearward movement of the terminal shock with increase of Mach number is not necessarily indicated by the preceding correlation between terminal-shock location and pressure-drop coefficient c_s. It would seem more likely that a given terminal-shock location resulting from other, more powerful, dynamical requirements should cause a particular value of c_s to exist, rather than conversely. These other dynamical requirements may be connected with the necessity for the streamline displacement at

infinity $\delta(M_o)$ to increase with Mach number in the present speed range. An increasing δ could be produced by a more extensive and intensive shock-boundary-layer wake, which in turn would require a longer and stronger terminal shock, such as would occur at the higher local Mach numbers farther to the rear of the airfoil.

It need hardly be emphasized that the calculations of this report, particularly those in this section, are of a provisional and exploratory character. At the present stage, not much more has been rigorously demonstrated than that the methods used herein can yield results of the right order of magnitude.

Finally, it is of interest to note that the condition used in this section, that shock back pressure shall equal free-stream pressure, can be regarded as a special case of a more general condition; namely, that the shock back pressure shall be as close as it can get to free-stream pressure. This more general condition is discussed in appendix D.

UPPER TRANSONIC FLOW WITH DETACHED SHOCK

Analysis. - The upper transonic or detached shock regime extends from free-stream Mach number 1 to that supersonic Mach number $M_{o,a}$ at which the shock ahead of the airfoil becomes attached to the leading edge, assumed sharp-edged. In the transonic small-perturbation case, $M_{o,a}$ is given by (reference 30 and appendix C),

$$\frac{M_{o,a}^2-1}{(\theta_L\Gamma)^{2/3}} = \frac{3}{2^{2/3}} = 1.890 \qquad (71)$$

where θ_L is the semivertex angle at the leading edge (fig. 9).

Calculation will now be made of the movement of the head shock (fig. 1) and of the supersonic part of the airfoil velocity distribution as a function of M_o. The terminal shock is assumed to start from the trailing edge (see preceding section) so that it need not be considered in the analysis. As in the preceding section, the supersonic part of the velocity distribution on the airfoil is assumed to be a Prandtl-Meyer distribution given by equation (54). This assumption increases in validity with the Mach number. At a Mach number of 1, the flow pattern derived by Guderley (reference 40) indicates the approximate validity of such an assumption, except in a small region near the beginning of the supersonic

velocity distribution that is relatively more substantially influenced by compression waves from the sonic boundary. The preceding assumption is therefore probably a much better one in the present speed range than in that of the preceding section.

As in the preceding section, by assuming a Prandtl-Meyer distribution the problem of calculating the supersonic part of velocity distributions in the upper transonic range is again reduced to determining one point of this distribution at each free-stream Mach number M_o in the range, which is necessary to evaluate the constant θ_e in equation (54). This calculation is performed along the same lines as in the preceding section. The continuity condition is first set up for the flow across a section AB in the y-direction (fig. 9), where A is a point on the shock, to be specified presently, at a distance y_w from the x-axis and B is the laterally opposite point on the airfoil at the same chordwise location x_w. Thus

$$Y = \int_Y^{y_w} (\rho v - 1)\,dy \tag{72}$$

The irrotationality condition (equation (5)) applies also in the present speed range, inasmuch as fluid rotation introduced by variable entropy increase across a curved shock in the small-perturbation transonic case, being of the order of the third power of the Mach number increment across the shock, is negligible. Substituting equation (5) into equation (72) and making the small-perturbation substitution of equation (10) for the density yields

$$Y = -\int_{\nu_w}^{\Lambda} \frac{\bar{\mu}\nu + \Gamma\nu^2}{C}\,d\nu \tag{73}$$

where ν_w is the velocity increment on the downstream side of the shock at A and Λ is the velocity increment at B.

A streamline-curvature function is now assumed as

$$C = C_a\left(\frac{\nu - \nu_w}{\Lambda - \nu_w}\right)^s \tag{74}$$

where s is a parameter to be determined as a function of x_w and K. Equation (74) satisfies the boundary condition at the airfoil and in addition states that the curvature is zero at point A. It is desirable that the streamline curvature should be zero at point A because if it were not, then the determination of the curvature at point A would greatly complicate the problem. Now a point A exists on a curved shock at which the streamline curvature just downstream of the shock is zero. It is called Crocco's point (references 38, 40, 41, 45, and 46) and is defined by the condition $(\partial v/\partial\theta)_{\text{along streamline}} = \infty$ (appendix C). Instead of choosing point A as Crocco's point, however, it will be chosen as the sonic point, that is, as that point at which the local Mach number just downstream of the shock is unity. The reason for this choice is the following: Because of the additional degree of freedom presented by the position of the shock relative to the airfoil, that is, determination of the distance y_w, one more condition in addition to those already given is necessary to make the problem determinate. If point A is the sonic point, a very simple such condition is obtained, because at the sonic point, $(\partial\theta/\partial v)_{\text{along AB}} = 0$ (appendix C). Hence, to the first order in the change of velocity between A and B (that is, in the small-perturbation case) the stream direction θ_w at A will equal the airfoil inclination θ_a at B. The violation of equation (74), because the curvature will not be zero at A, is probably not serious inasmuch as it is known that the sonic point and the point of maximum streamline deflection are quite close to each other on the shock polar and Crocco's point is between these two points (appendix C). Hence the streamline curvature should be close to zero at the sonic point A in the physical plane. It is noted that choice of a point with a particular property on the head shock to determine the path of integration in equation (72) makes the chordwise location x_w a function of the Mach number parameter K in the analysis. Hence the parameter s in equation (74) becomes a function only of K.

Substitution of equation (74) into equation (73) and integration yields

$$(YC_a)_{\theta_a = \theta_w} = -\left[\frac{(\bar{\mu}\nu_w+\Gamma\nu_w^2)}{(1-s)}(\Lambda-\nu_w)+\frac{(\bar{\mu}+2\Gamma\nu_w)}{(2-s)}(\Lambda-\nu_w)^2+\frac{\Gamma}{(3-s)}(\Lambda-\nu_w)^3\right] \tag{75}$$

in which the aforementioned condition $\theta_a = \theta_w$ is indicated in the subscript on the left side.

The distance y_w of the shock point A from the airfoil point B is obtained by integration of the irrotationality condition (equation (5)) with the curvature function (equation (74)) as

$$y_w - Y \tilde{=} y_w = \frac{\Lambda - \nu_w}{C_a(1-s)} \tag{76}$$

In order to satisfy the condition of zero curvature at $\nu = \nu_w$ by equation (74) and for convergence of the integrals leading to equations (75) and (76), it is necessary to restrict the range of values for the parameter s to

$$0 < s < 1 \tag{77}$$

The distance d of the normal element E of the shock from the leading edge O of the airfoil can be expressed as follows: The angle of inclination σ of the tangent AC to the shock at the sonic point A is given by (appendix C)

$$\cos \sigma = \sqrt{\bar{\mu}/2} \tag{78}$$

This inclination is somewhat steeper than that for a Mach wave, for which $\cos \sigma = \sqrt{\bar{\mu}}$, as is to be expected. The distance $\overline{CD}$ is thus given by

$$\overline{CD} = y_w \cot \sigma \approx y_w \cos \sigma \tag{79}$$

Introducing a factor A to allow for the reduction $\overline{CE}$ due to curvature of the shock between A and E therefore gives, using equation (76),

$$d+x_w = A\sqrt{\bar{\mu}/2}\ y_w = \frac{A\sqrt{\bar{\mu}/2}\ (\Lambda - \nu_w)}{C_a(1-s)} \tag{80}$$

The preceding equations will now be applied to the thin biconvex airfoil. For this contour, conditions at the chordwise location x_w analyzed here are given by equation (59) as

$$x_w = \frac{1}{2}\left(1 - \frac{\theta_w}{2\tau}\right) \tag{81}$$

$$(YC_a)_{\theta_a = \theta_w} = 2\tau^2 - \frac{\theta_w^2}{2} \tag{82}$$

It is convenient to proceed with the equations expressed explicitly in transonic-similarity form. At the sonic point behind a shock (appendix C),

$$\frac{\Gamma v_w}{\bar{\mu}} = -\frac{1}{2} \tag{83a}$$

$$\frac{\Gamma\theta_w}{\bar{\mu}^{3/2}} = \frac{1}{2^{3/2}} \tag{83b}$$

Substituting equation (81) into (80), equation (82) into (75), noting that the second term on the right side in equation (75) vanishes because of equation (83a), and expressing equations (75), (81), and (80) in similarity form with the aid of equations (83a) and (83b) and the definitions

$$K_1 \equiv \bar{\mu}/2(\tau\Gamma)^{2/3} = -K/2 \tag{84}$$

$$L \equiv \Gamma^{1/3}\,\Lambda/\tau^{2/3} \tag{85}$$

yields, respectively,

$$\frac{(YC_a)_{\theta_a = \theta_w}}{\tau^2} = 2 - \frac{K_1^3}{2} = \frac{K_1^2}{1-s}(L_w+K_1) - \frac{(L_w+K_1)^3}{3-s} \tag{86}$$

$$x_w = \frac{1}{2}\left(1 - \frac{1}{2}K_1^{3/2}\right) \tag{87}$$

$$d = \frac{A}{2}\frac{\sqrt{K_1}}{(1-s)}(L_w+K_1) - \frac{1}{2}\left(1 - \frac{1}{2}K_1^{3/2}\right) \tag{88}$$

The parameter s in equation (86) is next determined as a function of K_1. To begin with, as $K_1 \longrightarrow 0$, s must $\longrightarrow 1$, and in such a way

that $K_1^2/(1-s) \longrightarrow$ constant, for if not, then at $K_1 = 0$, $L_w < 0$ (by equation (86)), which is incorrect in view of the direction of curvature of the flow. It will be assumed that the variation of s with K_1 is given, not only near $K_1 = 0$, but throughout the entire upper transonic range $0 < K_1 < 3/2$ by

$$\frac{K_1^2}{1-s} = B \text{ (a constant)} \tag{89}$$

The value of this constant can be determined as follows: Equation (86) is similar in structure to the corresponding subsonic equation (56). It was assumed in the preceding section that equation (56) should comply with the potential-limit condition

$$\left(\frac{\partial K}{\partial L}\right)_x = \frac{1}{\left(\frac{\partial L}{\partial K}\right)_x} = 0 \tag{90}$$

at $x = x_l = 0.5$ throughout the lower transonic range. The subscript x in equation (90) indicates that x is held constant in the differentiation. Now, if a unique continuous solution exists at $M_o = 1$, then equation (86) should become equivalent to equation (56) at $M_o = 1$ and hence should obey the potential-limit condition analogous to equation (90) at $M_o = 1$ or $K_1 = 0$ and $x = 0.5$. An analogous condition to equation (90), rather than the same condition, is necessary because here $x = x_w$ is a function of K_1 and so cannot be held constant in differentiating L. However, inasmuch as

$$\frac{dL_w}{dK_1} = \left(\frac{\partial L}{\partial K_1}\right)_x + \left(\frac{\partial L}{\partial x}\right)_{K_1} \frac{dx_w}{dK_1} \tag{91}$$

and the second term on the right side is finite and, in fact, zero at $K_1 = 0$ by equation (87), it is seen that the analogous potential-limit condition to be applied to equation (86) is

$$\left(\frac{dK_1}{dL_w}\right)_{K_1 = 0} = 0 \tag{92}$$

The chordwise location at which equation (92) is applied is, at $K_1 = 0$, by equation (87), $x_w = 0.5$, which joins on continuously with the branch-point location for the biconvex airfoil in the lower transonic speed range. On an airfoil for which the $\theta_a = 0$ chordwise location differs from the branch-point chordwise location x_l previously derived, interpolation between these two locations as a function of K would be necessary in order to obtain the branch-point locations in the lower transonic asymmetric-flow range. Applying the condition of equation (92) to equation (86) results in, by equation (89),

$$B = \frac{3}{2} L_{w,l}^{2} \tag{93}$$

Inserting this value into equation (86) yields

$$L_{w,l} = \left[\frac{(YC_a)_{\theta_a = 0}}{\tau^2}\right]^{1/3} = 2^{1/3} = 1.260 \tag{94}$$

and, by equation (93),

$$B = \frac{3}{2^{1/3}} = 2.380 \tag{95}$$

The remaining constant A, occurring in equation (88), is evaluated by the boundary condition that the shock distance $d \rightarrow 0$ as $K_1 \rightarrow K_{1,a}$, where $K_{1,a}$ corresponds to the Mach number for attachment of the shock and is given by equations (71), (59), and (84) as $K_{1,a} = 3/2$. With these values for d and K_1 and by equations (89) and (95), equation (88) yields

$$(L_w + 3/2)\, A = 0.126 \tag{96}$$

On the other hand, equations (89), (95), and (86) yield a cubic for $L_w + 3/2$ at $K_1 = 3/2$, with the solution

$$L_w + \frac{3}{2} = 0.1318 \tag{97}$$

Hence

$$A = 0.955 \tag{98}$$

The constant A is of the expected order of magnitude, namely, somewhat less than unity, although perhaps too close to unity to indicate a high degree of quantitative accuracy.

The other boundary condition on shock distance, $d \to \infty$ as $K_1 \to 0$, is already satisfied by equation (88), which gives a limiting variation, using equation (89) and the preceding numerical values,

$$\lim_{K_1 \to 0} d \to \frac{ABL_l}{4K_1^{3/2}} = \frac{0.716}{K_1^{3/2}} \tag{99}$$

The variation of s with K_1, given by equation (89), and the various numerical constants just derived enable such quantities as the longitudinal shock distance d, the lateral shock distance y_w, the chordwise location x_w, and the velocity L_w at chordwise location x_w on the airfoil to be derived as functions of K_1 from equations (76) and (86) to (88). From $L_w(K_1)$, $x_w(K_1)$, which constitute the determination of a known point of the velocity distribution at each K_1, the supersonic part of the velocity distribution on the symmetric biconvex airfoil is obtained by the Prandtl-Meyer formula (54).

The various shock distances calculated as indicated are shown in figure 10. Some velocity distributions are shown in figure 7. The numerical values in figures 7 and 10 are plotted for a biconvex airfoil of = 0.1. These values, however, were actually derived from the similarity parameters calculated by the equations of this section, which yield only limiting values for $\tau = 0$, $M_o = 1$. As an indication of the error involved in applying the results of figures 7 and 10 to biconvex airfoils of finite thickness ratio, figure 10 indicates the Mach number for shock attachment to a $\tau = 0.1$ biconvex airfoil as 1.31; whereas the exact oblique-shock relations show it to be 1.48. Practical application of the results of this section therefore requires further investigation in the direction of the counterpart of the present calculation for τ and $\bar{\mu}$ finitely different from zero. (Calculations by integral methods of detached-shock configurations relative to thick bodies have recently been made by W. E. Moeckel, reference 47.)

Some comparisons with experiment. - Figure 7 has been cross-plotted in figure 11 to show the velocity increments Λ at the

$x = 0.5$ and $x = 0.8$ chordwise locations through the entire transonic speed range. From these velocity increments, local Mach numbers M have been calculated by equation (27), assuming $\Gamma_M = \Gamma = 1.2$ for over-all consistency with the determination of Λ. These Mach numbers are shown as the solid lines in figure 12. The relative constancy of M at $x = 0.5$ in the transonic range may be especially noted. (In the low subsonic and high supersonic ranges, M should approximately equal M_o.) This phenomenon is of particular interest in view of the rather independent derivations of the maximum local Mach number at the potential-limit Mach number $M_{o,l}$ and at sonic speed $M_o = 1$. The potential-limit derivation depended on the incompressible velocity distribution for the parameter r; whereas the sonic-speed derivation depended on a property at the sonic point of the shock polar $(\partial\theta/\partial\nu)_y = 0$. The relatively constant value of M at $x = 0.5$ throughout the transonic speed range is plausible from the expected tendency of the flow to maintain a maximum average value of $\rho v \sim 1$ along the line $x = x_l$, when both subsonic and supersonic velocities occur along this line.

The discontinuities in the theoretical curves for $x = 0.8$ at $M_o = 0.83$ and at $M_o = 0.94$ correspond to the assumed sudden appearance of the terminal shock at the potential-limit Mach number (and the condition $P_2 = 0$) and to the shock passing through the $x = 0.8$ location, respectively, (fig. 8).

Pressure distributions in the lower transonic range on 6- and 12-percent thick symmetric biconvex airfoils of 3-inch chord spanning a two-dimensional tunnel 20 inches high and 2 inches wide were measured in references 3 and 4. The Reynolds number based on airfoil chord was of the order of one million. The results were not corrected for tunnel-wall effect. Terminal-shock locations plotted in figure 8 were estimated herein from the given pressure distributions and schlieren photographs. The local Mach numbers given in reference 4 were presumably obtained by applying the finite-perturbation formulas (equations (6) and (26)) to the pressure differences actually measured. Accordingly, these formulas were used in obtaining velocity increments and local Mach numbers from the experimental results given. All velocity increments Λ, local Mach numbers M, and free-stream Mach numbers M_o were reduced from $\tau = 0.06, 0.12$ to $\tau = 0.10$ by the transonic similarity rules of equations (24), (25), and (31). The experimental results as thus reduced are shown in figures 8, 11, and 12.

Several points uncorrected by the transonic similarity rules are included in figures 11 and 12. It is seen that these rules do substantially correlate the different thickness-ratio results. The residual discrepancy in the results for $x = 0.5$ after correlation may be due to the finite difference between M_o and 1, to the finite-perturbation velocities involved, to differential tunnel-wall effects, or to differential Reynolds number effects. Also included in figures 11 and 12 are several points similarly reduced from the tests described in **reference 48**. These tests were made on a 6-percent thick, 4-inch chord symmetric biconvex airfoil in a two-dimensional tunnel 18 inches high and 4 inches wide. Reynolds number was of the order of one million. The discrepancy between the highest speed points of **reference 48** and the lowest speed points of references 3 and 4 is possibly due to larger tunnel-wall effects and the somewhat higher Reynolds number in the tests of **reference 48**.

Agreement of the present theory with the experimental results is considered to be good at least qualitatively. The theoretical calculations are, as previously noted, limiting calculations for $\tau = 0$ and $M_o = 1$. As an indication of the necessity of allowing for finite departures from at least the transonic limit $M_o = 1$ in order to attain closer agreement with experiment, several alternative theoretical local Mach number curves are included in figure 12. In one, the function $\Gamma_M(M_o)$ of equation (28a) was used in equation (27) to obtain local Mach numbers from the theoretical velocity increments of figure 11. In the other, the exact equation (26) was used. It is seen that the differences between these alternative curves is of the same order as the difference between theory and experiment. The experimental local Mach numbers appear, nevertheless, to be definitely lower and higher than the theoretical values at $x = 0.5$ and $x = 0.8$, respectively. It remains to be seen whether experiments at higher Reynolds number would not better the agreement with the (essentially infinite Reynolds number) theory. The changes with increase of Reynolds number may be expected to be in the direction for better agreement.

PRESSURE DRAG; USE OF MOMENTUM INTEGRAL

The flow patterns obtained in the preceding sections, together with the momentum equation in integral form, yield an estimate of the pressure drag of the symmetric biconvex airfoil in the transonic speed range. The pressure drag of an airfoil is defined as that portion of the total drag that can be obtained by an integration around the airfoil of the component in the free-stream (x-) direction of the normal force or pressure on the airfoil. The remaining

portion of the total airfoil drag, the skin friction, due to the tangential forces on the airfoil surface produced by viscous action in the boundary layer, will not be considered here. The skin friction, for example, on a 10-percent thick airfoil, is known to be small relative to the pressure drag in the transonic range.

In the range of continuous potential flow, that is, from Mach number zero to the potential-limit Mach number $M_{o,l}$, the pressure drag is zero, corresponding to the fact that the completely subsonic potential-flow field bounding the airfoil provides no mechanism for transporting x-direction momentum away from the airfoil. In the range of transonic flow with shock, however, the shock structure provides such a mechanism, both in the direct shock wake of decreased total head and in the additional wake due to boundary-layer thickening in traversing the terminal shock. In this range, a nonvanishing pressure drag is therefore obtained that could be directly calculated by integration over the airfoil of the x-component of the pressure. This direct integration can be carried out here over the rearward part of the symmetric biconvex airfoil for which velocity distributions have been previously derived. The contribution of the remaining forward part of the airfoil to the pressure drag can be obtained from knowledge of the conditions in the flow field by use of the momentum integral.

Integration of the x-component of the pressure between two chordwise locations x_a and x_b yields for the pressure-drag coefficient $c_{d,r}$ of this part of airfoil (upper and lower surface)

$$c_{d,r} \equiv \frac{D}{\frac{1}{2}\rho_o V_o^2 c} = 2\int_{x_a}^{x_b} P \tan\theta_a \, dx = -4\int_{x_a}^{x_b} \Lambda\theta_a dx \qquad (100)$$

in the small-perturbation case. For the symmetric biconvex airfoil equation (100) becomes, by equation (59a),

$$c_{d,r} = 4\tau\int_{\xi_a}^{\xi_b} \Lambda\xi d\xi \qquad (101)$$

Substituting the transonic small-perturbation limiting form (54) of the Prandtl-Meyer velocity distribution into equation (101) yields

$$c_{d,r} = \frac{\tau^{5/3}}{\Gamma^{1/3}}\left\{K(\xi_b^2 - \xi_a^2) + \frac{3}{2}\left(\frac{9}{2}\right)^{1/3}\left[(\xi_b - \xi_e)^{5/3}\left(\xi_b + \frac{3}{5}\xi_e\right) - (\xi_a - \xi_e)^{5/3}\left(\xi_a + \frac{3}{5}\xi_e\right)\right]\right\} \tag{102}$$

In the lower transonic range, equation (102) was used to calculate the pressure drag of the biconvex airfoil $\tau = 0.1$ from the midpoint $\xi_a = 0$ to the terminal-shock location $\xi_b = \xi_1$. The pressure drag from $\xi = \xi_1$ to the trailing edge $\xi = 1$ is zero, by the assumption made in the section LOWER TRANSONIC ASYMMETRIC FLOW WITH TERMINAL SHOCK that free-stream static pressure exists on the airfoil downstream of the terminal shock. In the upper transonic range, equation (102) was used to calculate the pressure drag of the biconvex airfoil from the chordwise location equal to that of the sonic point of the detached shock $\xi_a = \xi_w$ to the trailing edge $\xi_b = 1$.

The pressure-drag contribution of the remaining forward parts of the biconvex airfoil in these ranges was determined by the momentum integral. Thus, the net decrease of flux of x-momentum out of the region ABDE, (fig. 2)(momentum flux is here defined as static pressure plus flux of kinetic momentum) gives the pressure drag on the portion of the airfoil from the leading edge 0 to point A. As shown in detail in appendix B, the resulting expressions for the pressure drag on the biconvex profile are as follows:

(a) Lower transonic range; leading edge, $\xi = -1$, to midpoint $\xi = 0$

$$c_{d,f} = \frac{\tau^{5/3}}{\Gamma^{1/3}} L^3\left[-\frac{K}{2(3-r)} + \frac{2}{3}\frac{L}{(4-r)}\right] \tag{103}$$

(b) Upper transonic range; leading edge, $\xi = -1$, to $\xi = \xi_w$, $L = L_w$

$$c_{d,f} = \frac{\tau^{5/3}}{\Gamma^{1/3}}(L_w + K_1)\left[\frac{2}{3}\frac{(L_w + K_1)^3}{(4-s)} - \frac{K_1(L_w + K_1)^2}{(3-s)} + \frac{5}{6}\frac{K_1^3}{(1-s)}\right] \tag{104}$$

The resulting pressure drag on the symmetric biconvex airfoil is

$$c_d = c_{d,f} + c_{d,r} \tag{105}$$

and is shown in figure 13 as a function of free-stream Mach number. The finite value of $c_d = 0.015$ at the potential-limit Mach number $M_o = 0.83$ results from placing the terminal shock at the potential-limit chordwise location at this Mach number (see preceding section). As the terminal shock moves toward the trailing edge, the drag rapidly rises to a maximum value of $c_d = 0.098$ at sonic speed $M_o = 1$. There are several points of interest about this value. First, it is of the same order of magnitude as that derived by Guderley (reference 40) by an entirely different (hodograph) method for a somewhat differently shaped 10-percent-thick airfoil. Second, the value of $c_{d,f} = 0.017$ given at $M_o = 1$ by the lower transonic formula (equation (103)) was slightly different from the value 0.011 obtained at $M_o = 1$ from the upper transonic formula (104). This slight difference is due to r approaching a different value, 2, from $s(\longrightarrow 1)$ as $M_o \longrightarrow 1$. Inasmuch as this difference in $c_{d,f}$ is not great, and in view of the considerable differences in procedure on the two sides of sonic speed, the small difference in $c_{d,f}$ is to be regarded not as a defect but rather as indicating the consistency of the present approach. The occurrence of a drag maximum at $M_o = 1$ rather than somewhere in the vicinity is probably due to the approximations involved in the present calculation, especially that which assumes that the terminal shock starts at the trailing edge.

As the free-stream Mach number increases from sonic speed, the drag coefficient decreases because of the decreasing over-all pressure level. As the shock attaches and the field of flow becomes completely supersonic, the drag finally approaches the Ackeret rate of variation with Mach number, $1/\sqrt{M_o^2-1}$. Several drag coefficients have been calculated in the completely supersonic range by using the exact Prandtl-Meyer pressure distribution with initial conditions at the leading edge given by the exact oblique-shock relations of reference 49. The difference between the first such point, $c_d = 0.051$ at $M_o = 1.50$, at which sonic speed occurs behind the attached shock at the leading edge, and the point $c_d = 0.065$ at $M_o = 1.31$ by the present method, indicates again the approximation introduced into the

present results primarily by the transonic approximation $\bar{\mu} << 1$ (that is, setting all the Γ values equal to 1.2) and, probably to a lesser extent, by the small-perturbation approximation $\Lambda << 1$.

CONCLUDING REMARKS

The small-perturbation form of an integral method has been used, with the aid of simplifying assumptions indicated by experiment or other theory, to calculate approximate flow patterns for a symmetric biconvex airfoil through the transonic speed range. The wholly subsonic symmetric flow field develops symmetric continuous locally supersonic regions when the subsonic free-stream Mach number exceeds a definite (lower critical) value. Above an equally definite (potential limit) free-stream Mach number, no continuous symmetric solution exists by the present method. Above the potential-limit Mach number, the method yields both a physically unreal symmetric solution containing forbidden regions bounded by limiting lines and a physically real asymmetric solution containing an asymmetric locally supersonic region. Termination of this locally supersonic region on the downstream side by a shock required additional hypotheses concerning the shock. These hypotheses were quite unrelated to the limiting-line phenomenon. It was found possible to join the asymmetric solution continuously to the asymmetric solution that exists for slightly supersonic free-stream Mach numbers. The main results of the method, such as the variation of pressure drag with Mach number, relative constancy of local Mach number ahead of the terminal shock in the transonic range, and so forth, agree qualitatively with experimental data. More extensive experimental data are needed in the form of pressure distributions, wake surveys, and terminal-shock surveys on airfoils of simple shape under isolated airfoil conditions at high Reynolds numbers. The present method is probably simple and flexible enough to enable suitable alterations and extensions to be made, whether for more rigorous solutions of the cases treated, or to more general situations, such as airfoils with lift, bodies of revolution, and so forth.

National Advisory Committee for Aeronautics,
Lewis Flight Propulsion Laboratory,
Cleveland, Ohio, December 19, 1949.

APPENDIX A

SMALL-PERTURBATION APPROXIMATION OF CONTINUITY INTEGRAL

The exact form of the equation of continuity, equation (1), can be written as follows (see fig. 14):

$$\int_{0}^{y_0} dy_0 = \int_{Y}^{y_0+\delta} \rho v \cos \theta \, dy \tag{A1}$$

where δ is a possible lateral displacement of a streamline far from the airfoil. Subtracting y_0-Y from both sides of equation (A1), as in the section COMPRESSIBLE POTENTIAL FLOW, and proceeding to the limit $y_0 \longrightarrow \infty$ yields

$$Y-\delta = \int_{Y}^{\infty} (\rho v \cos \theta - 1) dy \tag{A2}$$

An expression for dy in terms of v and θ is next derived starting from the differential equations of motion in intrinsic form. These equations are (reference 35)

$$\frac{\partial v}{\partial n} = -Cv \tag{A3}$$

$$-\frac{C}{v}(M^2-1)\left(\frac{\partial v}{\partial \theta}\right)_s = \frac{\partial \theta}{\partial n} \tag{A4}$$

where

$$C = -\left(\frac{\partial \theta}{\partial s}\right)_s \tag{A5}$$

and the subscript s denotes values taken along a streamline.

Consider the variation of velocity v and stream direction θ along a line making an angle α_o with the free-stream direction (fig. 14). If z denotes distance measured along this line, then, using equations (A3) to (A5),

$$\frac{\partial v}{\partial z} = \left(\frac{\partial v}{\partial \theta}\right)_s \left(\frac{\partial \theta}{\partial s}\right)_s \frac{\partial s}{\partial z} + \frac{\partial v}{\partial n}\frac{\partial n}{\partial z}$$

$$= -\left(\frac{\partial v}{\partial \theta}\right)_s C \cos(\alpha_o-\theta) - Cv \sin(\alpha_o-\theta)$$

$$= -Cv \sin(\alpha_o-\theta)\left[\frac{1}{v}\left(\frac{\partial v}{\partial \theta}\right)_s \cot(\alpha_o-\theta) + 1\right] \qquad \text{(A6)}$$

$$\frac{\partial \theta}{\partial z} = \left(\frac{\partial \theta}{\partial s}\right)_s \frac{\partial s}{\partial z} + \frac{\partial \theta}{\partial n}\frac{\partial n}{\partial z}$$

$$= -C \cos(\alpha_o-\theta) - C\,\frac{(M^2-1)}{v}\left(\frac{\partial v}{\partial \theta}\right)_s \sin(\alpha_o-\theta)$$

$$= -C \sin(\alpha_o-\theta)\left[\cot(\alpha_o-\theta) + \frac{(M^2-1)}{v}\left(\frac{\partial v}{\partial \theta}\right)_s\right] \qquad \text{(A7)}$$

Equations (A6) and (A7) yield, respectively, for variations along z,

$$dz \sin(\alpha_o-\theta) = -\frac{dv}{C\left[v + \left(\frac{\partial v}{\partial \theta}\right)_s \cot(\alpha_o-\theta)\right]} \qquad \text{(A8)}$$

$$dz \sin(\alpha_o-\theta) = -\frac{d\theta}{C\left[\cot(\alpha_o-\theta) + \frac{(M^2-1)}{v}\left(\frac{\partial v}{\partial \theta}\right)_s\right]} \qquad \text{(A9)}$$

If the angle α_o is now taken as $\pi/2$, the line element dz becomes dy, and equations (A8) and (A9) become

$$dy \cos \theta = - \frac{dv}{C\left[v + \tan \theta \left(\frac{\partial v}{\partial \theta}\right)_s\right]} \tag{A10}$$

$$dy \cos \theta = - \frac{d\theta}{C\left[\tan \theta + \frac{(M^2-1)}{v}\left(\frac{\partial v}{\partial \theta}\right)_s\right]} \tag{A11}$$

Substituting equation (A10), the definition $v = 1+\nu$, the small-perturbation expressions $\cos \theta = 1 - \theta^2/2$, $\tan \theta = \theta$, and the expansion equation (10) of ρ in powers of ν into equation (A2) yields

$$Y-\delta = \int_Y^\infty \left[\mu\nu - \Gamma_c \nu^2 - \frac{\theta^2}{2} - \mu\nu\, \theta\nu_{\theta s}\right] \frac{d\nu}{C} \tag{A12}$$

in which

$$\Gamma_c = 1 + \frac{M_o^2}{2} - \frac{2-\gamma}{2} M_o^4 \tag{A13}$$

$$\nu_{\theta s} \equiv \left(\frac{\partial \nu}{\partial \theta}\right)_s \tag{A14}$$

The next higher order terms in the bracket of equation (A12) would be of order ν^3, $\nu\theta^2$, $\mu\nu^2\theta\nu_{\theta s}$. The order of magnitude of $\theta\nu_{\theta s}$ is ν. If equation (A12) is consistent with the transonic similarity rules, then $\theta^2 \sim \mu\nu^2$. The two terms involving θ in equation (A12) therefore can at most only affect the function $\Gamma_c(M_o)$ but not its limiting value $\Gamma_c(1) = \Gamma = (\gamma+1)/2$. Thus the small-perturbation equation (4) of the continuity integral is correct to the order ν in the subsonic range $\mu \sim 1$ and to the order ν^2 with $\Gamma_c = \Gamma$ in the transonic range $\mu \ll 1$. The small-perturbation form of the irrotationality condition (equation (5)) is seen from equation (A10) to be correct to the first order in ν and θ.

In the important special case where the airfoil has fore-and-aft symmetry, equations (4) and (5) hold exactly at the midchord location, for here, by symmetry, $\theta = 0$ in equations (A1) and (A10).

In the neighborhood of such a location and, more generally, in the neighborhood of any $\theta = 0$ location on an airfoil, it may therefore be expected that the essential small-perturbation approximations are those involving the velocity increment ν, as in equation (10) rather than those involving the flow direction θ. This expectation is the justification for the use of Γ_c rather than Γ in the continuous-potential-flow calculations of this paper.

APPENDIX B

SMALL-PERTURBATION APPROXIMATION OF MOMENTUM INTEGRAL

The momentum principle in integral form states that the vector rate of flow of momentum out of a fixed volume of space equals the vector-integrated pressure on the bounding surface of the volume. Applying this principle to the two-dimensional region ABDE (fig. 14) gives, for components in the x-direction,

$$\underset{ED}{\int_0^{y_o}} (p_o+\rho_o v_o^2)dy + \underset{DB}{\int_{y_o}^{y_o+\delta}} p_o dy = \underset{AB}{\int_Y^{y_o+\delta}} (p+\rho v^2 \cos^2\theta)dy + \underset{EOA}{\int_o^Y} p_a dy \tag{B1}$$

in which the paths of integration are indicated under the respective integral signs. Rearranging the terms of equation (B1) as with the continuity equation (A1), proceeding to the limit $y_o \longrightarrow \infty$, denoting by p, ρ, and v fractions of the respective free-stream quantities, and noting that $\rho_o v_o^2/p_o = \gamma M_o^2$ results in

$$Y-\delta = \int_o^Y \frac{p_a-1}{\gamma M_o^2}\,dY + \int_Y^{y_o} \left[\frac{p-1}{\gamma M_o^2} + (\rho v^2 \cos^2\theta - 1)\right]dy \tag{B2}$$

Subtraction of the continuity equation (A2) then yields for the pressure-drag coefficient $c_{d,f}$ on the airfoil from the leading edge to the point A (including a factor 2 for both surfaces of the symmetric airfoil),

$$c_{d,f} = \frac{4}{\gamma M_o^2}\int_o^Y (p_a-1)dy = -4\int_Y^{\infty} \left[\frac{p-1}{\gamma M_o^2} + \rho v \cos\theta(v\cos\theta - 1)\right]dy \tag{B3}$$

Substituting the definition $v = 1+\nu$, the expansion $\cos\theta = 1 - \theta^2/2 + \ldots$, the expansions for p and ρ as power series in ν obtained from equation (6), and the irrotationality expression (A10) into equation (B3) yields

$$c_{d,f} = 4\int_0^{\Lambda}\left[-\frac{\mu}{2}\nu^2 + \frac{2}{3}\Gamma_m\nu^3 + \frac{\theta^2}{2} + \frac{\mu}{2}\nu^2\theta v_{\theta s}\right]\frac{d\nu}{C} \qquad (B4)$$

where

$$\Gamma_m = \frac{3}{2}\left(\frac{1+M_o^2}{2} - \frac{2-\gamma}{3}M_o^4\right) \qquad (B5)$$

and $v_{\theta s}$ is defined in equation (A14). Equation (B4) shows why the momentum integral equation (B2)(or rather the derivative of equation (B2) with respect to Y) is inconvenient to use along with equation (4) in solving the velocity-distribution problem. The flow-direction term $\theta^2/2$ in equation (B4) is of the same order of magnitude as the velocity term $-(\mu/2)\nu^2$ and so cannot be neglected in the small-perturbation case, as was the same term in the continuity integral equation (A12). The other θ term in equation (B4) is of order $\mu\nu^3$ and, as in the continuity integral, at worst merely modifies the function $\Gamma_m(M_o)$ but not its limiting value at sonic speed $\Gamma_m(1) = \Gamma = (1+\gamma)/2$. Thus, in this paper, of the three first integrals of the differential equations of motion - that is, conservation of energy, mass, and momentum - the first two (the first as Bernoulli's equation) were used in calculating the basic flow pattern, and the x-component of the third integral, on the basis of the calculated flow pattern, was used to determine a portion of the pressure drag. The lift and the moment of the forces acting on different portions of the airfoil could similarly be calculated from conditions in the flow field by the y-component momentum integral and the angular momentum integral, respectively.

For the calculation of the pressure drag on the forward portion of the biconvex airfoil in the lower transonic range, the forward portion extended to midchord. Hence the two terms involving θ in equation (B4) were considered as vanishing to a sufficient approximation. The resulting integration of equation (B4) using the curvature function (equation (33)) then yields equation (103). In the upper transonic range, the forward portion of the airfoil

extended to the $\theta = \theta_w$ location and θ was held constant at this value in the integration of equation (B4). The term involving $\nu_{\theta s}$ in equation (B4) vanishes in the limiting case $M_o = 1$ or $\Gamma_m = \Gamma$, for which the calculations in this range were made. Integration of equation (B4), using the curvature function and other relations pertaining to the upper transonic range (see section UPPER TRANSONIC FLOW WITH DETACHED SHOCK) leads to equation (104).

APPENDIX C

TRANSONIC SMALL-PERTURBATION APPROXIMATION OF OBLIQUE-SHOCK RELATIONS

An element of oblique-shock front, inclined at an angle σ to a free-stream flow at Mach number M_o (fig. 9) produces a flow deflection θ given by (reference 49)

$$\left(\frac{\gamma-1}{\gamma+1}\right)\left[\frac{4}{(\gamma-1)M_o^2}+1-\cos 2\sigma\right]=\sin 2\sigma \tan(\sigma-\theta) \tag{C1}$$

The corresponding velocity ratio v just downstream of the element is

$$v=\frac{\cos\sigma}{\cos(\sigma-\theta)} \tag{C2}$$

Elimination of σ between equations (C1) and (C2) yields the equation of the shock polar. A relation between the slope $(\partial v/\partial\theta)_{sh}$ of the tangent to the shock polar, that is, the rate of change of velocity ratio with respect to stream direction along the downstream side of the shock and the similar rate of change along a streamline $(\partial v/\partial\theta)_s$ at the same downstream point of the shock, is obtained by dividing equation (B8) by equation (A9) and replacing α_o by σ; thus,

$$\left(\frac{\partial v}{\partial\theta}\right)_{sh}=\frac{v+\left(\frac{\partial v}{\partial\theta}\right)_s\cot(\sigma-\theta)}{\cot(\sigma-\theta)+\frac{(M^2-1)}{v}\left(\frac{\partial v}{\partial\theta}\right)_s} \tag{C3}$$

A similar relation for the rate of change of velocity with stream direction in the y-direction at a point on the downstream side of the shock element is given by setting $\sigma=\pi/2$ in (C3),

$$\left(\frac{\partial v}{\partial\theta}\right)_y=\frac{v+\tan\theta\left(\frac{\partial v}{\partial\theta}\right)_s}{\tan\theta+\frac{(M^2-1)}{v}\left(\frac{\partial v}{\partial\theta}\right)_s} \tag{C4}$$

For small perturbations $v - 1 = \upsilon \ll 1$, equations (C1) and (C2) become

$$\Gamma\upsilon = -\Gamma\theta \tan\sigma = -\frac{\bar{\mu}}{M_o^2} + \cos^2\sigma \tag{C5}$$

Also, making the transonic approximation $\cos\sigma \sim \sqrt{M_o^2 - 1} = \sqrt{\bar{\mu}} \ll 1$ and using equation (27) with $\Gamma_M = \Gamma$ yields, in place of equations (C5), (C4), and (C3),

$$\Gamma\theta = \bar{\mu}\cos\sigma - \cos^3\sigma \tag{C6}$$

$$\Gamma\upsilon = -\Gamma\theta/\cos\sigma = -\bar{\mu} + \cos^2\sigma \tag{C7}$$

$$\left(\frac{\partial\upsilon}{\partial\theta}\right)_{sh} = \frac{1 + \cos\sigma\,(\partial\upsilon/\partial\theta)_s}{\cos\sigma + (\bar{\mu}+2\Gamma\upsilon)(\partial\upsilon/\partial\theta)_s} \tag{C8}$$

$$\left(\frac{\partial\theta}{\partial\upsilon}\right)_y = (\bar{\mu}+2\Gamma\upsilon)\left(\frac{\partial\upsilon}{\partial\theta}\right)_s \tag{C9}$$

Equation (C7) can be differentiated to yield

$$\Gamma\left(\frac{\partial\upsilon}{\partial\sigma}\right)_{sh} = -2\cos\sigma \tag{C10}$$

$$\left(\frac{\partial\upsilon}{\partial\theta}\right)_{sh} = \frac{2\cos\sigma}{\bar{\mu} - 3\cos^2\sigma} \tag{C11}$$

Equations (C8), (C9), and (C10) combine to give

$$\left(\frac{\partial\upsilon}{\partial\theta}\right)_s = -\frac{(5\cos^2\sigma - \bar{\mu})}{\cos\sigma\,(7\cos^2\sigma - 3\bar{\mu})} \tag{C12}$$

$$\left(\frac{\partial\theta}{\partial\upsilon}\right)_y = -\frac{(2\cos^2\sigma - \bar{\mu})(5\cos^2\sigma - \bar{\mu})}{\cos\sigma\,(7\cos^2\sigma - 3\bar{\mu})} \tag{C13}$$

The ratio of the local curvature $C_{sh} = -(\partial\sigma/\partial z)_{sh}$ of a shock front to the curvature of the streamline just downstream of the shock element is obtained by dividing equation (A8) by $(d\sigma)_{sh}$, setting $\alpha_o = \sigma$, and going to the transonic small-perturbation limit. Thus,

$$\frac{C_{sh}}{C} = \frac{\Gamma(-\bar{\mu} + \cos^2\sigma)}{\cos\sigma\,(3\bar{\mu} - 7\cos^2\sigma)} \tag{C14}$$

The conditions at various points on the shock polar in the small-perturbation transonic range can now be determined by the preceding equations. Crocco's point, for example, is defined by $(\partial\upsilon/\partial\theta)_s = \infty$. Equations (C12) and (C14) show that this condition implies zero streamline curvature if the shock front itself has finite curvature, which is usually the case for a detached shock wave. Crocco's condition yields, by equation (C12),

$$\cos^2\sigma = 3/7\,\bar{\mu} \tag{C15}$$

for the inclination of the shock front in the physical plane at Crocco's point. Using equation (C15), the various flow quantities υ, θ, and the local Mach number M just downstream of the shock element can be determined from equations (C6), (C7), and (27) with $\Gamma_M = \Gamma$.

The derivative $(\partial\theta/\partial\upsilon)_y$ (equation (C13)) is infinite at Crocco's point, zero at the sonic point (defined by $M = 1$), and zero also at a subsonic point of the shock polar defined by $\cos^2\sigma = 1/5\,\bar{\mu}$. At this last point, the downstream streamline starts out at constant pressure, inasmuch as here $(\partial\upsilon/\partial\theta)_s = 0$ by equation (C12).

The properties of various points on the shock polar in the small-perturbation transonic limit, determined in the manner indicated, are listed in similarity form in table II. Equations (64) and (68) to (70) are obtained from the values of $\Gamma\upsilon/\bar{\mu}$ given in the table. The velocity increment υ in the table is $(v_2/v_1) - 1$, and hence equals $\Lambda_1 - \Lambda_2$ in the section LOWER TRANSONIC ASYMMETRIC FLOW WITH TERMINAL SHOCK. Similarly, $\bar{\mu}$ in table I is $-\mu + 2\Gamma\Lambda_1$ in the same section.

Further discussion of the shock polar in the transonic small-perturbation limit is given by Guderley (reference 38), who shows, in particular, that from Crocco's point to the point of maximum

deflection on the shock polar, the oblique shock in the physical plane is attached to the vertex of a wedge with curved sides and has infinite curvature at the vertex ($C_{sh}/C = \infty$); reference 38 also shows that the point of maximum deflection on the shock polar corresponds to the point of shock detachment from the vertex, which had been doubted by Crocco (reference 46) and more recently by Thomas (reference 50).

TABLE II

	Definition	$\frac{1}{\sqrt{\mu}}\left(\frac{\partial\theta}{\partial\upsilon}\right)_y$	$\frac{\cos^2\sigma}{\mu}$	$\frac{\cos\sigma}{\sqrt{\mu}}$	$\frac{\Gamma\upsilon}{\mu}$	$\frac{\Gamma\theta}{\mu^{3/2}}$	$\frac{\Gamma^{1/3}\upsilon}{\theta^{2/3}}$	$\frac{M^2-1}{\mu}$
Mach wave	$\nu = 0$	-1	1	1	0	0	0	1
Sonic point	$M = 1$	0	1/2	0.707	-0.500	0.354	-1	0
Crocco's point	$\left(\frac{\partial\theta}{\partial\upsilon}\right)_s = 0$	∞	3/7	0.655	-0.571	0.374	-1.1	-0.143
Maximum deflection	$\left(\frac{\partial\theta}{\partial\upsilon}\right)_{sh} = 0$	$-1/\sqrt{3}$	1/3	0.577	-0.667	0.385	-1.260	-0.300
Constant pressure	$\left(\frac{\partial\upsilon}{\partial\theta}\right)_s = 0$	0	1/5	0.447	-0.800	0.358	-1.587	-0.600
Normal shock	$\theta = 0$	∞	0	0	-1	0	∞	-1

APPENDIX D

TERMINAL-SHOCK CONDITION IN LOWER TRANSONIC RANGE

The condition that for finite perturbation of the flow the terminal shock in the lower transonic range be such that its back pressure is as close as it can get to free-stream pressure may be regarded as a rough statement, for a specific purpose, of the theorem that the equations of motion can be derived from the variational principle

$$\delta \iint (p_o - p)\, dx\, dy = 0 \qquad (D1)$$

where p is local pressure at a point (x,y) and p_o is the free-stream pressure at infinity. This theorem has been established for nonviscous flow fields containing curved shocks (references 16, 43, and 51 and unpublished results of Chi-Teh Wang). It is assumed here to hold at high Reynolds number in the lower transonic range Moreover, the extremum value of the integral in equation (D1) is assumed to be the same as for irrotational flow, namely, a minimum.

Consider a stream tube of flow just outside the boundary layer (fig. 15). In this stream tube, the flow accelerates isentropically from free-stream pressure and free-stream Mach number at station 0 to a supersonic condition at station 1, reverts through a normal shock to subsonic conditions at station 2, and returns ultimately to free-stream pressure, but not to free-stream velocity, at station 3. The flow from station 2 to station 3 need not be assumed isentropic. If the normal shock is assumed to occur in a diverging portion of the stream tube, as is indicated by stability considerations (reference 52), then the maximum velocity, or minimum pressure, on the airfoil occurs just ahead of the shock at station 1. If the shock does not form in a diverging portion of the stream tube, then the pressure coefficient to be derived is that just ahead of the shock, not the minimum in the stream tube. The small-perturbation assumption is not made.

The shock back pressure p_2 is now expressed as a fraction of free-stream pressure p_o. By the isentropic relation, the ratio of the pressure just ahead of the shock p_1 to the free-stream pressure p_o is given by

$$\frac{p_1}{p_o} = \left(\frac{1 + \frac{\gamma-1}{2} M_o^2}{1 + \frac{\gamma-1}{2} M_1^2}\right)^{\frac{\gamma}{\gamma-1}} \tag{D2}$$

The ideal pressure ratio across the shock is given by the Rankine-Hugoniot relation

$$\left(\frac{p_2}{p_1}\right)_{id} = \frac{2\gamma}{\gamma+1} M_1^2 - \frac{\gamma-1}{\gamma+1} \tag{D3}$$

As in the section on lower transonic asymmetric flow, to allow for the possibility that the pressure rise across the actual shock region of finite extent is different, for whatever reason, from the pressure rise across an ideal normal shock, a shock-pressure-drop coefficient is introduced: (The desirability of considering the influence of the shock-boundary-layer interaction in this connection was pointed out to the author by A. Silverstein.)

$$c_s = \frac{\Delta p_s}{\frac{1}{2}\rho_1 v_1^2} = \frac{\Delta p_s}{\frac{\gamma}{2} p_1 M_1^2} \tag{D4}$$

such that the actual pressure ratio across the shock is given by

$$\frac{p_2}{p_1} = \left(\frac{p_2}{p_1}\right)_{id} - \frac{\Delta p_s}{p_1} \tag{D5}$$

Equations (D2) to (D5) combine to give for the actual shock back pressure ratio

$$\frac{p_2}{p_o} = \left(\frac{1 + \frac{\gamma-1}{2} M_o^2}{1 + \frac{\gamma-1}{2} M_1^2}\right)^{\frac{\gamma}{\gamma-1}} \left(\frac{2\gamma}{\gamma+1} M_1^2 - \frac{\gamma-1}{\gamma+1} - c_s \frac{\gamma}{2} M_1^2\right) \tag{D6}$$

For given M_o and c_s, this expression is found to have a maximum at a value of M_1 given by

$$M_1 = \sqrt{\frac{\gamma+3 - c_s(\gamma+1)}{2 - c_s(\gamma+1)/2}} \tag{D7}$$

The maximum shock back pressure ratio is accordingly

$$\left(\frac{p_2}{p_o}\right)_{max} = \left(1 + \frac{\gamma-1}{2} M_o^2\right)^{\frac{\gamma}{\gamma-1}} (\gamma+1-c_s) \left[\frac{4-c_s(\gamma+1)}{(\gamma+1)(\gamma+1-c_s)}\right]^{\frac{\gamma}{\gamma-1}} \tag{D8}$$

It is now inferred, from the condition that shock back pressure be as close as possible to free-stream pressure, that if $(p_2/p_o)_{max} < 1$, then the shock Mach number M_1 is given by equation (D7), whereas if $(p_2/p_o)_{max} > 1$, the shock Mach number M_1 is given by equation (D6) with $p_2/p_o = 1$.

The ideal-shock case $c_s = 0$ is discussed first. Here the free-stream Mach number M_o, at which $(p_2/p_o)_{max} = 1$, is 0.78. Hence, by equation (D7), the shock Mach number M_1 for free-stream Mach numbers $M_o < 0.78$ is given by

$$M_1 = \sqrt{\frac{\gamma+3}{2}} = 1.483 \qquad (\gamma = 1.4) \tag{D9}$$

For free-stream Mach numbers in the range $0.78 < M_o < 1$, equation (D6) with $p_2/p_o = 1$ and $c_s = 0$ gives a relation between M_1 and M_o. The preceding relations between M_1 and M_o can be converted into relations between the shock pressure coefficient

$$P_1 \equiv \frac{p_1 - p_o}{\frac{1}{2}\rho_o v_o^2} = \frac{2}{\gamma M_o^2}\left(\frac{p_1}{p_o} - 1\right) \tag{D10}$$

and M_o by equation (D2). The result is shown in figure 16. Shown for comparison are the pressure-coefficient curves for sonic velocity ($M_1 = 1$ in equation (D2)) and for perfect vacuum ($M_1 = \infty$ in equation (D2)).

Included in figure 16 are some experimental data given in references 44 and 53. The data of reference 53 consist of the minimum pressures measured on the wings of various airplanes in both low-speed supercritical flight (stalled pull-ups) and in high-speed supercritical flight (dive pull-outs). Of the six circle data points in figure 16, the three points at free-stream Mach numbers of 0.42, 0.445, and 0.645 represent minimums of all the pressures measured on the wings of the P-47C-1, the XP-51, and the SB2C-1 airplanes, respectively, in stalled pull-ups. The cluster of three points at approximately $M_o = 0.73$ represents minimum pressures selected in reference 53 from the pressure distributions measured on the wings of the XP-51 airplane in successive dive pull-outs. A further dive pull-out point for the XF2A-2 airplane coincides with the middle one of this cluster of three points. The data of reference 44 were obtained on a NACA 4412 airfoil spanning the Langley 24-inch high-speed closed circular tunnel. The variation of minimum pressure on the upper surface with Mach number at an angle of attack of the airfoil of $1^\circ 52.5'$ was taken as representative of their results. Further wind-tunnel data of the same type are given in reference 24.

Comparison of the experimental data with the theoretical limit curve shows that the limit pressures indicated by the theory are, in fact, approached or reached but not exceeded. The leveling off of the pressure distribution of reference 44 somewhat below a local Mach number of 1.5 may be due to low Reynolds number, wind-tunnel effect, or both. Thus the concept of a limit curve derived from a shock condition independent of Reynolds number and airfoil shape appears to have some significance, at least in the limit of large Reynolds numbers (single normal terminal shock), isolated airfoils, and for an airfoil shape that permits high local Mach number supersonic regions to develop at low free-stream Mach numbers.

Consider now the effect of shock pressure-drop coefficient c_s. As noted in the section LOWER TRANSONIC ASYMMETRIC FLOW WITH TERMINAL SHOCK, values of c_s in the approximate range 0.1 to 0.5 occur experimentally. Assume for definiteness a value $c_s = 0.33$. The effect of this value of c_s in equations (D6) to (D8) is to increase the shock Mach number M_1 yielding maximum p_2/p_o to 1.5 and to shift the free-stream Mach number M_o at which $(p_2/p_o)_{max} = 1$ to $M_o = 1$. Hence, the portion ABCD of the $c_s = 0$ limit curve (fig. 16) would be eliminated and replaced by the curve BE, slightly shifted to correspond to $M_1 = 1.5$ instead of 1.483. The introduction of a shock pressure-drop coefficient c_s thus yields practically the same value of limit shock Mach number, and hence minimum pressure, as when $c_s = 0$ in the range $M_o < 0.78$. It may be

noted that the value $c_s = 0.33$ yields the pressure ratio $p_2/p_o = 0.527$ in equation (D6), that is, the pressure ratio corresponding to locally sonic velocity in isentropic flow, which provides an interpretation for the statement occasionally made that sonic velocity occurs behind the terminal shock.

The shock condition as thus far developed applies to finite and, in fact, quite large velocity perturbations and where $1-M_o$ can, and possibly should, be of the order 1. The transition to the transonic small-perturbation case is equivalent to replacing the branch AB of the limit curve (fig. 16) (or its modification for $c_s \neq 0$) by the tangent to AB at the point A. This fact is seen from equation (67), which is the limiting form of equation (D6) for $\mu = 1-M_o^2 \longrightarrow 0$ and $M_1^2-1 \longrightarrow 0$. For constant c_s near $M_o = 1$ and by the shock back pressure condition $P_2 = 0$ in this range, equation (67) yields $-2\Lambda_1 (= P_1)$ as a linear function of $1-M_o$, tangent to equation (D6) at $M_o = 1$.

As remarked in the section LOWER TRANSONIC ASYMMETRIC FLOW WITH TERMINAL SHOCK, application of the shock condition $p_2/p_o = 1$ or $P_2 = 0$ in equation (67) implies approximately zero pressure change along the airfoil downstream of the shock. If this condition exists regardless of airfoil shape, a severe separation of the boundary layer must occur in traversing the shock. Similarly, for finite perturbations at lower free-stream Mach numbers, the present analysis applies only if the boundary layer can so vary in thickness as to provide sufficient flexibility in the airfoil boundary condition for the terminal shock to be free to stabilize at different local Mach numbers along the airfoil. Only then does the possibility arise of choosing one of these local Mach numbers in accordance with equation (D1) for shock location, independently of airfoil shape.

With such freedom of shock location, equation (D1) also indicates that the terminal shock will form in a diverging portion of stream tube, as this provides less variation of static pressure than if the shock formed (at the same local Mach number) in a converging portion of the stream tube, which would necessarily be preceded by a diverging part. Where substantial pressure change does occur downstream of the shock, the terminal-shock condition given herein requires modification; for example, in the small-perturbation case the P_2 term in equation (67) would have to be retained.

Finally, it is of interest to note that the shock Mach number given by equation (D9) is also that for which the streamline curvature vanishes just downstream of a normal-shock element of finite

curvature (references 18 and 43). This property is derived by finite-perturbation considerations analogous to those of appendix C; thus no close connection with the present derivation of equation (D9) appears to exist. Inasmuch as a separating boundary layer traversing a shock should, however, tend to produce zero streamline curvature downstream of the shock element, this property of equation (D9) may also help to explain terminal-shock stabilization at approximately $M_1 = 1.5$.

APPENDIX E

SYMBOLS

The more important symbols used in this report are as follows:

C streamline curvature, $-\left(\frac{\partial\theta}{\partial s}\right)_s$

c chord length, taken as unity

$c_d \equiv D(\text{drag})/\frac{1}{2}\rho_o v_o^2 c$, section drag coefficient

$c_s \equiv \Delta p_s/\frac{1}{2}\rho_1 v_1^2$, shock-pressure-drop coefficient

D drag

d distance of normal element of detached shock from leading edge

$K \equiv -2K_1 = (1-M_o^2)/(\tau\Gamma)^{2/3}$, transonic similarity parameter, (equations (12c) and (84))

$L \equiv \Gamma^{1/3}\Lambda/\tau^{2/3}$, velocity parameter, (equations (58b) and (85))

M local Mach number, ratio of local velocity to local velocity of sound

$P \equiv (p-p_o)/\frac{1}{2}\rho_o v_o^2$, pressure coefficient

p pressure (fraction of free-stream value)

r,s curvature function parameters, (equations (33) and (74))

$V \equiv 1 + \Lambda$, resultant velocity at airfoil (fraction of free-stream value)

$v \equiv 1 + \upsilon$, resultant velocity (fraction of free-stream value)

$x \equiv \frac{1}{2}(1+\xi)$, chordwise location, distance in free-stream direction

Y ordinate of airfoil

y lateral distance perpendicular to free-stream direction

$z \equiv v/\Lambda$, (distance in appendix C)

$\Gamma \equiv 1 + \frac{M_o^2}{2} - \frac{2-\gamma}{2} M_o^2$, (equation (11c))

$\Gamma_c \equiv (\gamma+1)/2$, (equation (11d))

$\Gamma_M \equiv M_o^2 \left(1 + \frac{\gamma-1}{2} M_o^2\right)$, (equation (28a))

γ ratio of specific heats, 1.4

δ streamline displacement at infinity, figure 2

θ angle between local stream direction and free-stream direction, figure 2

$\lambda \equiv \left(\frac{2-r}{3-r}\right) \frac{\Gamma_c \Lambda}{\mu}$, (equation (37a))

$\mu \equiv -\bar{\mu} = 1-M_o^2$

ρ density (fraction of free-stream value)

σ angle between shock element and free-stream direction

τ thickness ratio, ratio of maximum thickness to chord length

$\chi \equiv \frac{(2-r)^3}{(3-r)^2} \frac{\Gamma_c^2 Y C_a}{\mu^3}$, (equation (37b))

$\sim$ of the order of magnitude of

Subscripts:

a at airfoil

e calculated sonic point of Prandtl-Meyer distribution

i incompressible or low speed

l potential limit

o free-stream condition

w sonic point of oblique shock

1,2 upstream and downstream of terminal shock, respectively

REFERENCES

1. Stack, J.: Compressible Flows in Aeronautics. Jour. Aero. Sci., vol. 12, no. 2, April 1945, pp. 127-143; discussion, pp. 143-148.

2. Ackeret, J., Feldmann, F., and Rott, N.: Investigations of Compression Shocks and Boundary Layers in Gases Moving at High Speed. NACA TM 1113, 1947.

3. Liepmann, Hans Wolfgang: The Interaction between Boundary Layer and Shock Waves in Transonic Flow. Jour. Aero. Sci., vol. 13, no. 12, Dec. 1946, pp. 623-637.

4. Liepmann, Hans Wolfgang, Askenas, Harry, and Cole, Julian D.: Experiments in Transonic Flow. Tech. Rep. No. 5667, Air Materiel Command, U.S. Air Forces, Feb. 19, 1948. (Prepared by C.I.T., June 1947, under AAF Contract No. W33-038ac-1717 (11592).)

5. von Kármán, Theodore: Supersonic Aerodynamics - Principles and Applications. Jour. Aero. Sci., vol. 14, no. 7, July 1947, pp. 373-402; discussion, pp. 403-409.

6. Kaplan, Carl: The Flow of a Compressible Fluid past a Curved Surface. NACA Rep. 768, 1943.

7. Hantzsche, W.: Die Prandtl-Glauertsche Näherung als Grundlage für ein Iterationsverfahren zur Berechnung kompressibler Unterschallströmungen. Zeitschr. f. angew. Math. Mech., Bd. 23, Nr. 4, Aug. 1943, S. 185-199.

8. Guderley, Gottfried, and Yoshihara, Hideo: On the Compressible Potential Flow over a Closed Body. Tech. Rep. No. F-TR-2176-ND, Tech. Intell., Air Materiel Command (Wright-Patterson Air Force Base), Dec. 1947.

9. Lighthill, M. J.: The Hodograph Transformation in Trans-sonic Flow. Proc. Roy. Soc. London, vol. 191, no. A1026, ser. A, Nov. 18, 1947, pp. 323-369.

10. Ferguson, D. F., and Lighthill, M. J.: The Hodograph Transformation in Trans-sonic Flow. IV. Tables. Proc. Roy. Soc. London, vol. 192, no. A1028, ser. A, Dec. 23, 1947, pp. 135-142.

11. Tsien, Hsue-Shen, and Kuo, Yung-Huai: Two-Dimensional Irrotational Mixed Subsonic and Supersonic Flow of a Compressible Fluid and the Upper Critical Mach Number. NACA TN 995, 1946.

12. Kuo, Yung-Huai: Two-Dimensional Irrotational Transonic Flows of a Compressible Fluid. NACA TN 1445, 1948.

13. Bergman, Stefan: Two-Dimensional Transonic Flow Patterns. Am. Jour. Math., vol. LXX, 1948, pp. 856-891.

14. Gelbart, Abe: On Subsonic Compressible Flows by a Method of Correspondence. I - Methods for Obtaining Subsonic Circulatory Compressible Flows about Two-Dimensional Bodies. NACA TN 1170, 1947.

15. Bartnoff, Shepard, and Gelbart, Abe: On Subsonic Compressible Flows by a Method of Correspondence. II - Application of Methods to Studies of Flow with Circulation about a Circular Cylinder. NACA TN 1171, 1947.

16. Wang, Chi-Teh: Variational Method in the Theory of Compressible Fluid. Jour. Aero. Sci., vol. 15, no. 11, Nov. 1948, pp. 675-685.

17. Göthert, B., and Kawalki, K. H.: The Compressible Flow past Various Plane Profiles near Sonic Velocity. NACA TM 1203, 1949.

18. Emmons, Howard W.: Flow of a Compressible Fluid past a Symmetrical Airfoil in a Wind Tunnel and in Free Air. NACA TN 1746, 1948.

19. Emmons, Howard W.: The Theoretical Flow of a Frictionless, Adiabatic, Perfect Gas Inside of a Two-Dimensional Hyperbolic Nozzle. NACA TN 1003, 1946.

20. Maccoll, J. W., and Codd, J.: Theoretical Investigations of the Flow around Various Bodies in the Sonic Region of Velocities. Theoretical Res. Rep. No. 17145, Armament Res. Dept., British M.O.S., Sept. 1945.

21. Tsien, H. S., and Finston, M.: Interaction between Parallel Streams of Subsonic and Supersonic Velocities. Jour. Aero. Sci., vol. 16, no. 9, Sept. 1949, pp. 515-528.

22. Lees, Lester: Remarks on the Interaction between Shock Waves and Boundary Layer in Transonic and Supersonic Flow. Rep. No. 120, Aero. Eng. Dept., Princeton Univ., Nov. 1, 1947. (Available from Library of Congress as No. U-50566.)

23. Allen, H. Julian, Heaslet, Max. A., and Nitzberg, Gerald E.: The Interaction of Boundary Layer and Compression Shock and Its Effect upon Airfoil Pressure Distributions. NACA RM A7A02, 1947.

24. Nitzberg, Gerald E., and Crandall, Stewart: A Study of Flow Changes Associated with Airfoil Section Drag Rise at Supercritical Speeds. NACA TN 1813, 1949.

25. Stodola, A.: Steam and Gas Turbines. Vol. II. McGraw-Hill Book Co., Inc., 1927. (Reprinted, Peter Smith (New York), 1945.)

26. Perl, W., and Moses, H. E.: Velocity Distributions on Symmetrical Airfoils in Closed Tunnels by Conformal Mapping. NACA TN 1642, 1948.

27. Oswatitsch, K., and Wieghardt, K.: Theoretical Analysis of Stationary Potential Flows and Boundary Layers at High Speed. NACA TM 1189, 1948.

28. Greene, Leonard Michael: The Attentuation Method for Compressible Flow Systems. Jour. Aero. Sci., vol. 12, no. 3, July 1945, pp. 329-338.

29. Perl, W.: Calculation of Compressible Flows past Aerodynamic Shapes by Use of the Streamline Curvature. NACA TN 1328, 1947.

30. von Kármán, Theodore: The Similarity Law of Transonic Flow. Jour. Math. Phys., vol. XXVI, no. 3, Oct. 1947, pp. 182-190.

31. Glauert, H.: The Elements of Aerofoil and Airscrew Theory. Cambridge Univ. Press (London), 2d ed., 1948, p. 43.

32. Perl, W.: Relation between the Limiting Line Phenomenon and the Kármán Transonic Similarity Theory. The Phys. Rev., vol. 73, no. 10, 2d ser., May 15, 1948, p. 1254.

33. Kaplan, Carl: On Similarity Rules for Transonic Flows. NACA Rep. 894, 1948.

34. Perl, W., and Green, L. J.: The Two-Dimensional Incompressible Potential Flow over Corrugated and Distorted Infinite Surfaces. NACA ARR E5A05, 1945.

35. von Kármán, Th.: Compressibility Effects in Aerodynamics. Jour. Aero. Sci., vol. 8, no. 9, July 1941, pp. 337-356.

36. Tsien, Hsue-shen: The "Limiting Line" in Mixed Subsonic and Supersonic Flow of Compressible Fluids. NACA TN 961, 1944.

37. Tsien, Hsue-shen, and Fejer, Andrej: A Method for Predicting the Transonic Flow over Airfoils and Similar Bodies from Data Obtained at Small Mach Numbers. Rep. submitted by GALCIT to Air Tech. Service Command, AAF, Dec. 31, 1944. (Available from CADO as ATI No. 16128.)

38. Guderley, K. Gottfried: Considerations of the Structure of Mixed Subsonic-Supersonic Flow Patterns. Tech. Rep. No. F-TR-2168-ND, Tech. Intell., Air Materiel Command (Wright Field), Oct. 1947.

39. Friedrichs, K. O.: On the Non-occurrence of a Limiting Line in Transonic Flow. Communications on Appl. Math. (New York Univ.), vol. 1, no. 3, Sept. 1948, pp. 287-301.

40. Guderley, K. Gottfried: Singularities at the Sonic Velocity. Tech. Rep. No. F-TR-1171-ND, Tech. Intell., Air Materiel Command (Wright-Patterson Air Force Base), June 1948.

41. Guderley, Gottfried: New Aspects of Transonic Flow Theory. Tech. Data Digest, vol. 12, no. 9, Nov. 1, 1947, pp. 5-18.

42. Theodorsen, Theodore: A Condition on the Initial Shock. NACA TN 1029, 1946.

43. Lin, C. C., and Rubinov, S. I.: On the Flow behind Curved Shocks. Jour. Math. Phys., vol. XXVII, no. 2, July 1948, pp. 105-129.

44. Stack, John, Lindsey, W. F., and Littell, Robert E.: The Compressibility Burble and the Effect of Compressibility on Pressures and Forces on an Airfoil. NACA Rep. 646, 1938.

45. Busemann, Adolf: A Review of Analytical Methods for the Treatment of Flow with Detached Shocks. NACA TN 1858, 1949.

46. Crocco, Luigi: Singolarità della Corrente Gassosa Iperacustica Nell' Intorno di Una Prora a Diedro. L'Aerotecnica, Vol. XVII, fasc. 6, Giugno 1937, pp. 519-534.

47. Moeckel, W. E.: Approximate Method for Predicting Form and Location of Detached Shock Waves Ahead of Plane or Axially Symmetric Bodies. NACA TN 192[illegible], 1949.

48. Lindsey, W. F., Daley, Bernard N., and Humphreys, Milton D.: The Flow and Force Characteristics of Supersonic Airfoils at High Subsonic Speeds. NACA TN 1211, 1947.

49. The Staff of the Ames 1- by 3-Foot Supersonic Wind-Tunnel Section: Notes and Tables for Use in the Analysis of Supersonic Flow. NACA TN 1428, 1947.

50. Thomas, T. Y.: On the Stability and Instability of Shock Waves. Proc. Nat. Acad. Sci., vol. 34, no. 11, Nov. 1948, pp. 526-530.

51. Bateman, H.: Partial Differential Equations of Mathematical Physics. Dover Pub. (New York), 1944, p. 164.

52. Kantrowitz, Arthur: The Formation and Stability of Normal Shock Waves in Channel Flows. NACA TN 1225, 1947.

53. Rhode, Richard V.: Correlation of Flight Data on Limit Pressure Coefficients and Their Relation to High-Speed Burbling and Critical Tail Loads. NACA ACR L4I27, 1944.

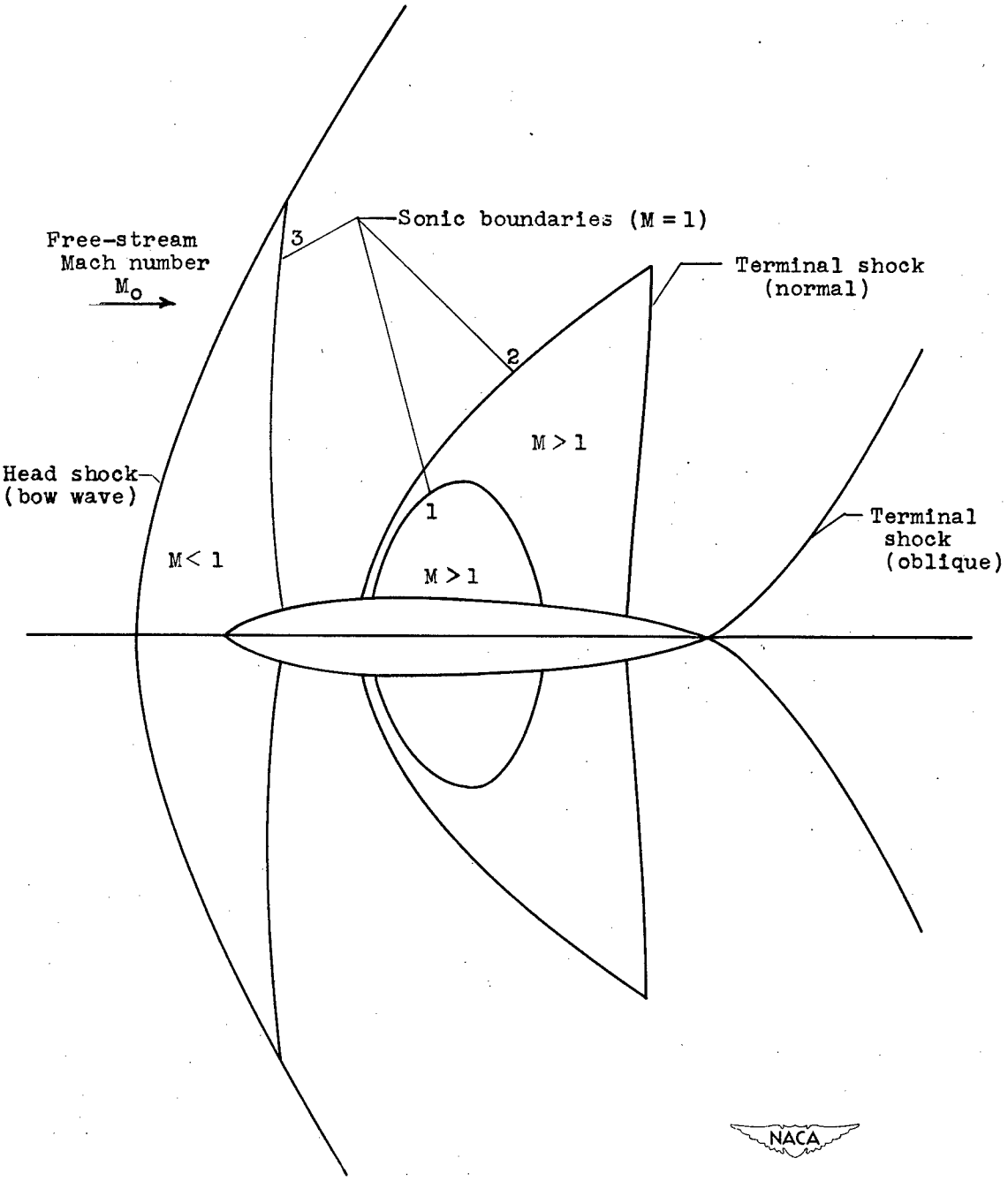

Figure 1. - Schematic superposition of three transonic flow patterns about symmetric airfoil.

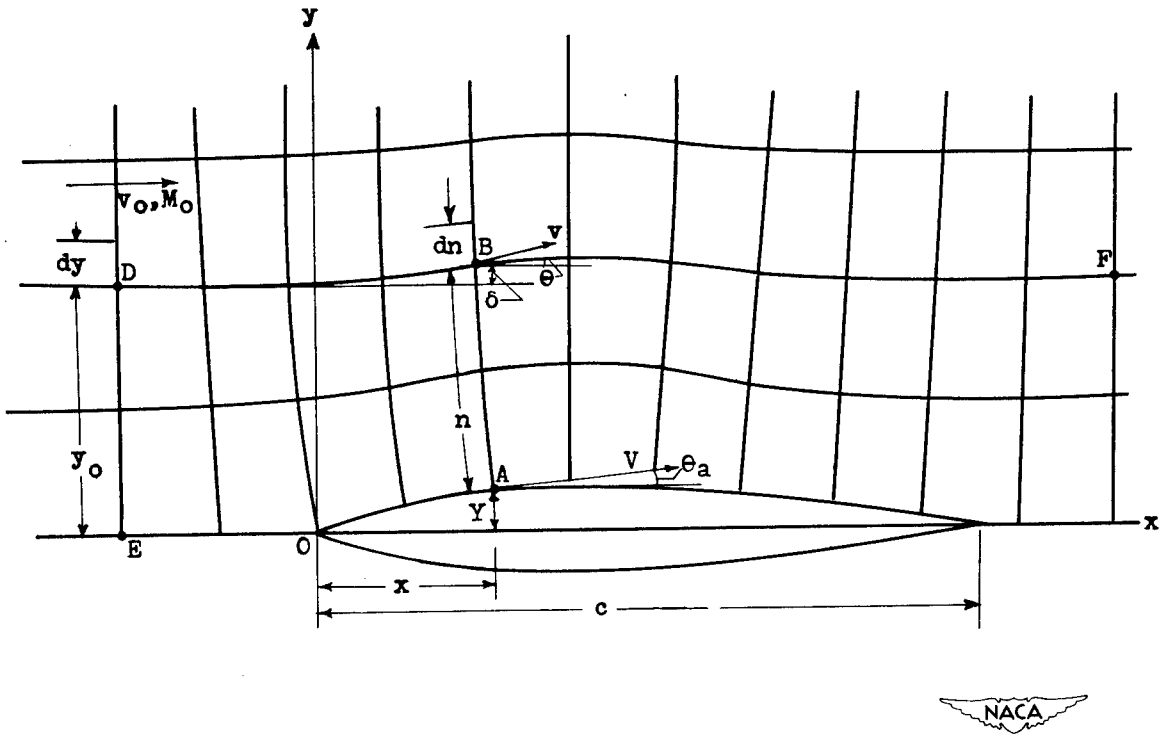

Figure 2. - Symmetric compressible potential flow.

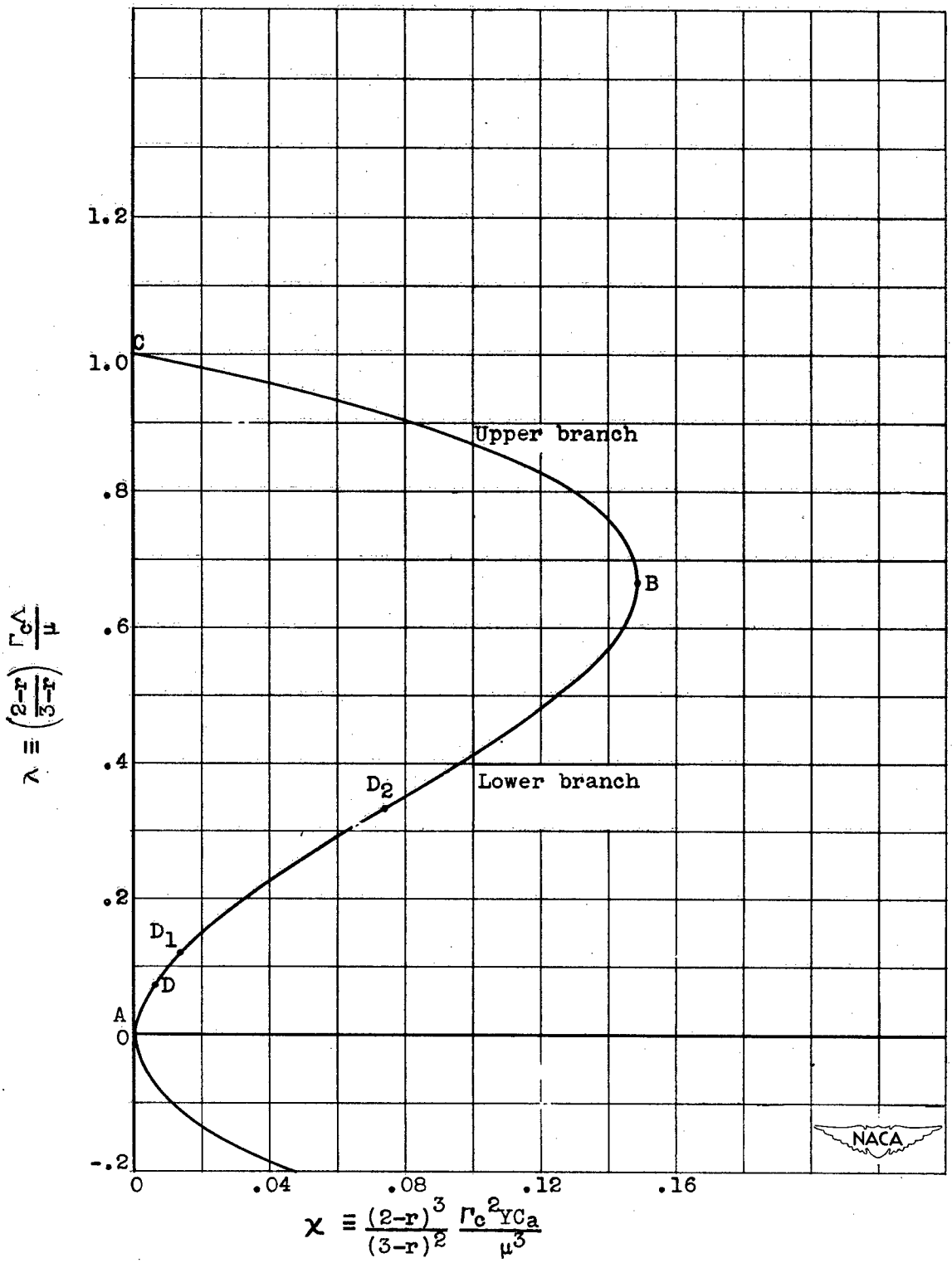

Figure 3. - Plot of equation (38): $\chi = \lambda^2 - \lambda^3$.

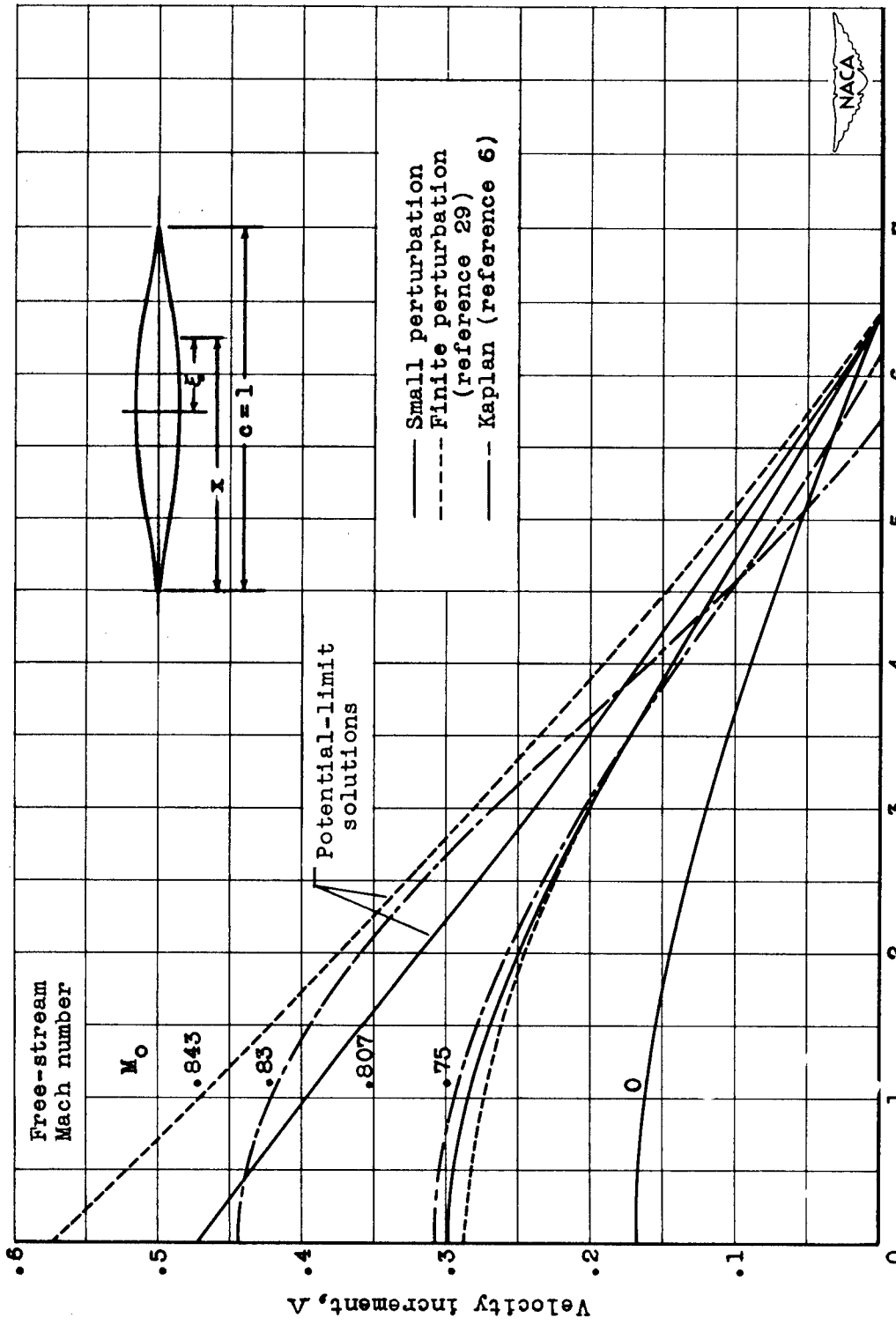

Figure 4. - Velocity distributions on $\tau = 0.1$ Kaplan section in continuous potential flow.

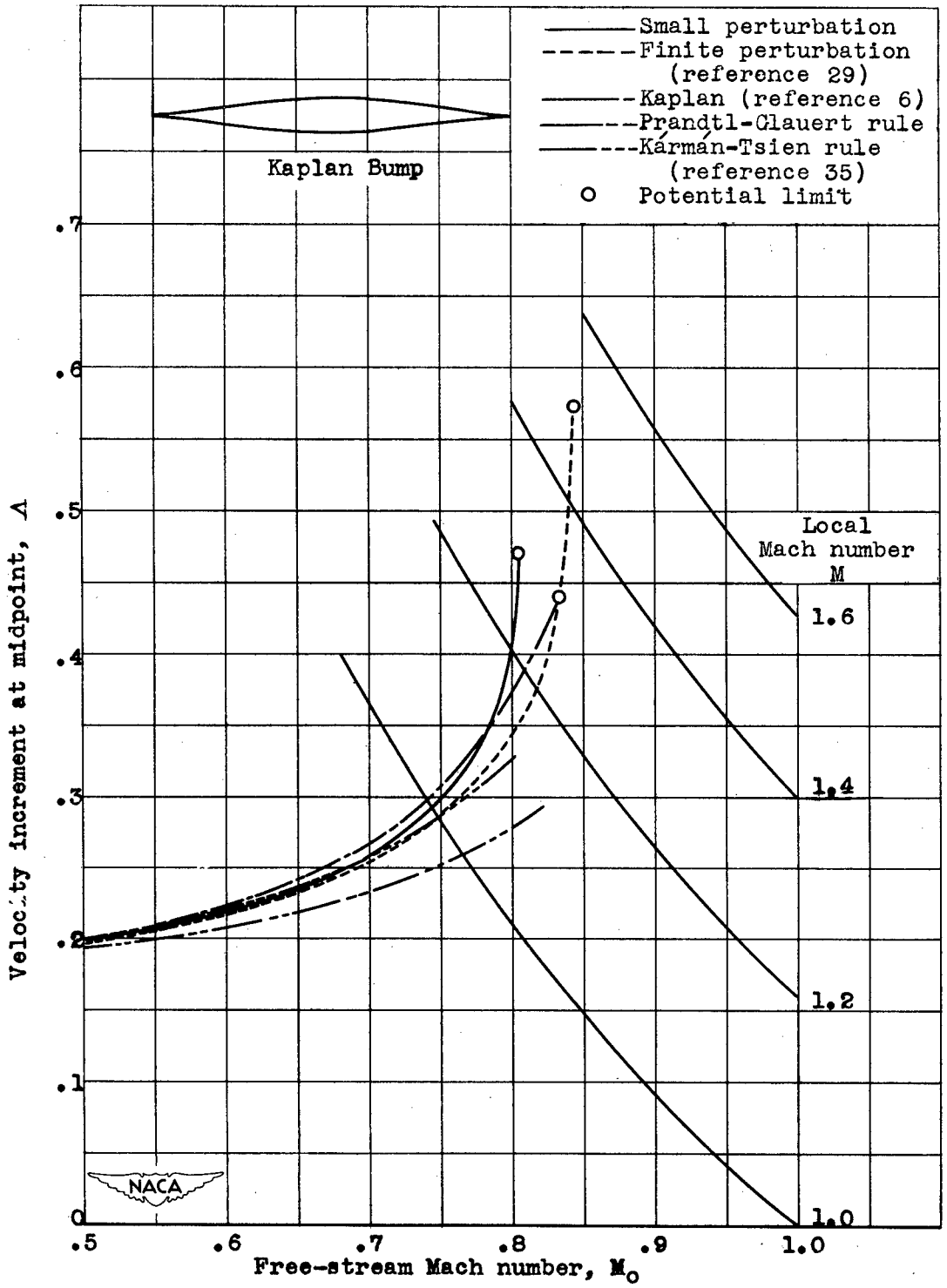

(a) Kaplan section.

Figure 5. - Effect of Mach number on maximum velocity increment of various τ = 0.1 sections. x = 0.5.

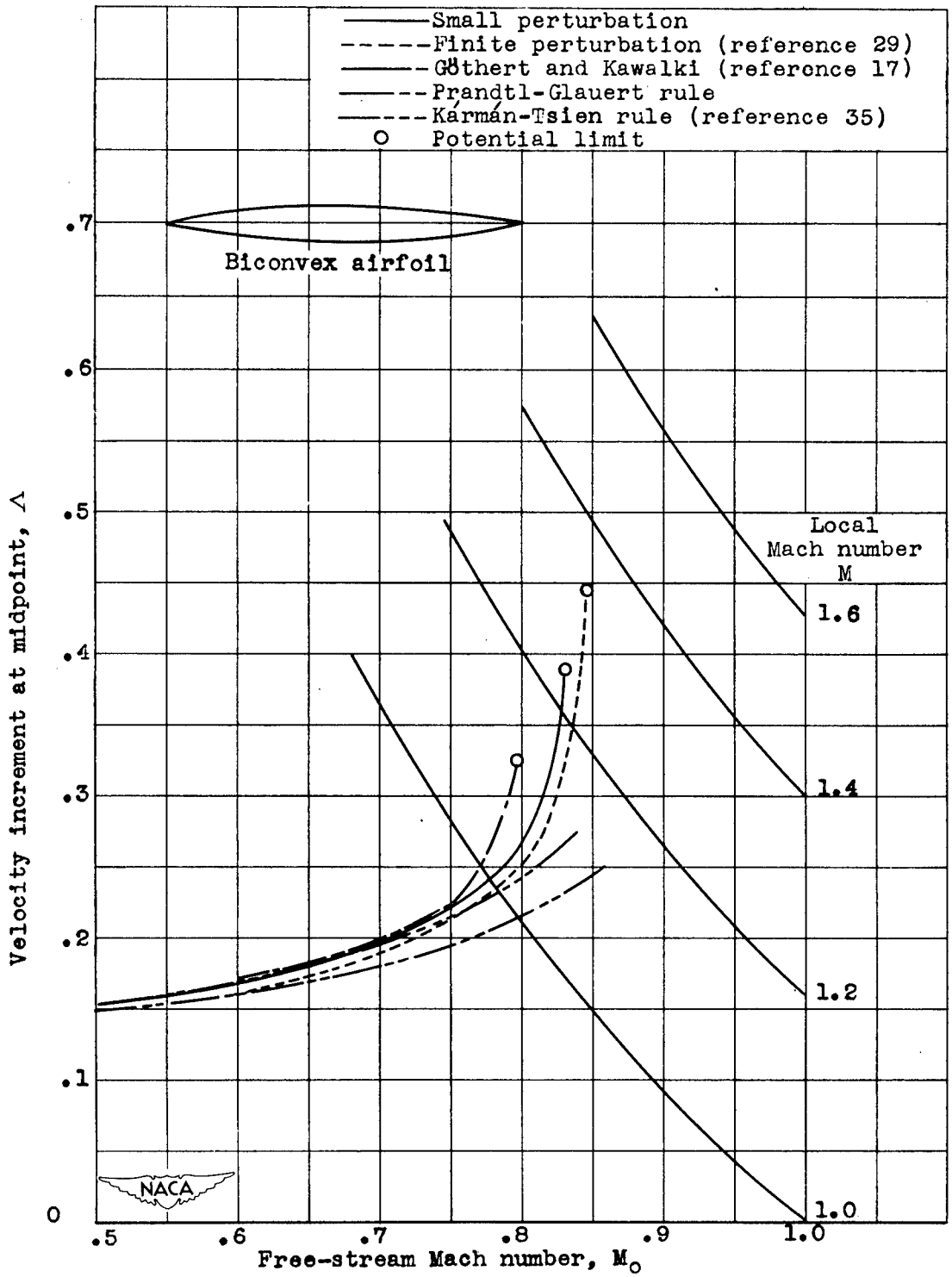

(b) Symmetric biconvex section.

Figure 5. - Continued. Effect of Mach number on maximum velocity increment of various τ = 0.1 sections. x = 0.5.

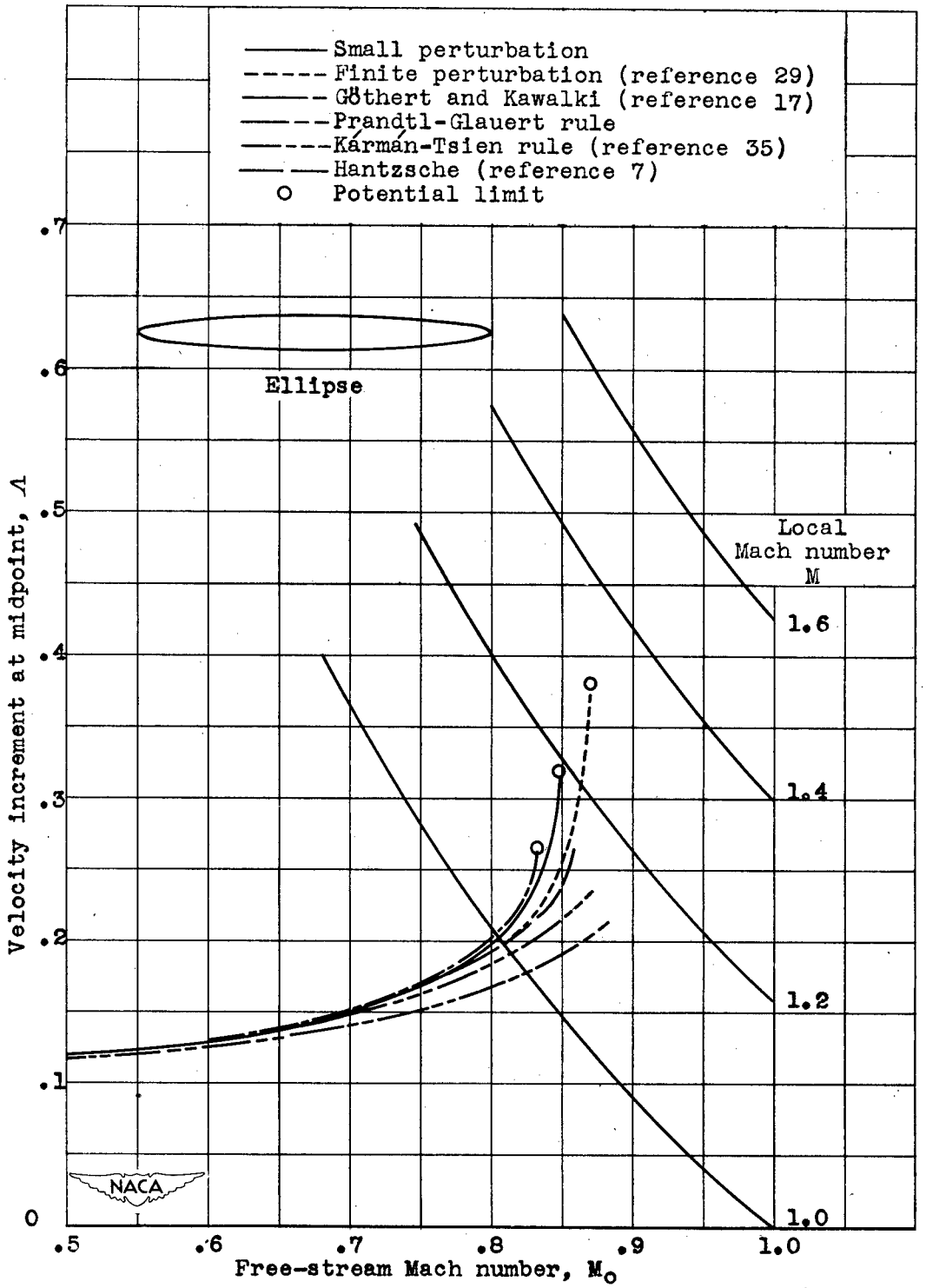

(c) Elliptic section.

Figure 5. - Concluded. Effect of Mach number on maximum velocity increment of various $\tau = 0.1$ sections. $x = 0.5$.

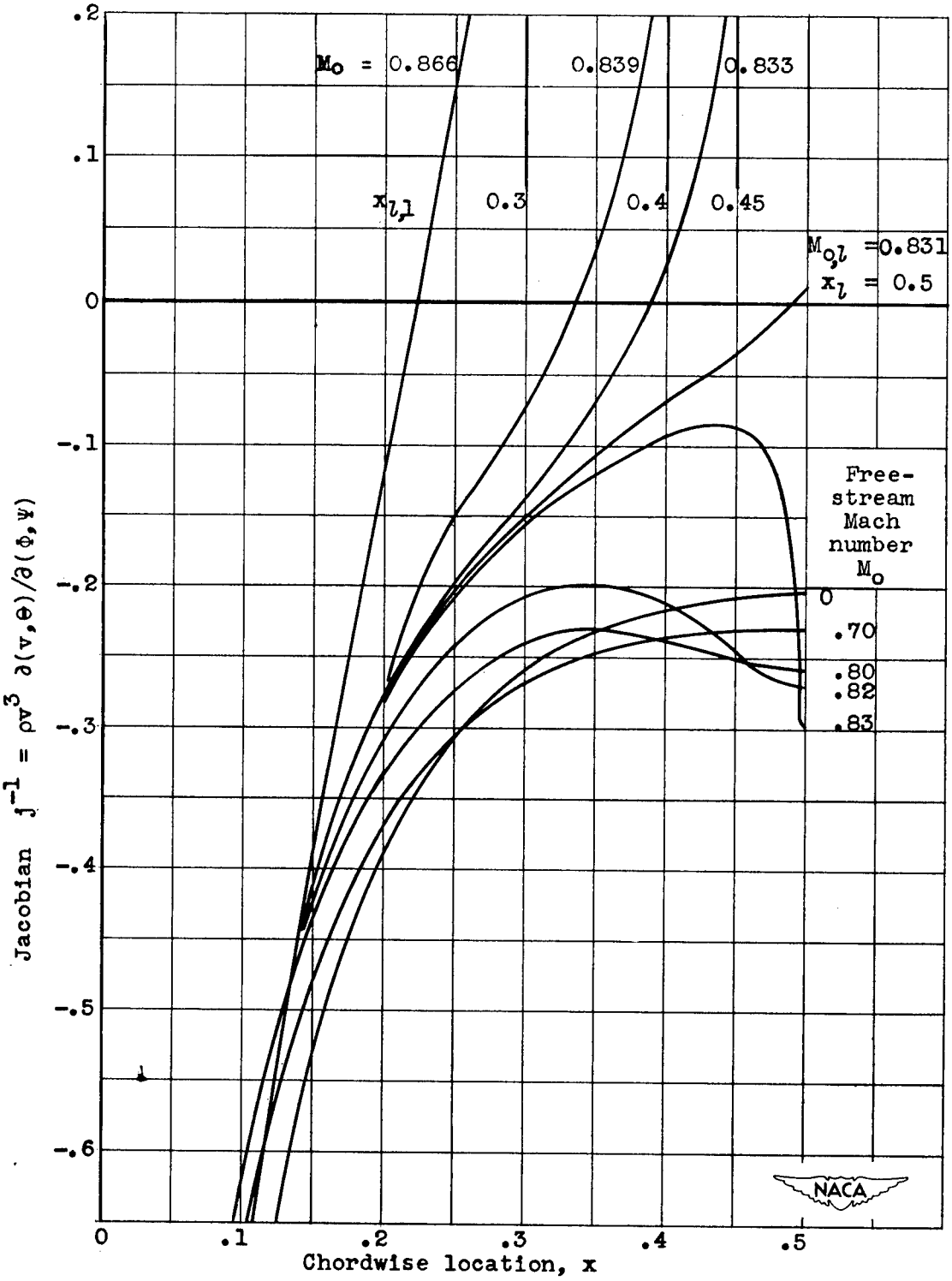

Figure 6. - Jacobian of transformation from physical to hodograph plane. Symmetric biconvex airfoil, $\tau = 0.1$.

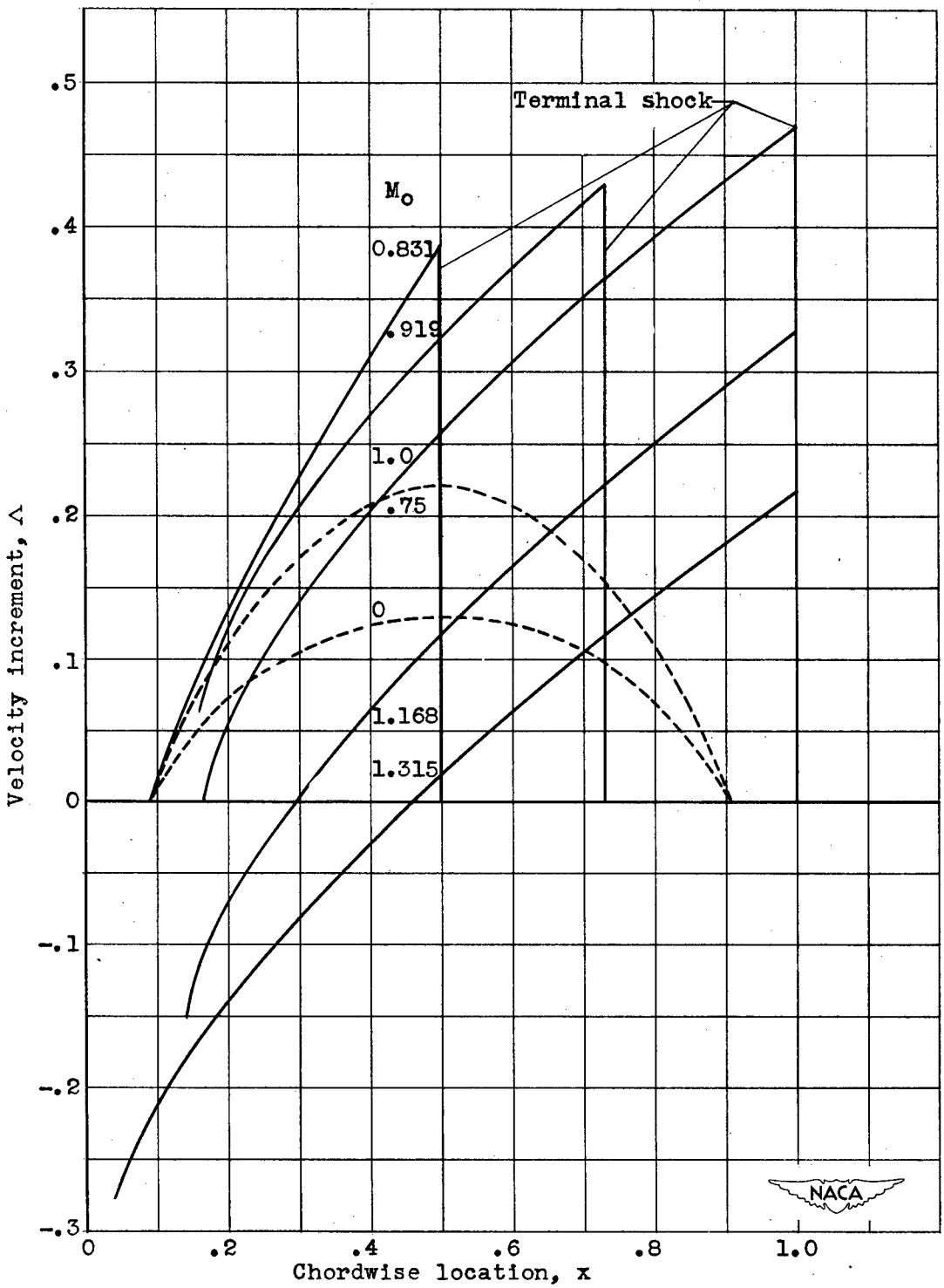

Figure 7. - Velocity distributions on $\tau = 0.1$ symmetric biconvex airfoil in subsonic and transonic range.

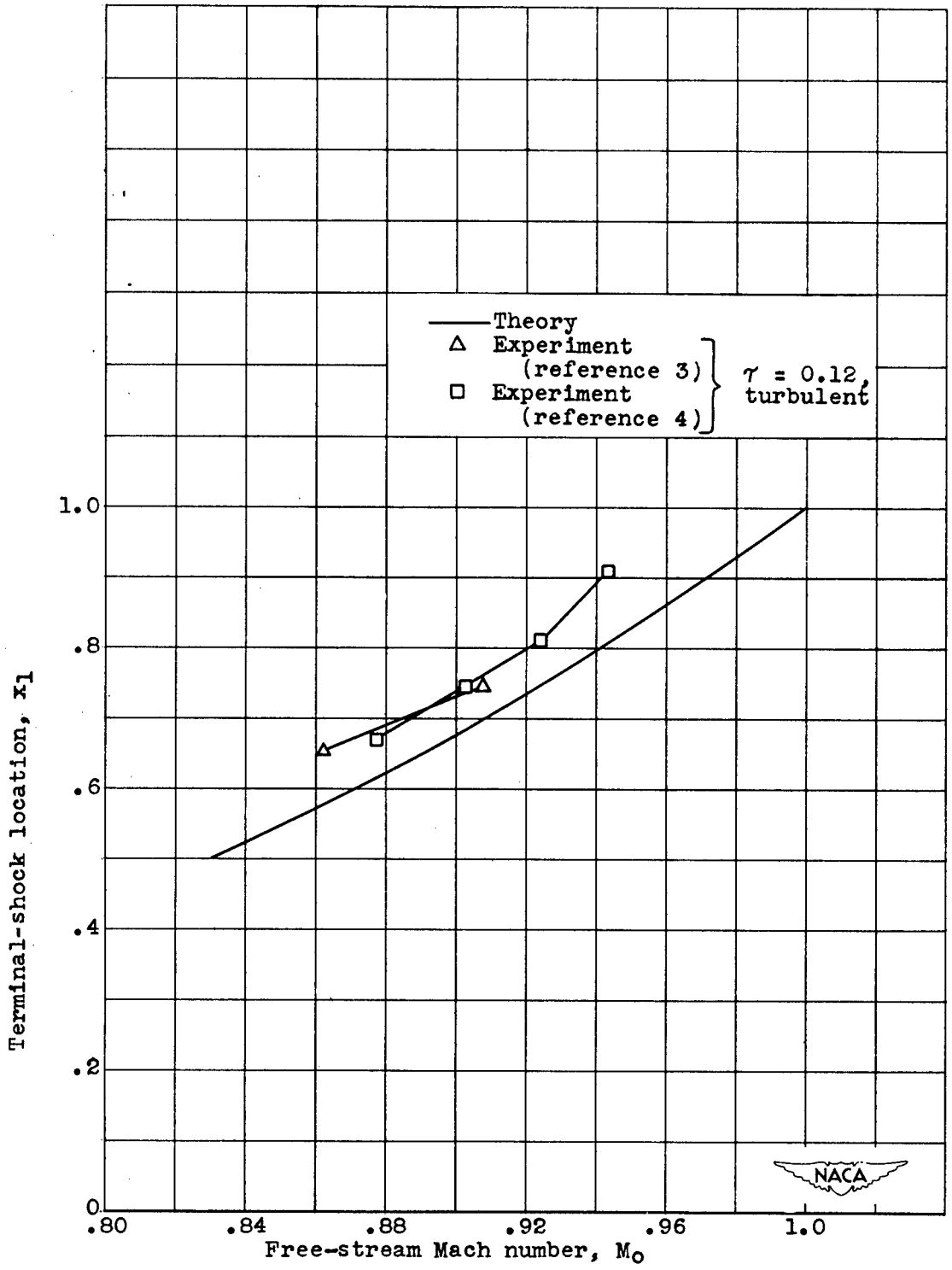

Figure 8. - Terminal-shock location on $\tau = 0.1$ symmetric biconvex airfoil in lower transonic range. Limiting calculation for $\tau \to 0$, $M_0 \to 1$. Plotted by transonic similarity rules for $\tau = 0.1$.

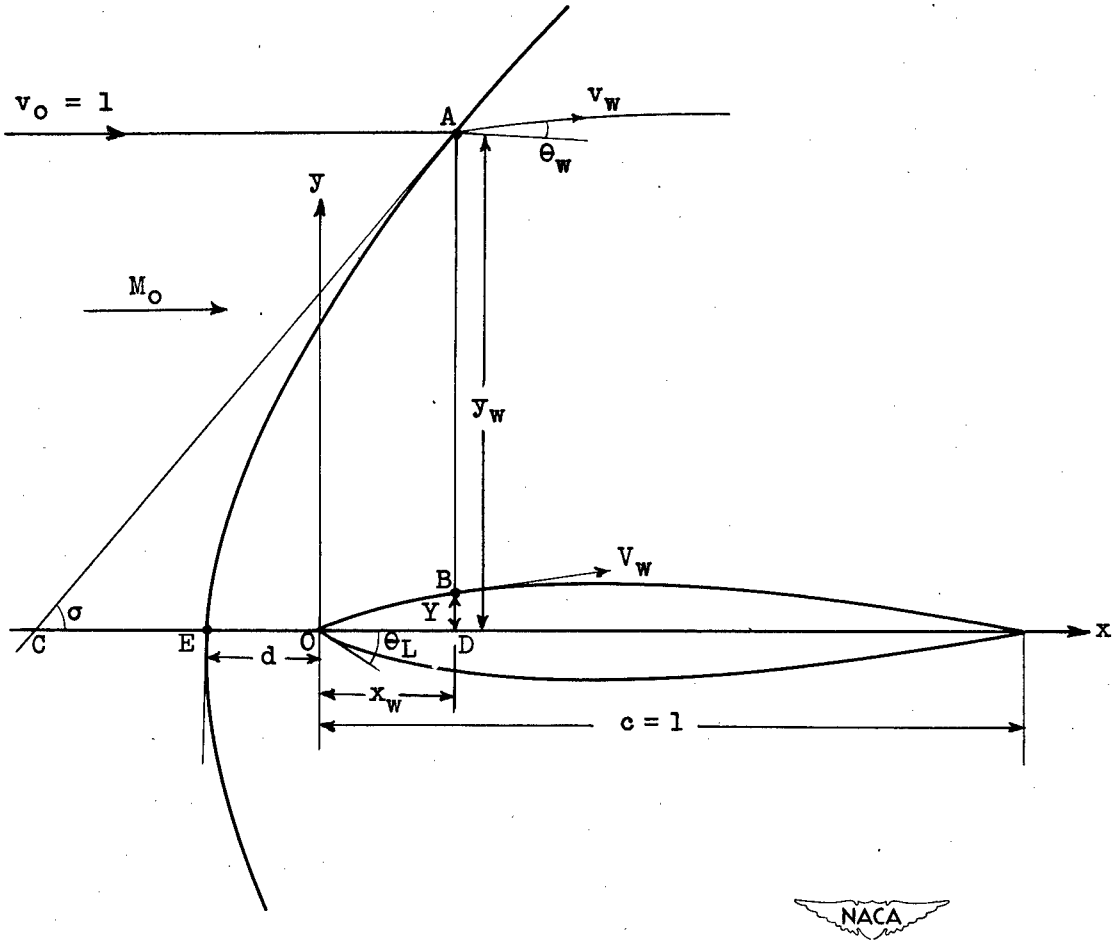

Figure 9. - Upper transonic or detached shock range.

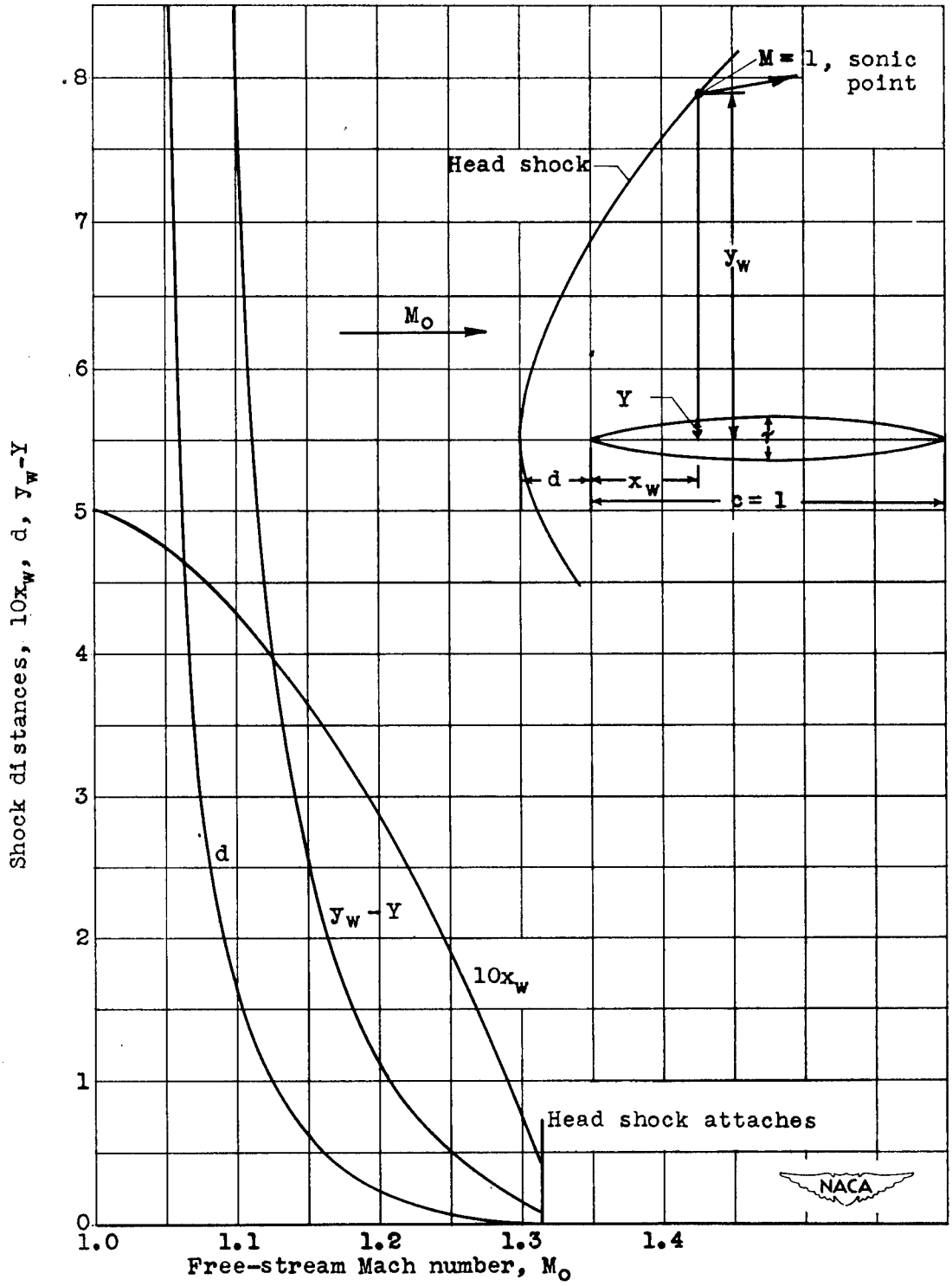

Figure 10. - Detached-shock location relative to $\tau = 0.1$ symmetric biconvex airfoil in upper transonic range. Limiting calculation for $\tau \to 0$, $M_o \to 1$. Plotted by transonic similarity rules for $\tau = 0.1$.

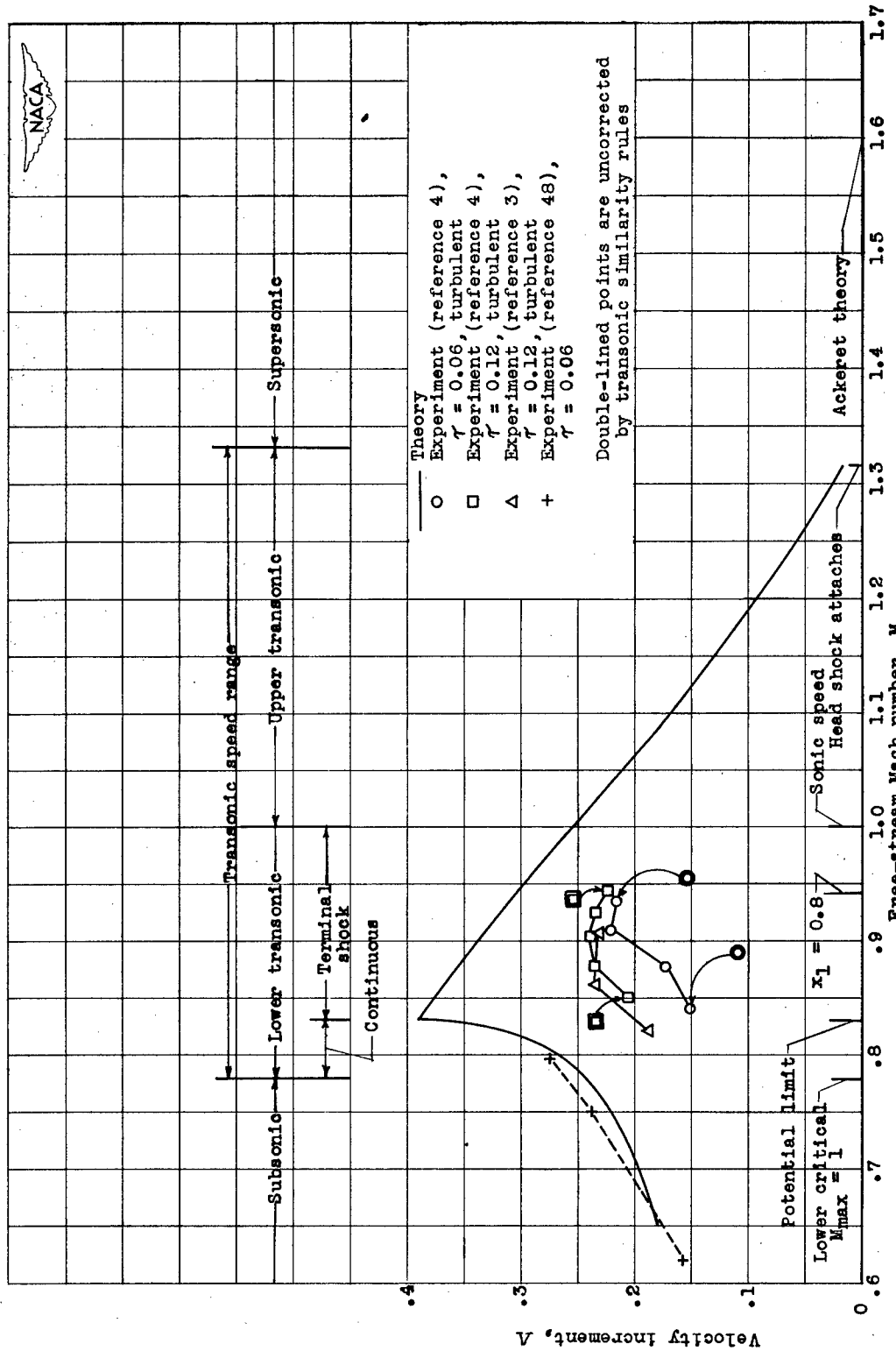

(a) x = 0.5.

Figure 11. - Velocity on symmetric biconvex airfoil in transonic range. Limiting calculation for $\tau \to 0$, $M_0 \to 1$.
Plotted by transonic similarity rules for $\tau = 0.1$.

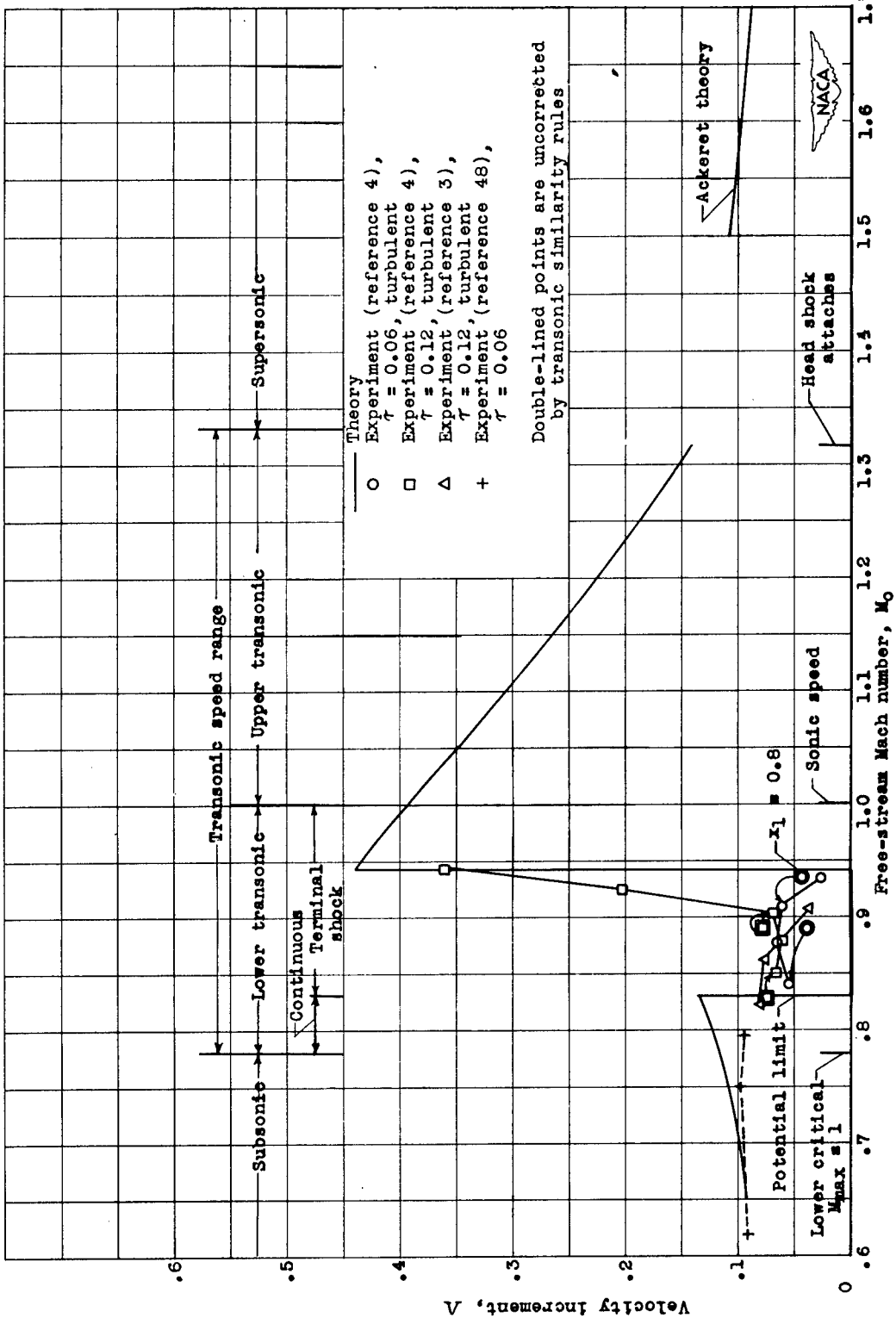

(b) x = 0.8.

Figure 11. - Concluded. Velocity on symmetric biconvex airfoil in transonic range. Limiting calculation for $\tau \to 0$, $M_o \to 1$. Plotted by transonic similarity rules for τ = 0.1.

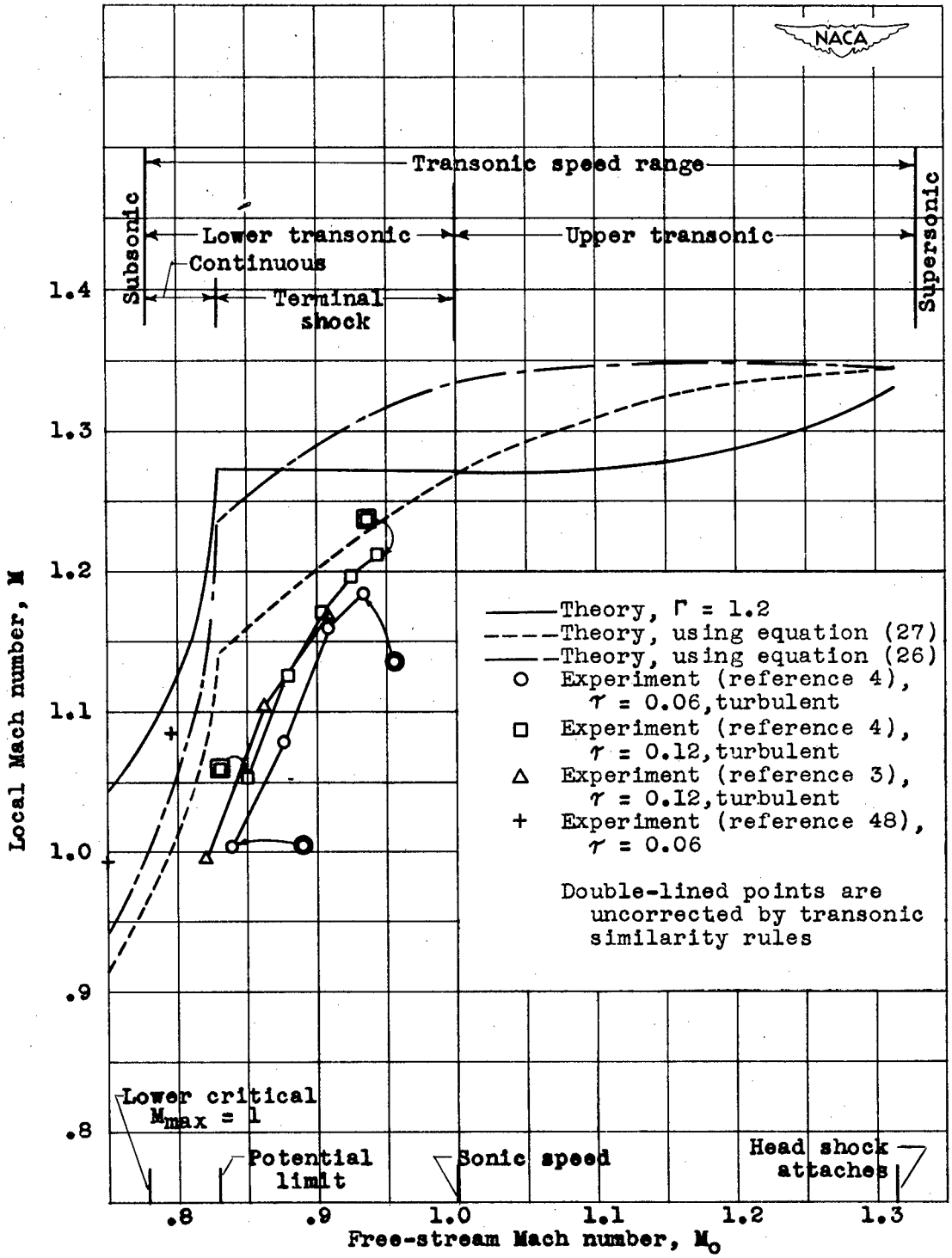

(a) x = 0.5.

Figure 12. - Local Mach number on symmetric biconvex airfoil in transonic range. Limiting calculation for $\tau \to 0$, $M_0 \to 1$. Plotted by transonic similarity rules for $\tau = 0.1$.

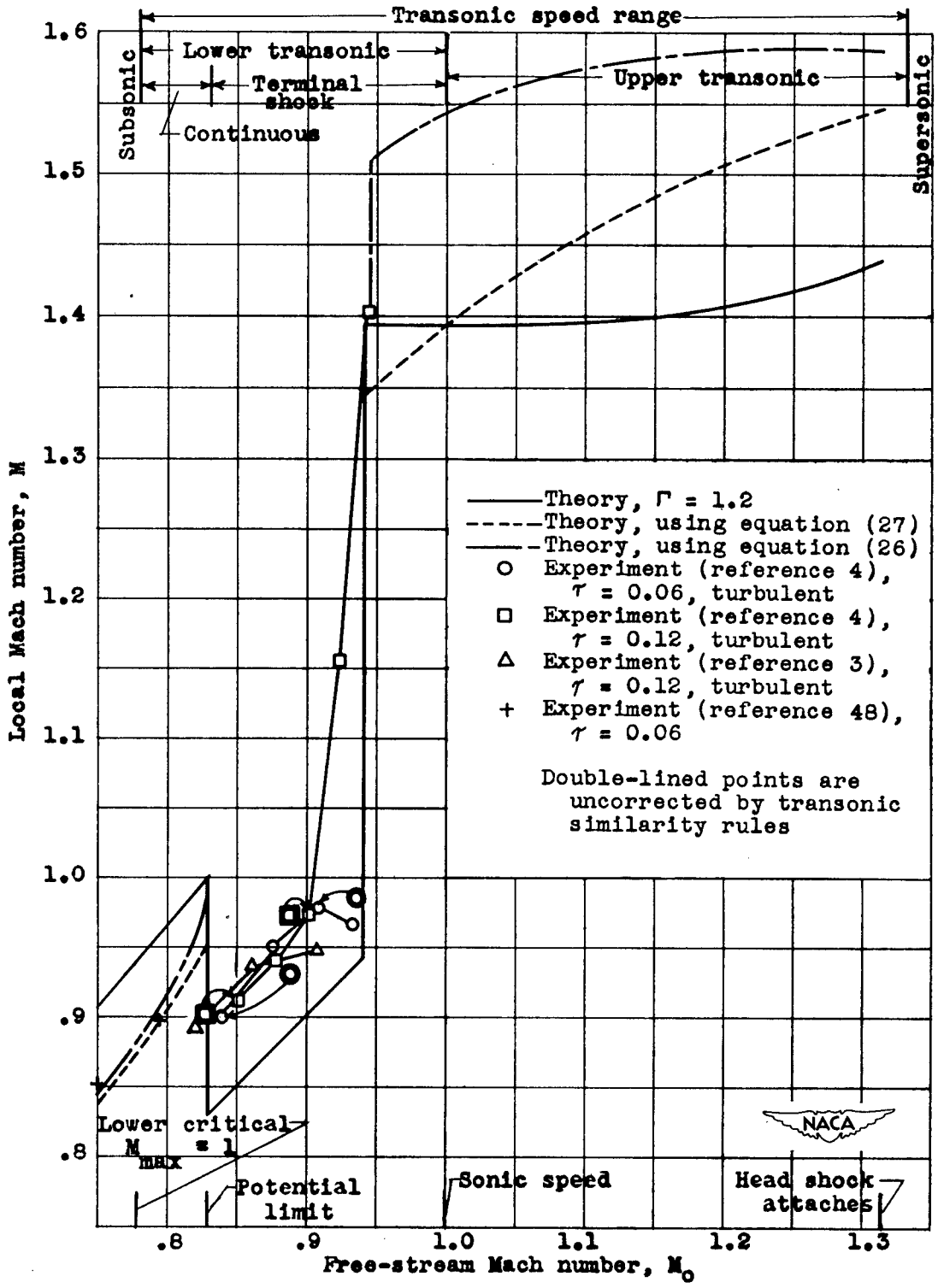

(b) x = 0.8.

Figure 12. - Concluded. Local Mach number on symmetric biconvex airfoil in transonic range. Limiting calculation for $\tau \to 0$, $M_o \to 1$. Plotted by transonic similarity rules for $\tau = 0.1$.

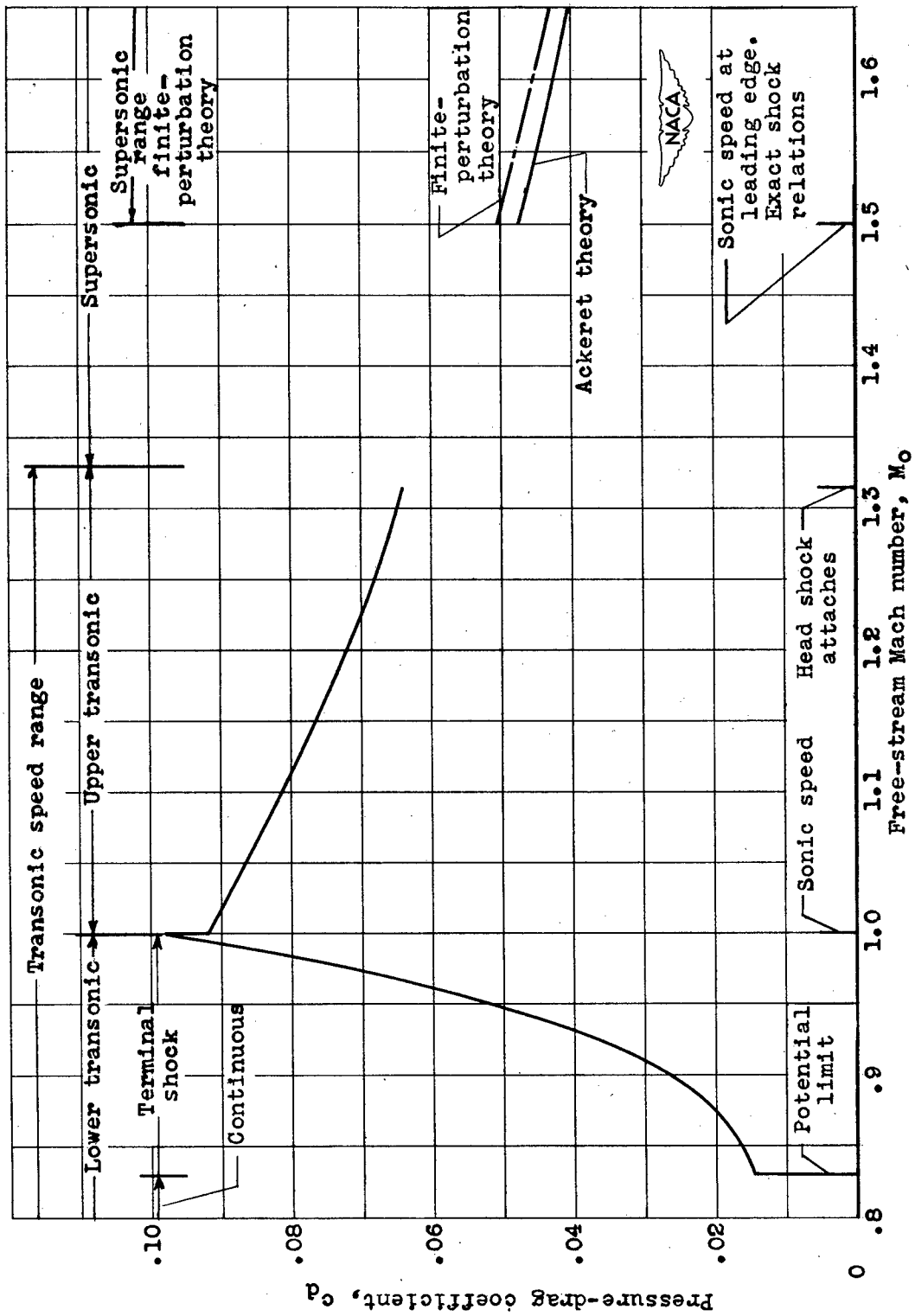

Figure 13. - Pressure drag on symmetric biconvex airfoil in transonic range. Limiting calculation for $\tau \to 0$, $M_o \to 1$. Plotted by transonic similarity rules for $\tau = 0.1$.

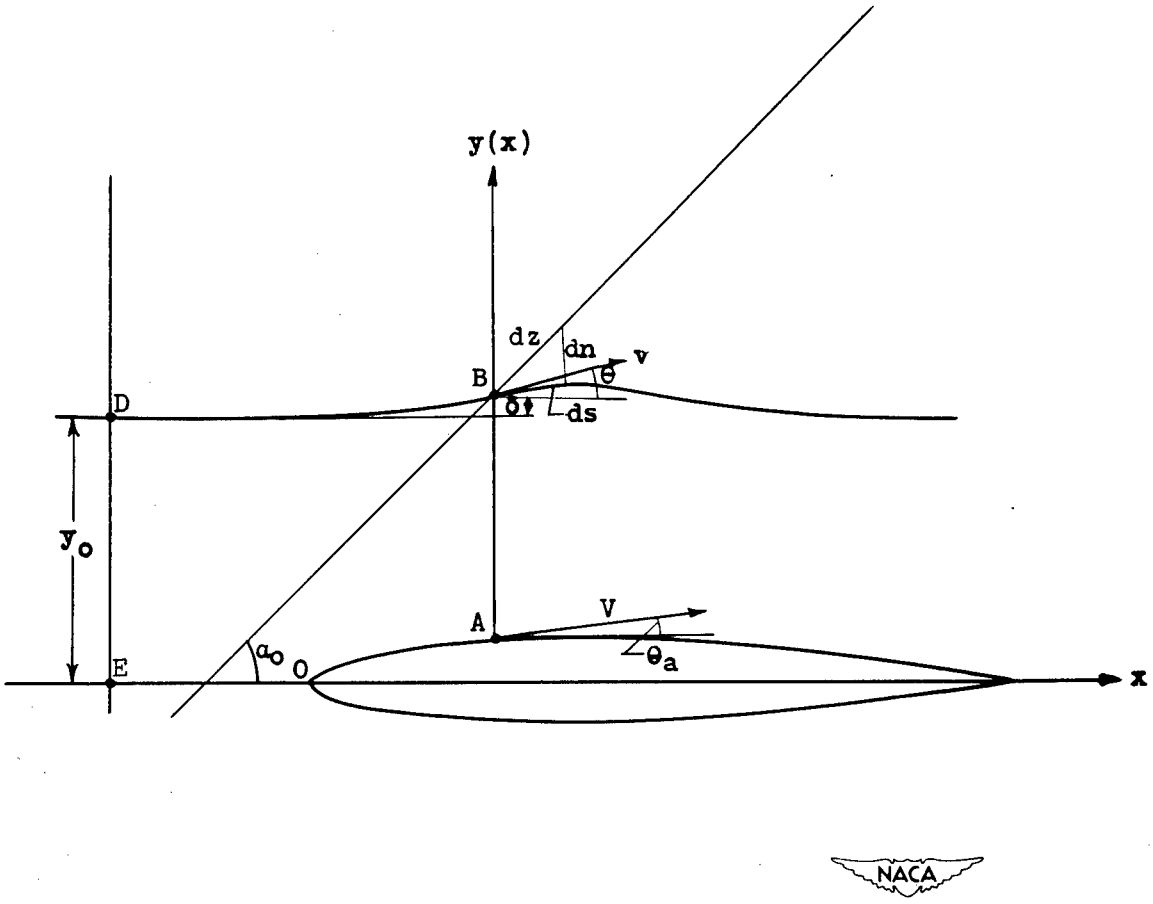

Figure 14. - Symmetric compressible potential flow.

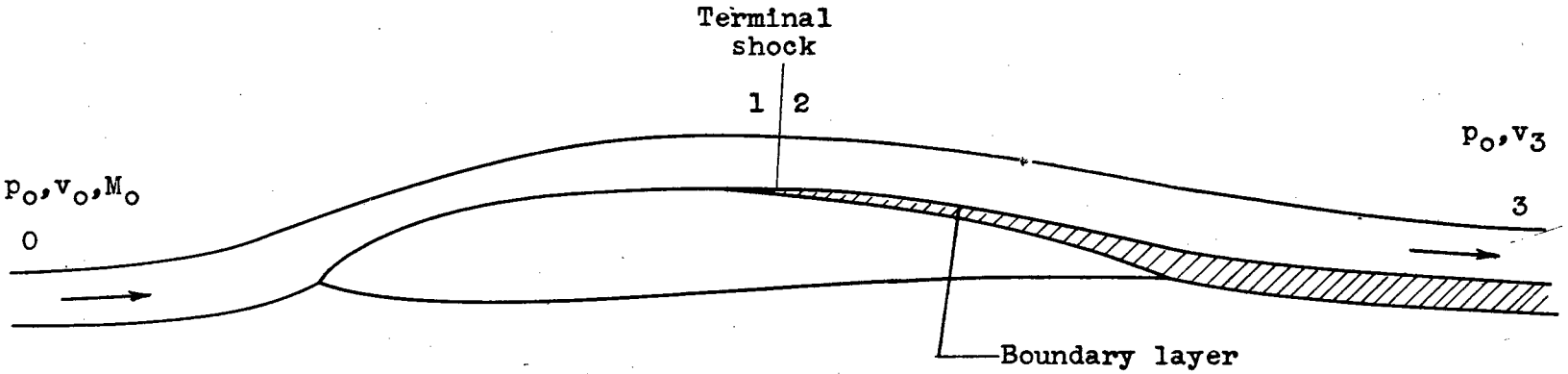

Figure 15. - Representation of stream tube in lower transonic range.

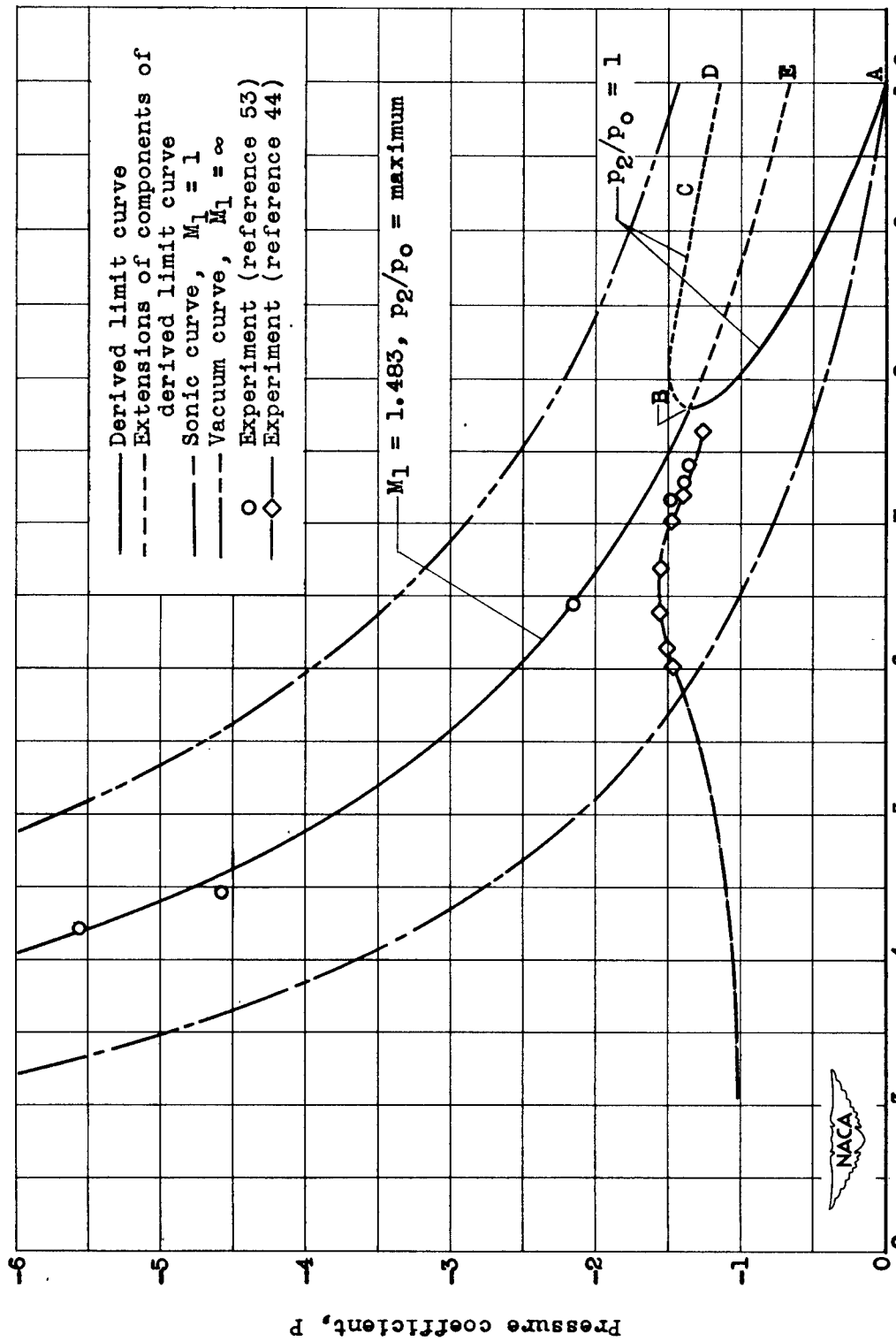

Figure 16. - Terminal-shock limiting-pressure coefficient on airfoils in lower transonic range.